SILICON SURFACE PASSIVATION FOR DEVICES

N. A. S. A. RESEARCH GRANT

NGR 36-003-067

School of Engineering

CASE WESTERN RESERVE UNIVERSITY

Cleveland, Ohio - 44106

Prof. Alan B. Kuper - Principal Investigator
Sept. 1968 - June 1969

Prof. Eugene T. Yon - Principal Investigator
June 1969 - Sept. 1969

Prepared by: EUGENE T. YON

NATIONAL AERONAUTICS AND SPACE ADMINISTRATION
Electronics Research Center
Cambridge, Massachusetts
F. J. Cocca, Grant Monitor

September 1, 1969

TABLE OF CONTENTS

INTRODUCTION

This report covers the research effort during the period of September 1, 1968 - September 1, 1969. The total effort involved four research projects. These were:

I. Effects of Gold Contamination in MOS Devices

II. Water Contamination in Thermal Oxide on Silicon

III. Interface State Measurement by MOS Low Temperature Transient Capacitance

IV. Device Screening Tests

The body of this report is divided into four major sections corresponding to each research project. Project I has been partially described in the previous year's report and only a final summary is given here. Projects II and III have been completed this year and are completely described. Project IV was initiated in the later part of this year, therefore, only partial results are reported. This project is being continued and expanded into the primary research effort for the coming year.

I. EFFECTS OF GOLD CONTAMINATION IN MOS DEVICES

Since gold in silicon can give rise to two energy levels deep within the forbidden bandgap, it can be important in determining the electrical behavior of semiconductor devices[1]. In silicon planar technology, the effect of gold is most important near the oxide-silicon interface. Theoretical and experimental studies have been made to investigate the effect of gold on the interface system[2, 3].

Cagnina and Snow[2] have calculated the effect of a uniform concentration of gold in the silicon on the MOS capacitance characteristic. The principle effect of the gold is a change of the capacitance curve minimum, dependent on the ratio of gold concentration to doping level. Experimental curves of gold diffused samples had a capacitance lowering in agreement with the theory. In addition to this shift in capacitance, they also observed a change of interface charge and inferred that the gold responsible for the change must be close to the oxide-silicon interface.

The purpose of the present research was to investigate further the electrical effects of gold in the interface system and to correlate these effects with radiochemically determined gold concentration profiles.

1. Experimental Methods

In this study, gold was diffused into a sample either from the

backside of the silicon wafer or from the outer surface of the front oxide. The gold source was an evaporated gold film. After diffusion, MOS capacitors were fabricated on the samples and the electrical effects of the diffused gold were measured. The samples were then neutron-activated and the gold concentration profiles determined. These concentration profiles were then compared with the corresponding electrical results.

1.1 Gold Diffusion

For gold diffusion into the silicon bulk from the back, the samples were first thermally oxidized to a thickness of 5000Å. The back oxide was then removed with HF and gold was immediately vacuum evaporated onto the exposed backside silicon. Gold diffusion was done at 1000°C in dry nitrogen. The 5000Å top oxide was used to minimize spurious contamination of the sample from contact with the boat, and was etched back to 2000Å for the electrical measurements.

For gold diffusion into the oxide, a 1μ oxide was initially grown on the sample. A large region in the center of the top oxide was then etched back to 2000Å and gold was vacuum evaporated on a portion of this 2000Å oxide. The sample was then diffused at 1000°C in dry nitrogen. The thick oxide around the edges and back of the sample minimized spurious contamination from the boat and

furnace during diffusion.

1.2 Electrical Measurements

Before electrical measurement, the excess metallic gold left on the sample after diffusion was removed by aqua regia. 20 mil diameter aluminum dots were evaporated onto the top oxide to form the MOS field plates. The sample back was then etched CP4 and a large area gold back contact was evaporated.

MOS capacitance voltage characteristics were measured at 1MHz with a Boonton 71A capacitance meter in a capacitance-voltage plotting setup.

MOS conductance voltage characteristics were measured point by point at 1MHz with a Boonton 75A-S8 capacitance bridge.

1.3 Radiochemical Techniques

After the electrical measurements were performed, the contact electrodes were removed and the samples were cleaned and wrapped in aluminum foil for shipment to the reactor. Neutron activation was done at Argonne National Laboratory for 2-3 days in a water cooled hole having a flux of about 3×10^{13} neutrons/cm^2/sec.

Following activation, the samples were mounted and masked with apiezon wax on individual holders such that only a portion of the surface was exposed. This exposed area was used for etch

sectioning. The sectioning was done by etching in planar cuts starting at the outer surface of the top oxide and proceeding into the silicon. An etching was followed by soaking in a gold stripping solution to prevent plated gold from one etched section being transferred to the next. Etches used were 5:1 HF for the oxide and Iodine etch B (1:5 HF to HNO_3 mixed 1:1 with iodine saturated acetic acid) for the silicon.

Counting was done by scintillation spectrometry on the 0.4 Mev. gamma photopeak of Au^{198}. A four inch $N_AI(Th)$ well type scintillation crystal was used with a 256 channel pulse height analyzer. Typical overall experimental sensitivity was 10^8 atoms per count per minute with a background of 30 cpm. Calibration was done by counting a small sample of known gold content that was activated with the other samples.

2. Results and Discussion

Diffusion of gold into the top oxide and directly into the bulk from the back of the wafer was done for various times at 1000^oC for n and p-type (phosphorus) results will be presented here, as the majority of the work was done with n-type material.

Results on neutron activation analysis of samples having gold diffused into the silicon bulk from the back is shown in Figure 1. The figure shows that the gold concentration in the bulk silicon is

uniform within at least 1.5μ of the interface. The bulk gold concentration in the silicon initially increases rapidly with time and saturates after 60 minutes. After this time, the major change in the concentration profile is an increased penetration of gold into the oxide. The first data point in the silicon at the interface was for a 1500Å section and was always of a higher concentration than that found in the silicon bulk, thus there is a definite pile up of gold in the silicon within 1500Å of the interface. The concentration of gold in this first section though could actually be higher than indicated by the profiles*.

The experimentally observed change in effective interface charge as seen in Fig. 2 had the form shown in Fig. 4, and was independent of sample resistivity over the range studied of 10 to 0.1Ω cm. The variation of effective surface charge is most likely associated with the piled up gold in the silicon near the interface since only a capacitance minimum lowering was predicted for the bulk gold. Capacitance minimum data is compared with bulk gold measurement in Fig. 3. Figure 4 shows that the shift of surface

---

*The difficulty in determining the actual concentration of gold in the first silicon cut is an experimental one. The problem lies in the fact that it was necessary to follow an etching with two gold stripping soaks to prevent spurious transfer of gold from one section to another. If there is a sharp pile up of gold in the silicon very near the interface, the gold stripping soaks associated with the last oxide section could leach away an appreciable amount of this piled-up gold.

state charge reaches a maximum at about 30 minutes and then slowly decreases with time. The radiochemical data of Fig. 1 shows that gold in the silicon saturates after about 60 minutes with appreciable gold diffusing into the oxide before this time. This suggests that gold in the silicon near the interface, if negatively charged, could explain the initial positive shift of surface state charge. If gold in the oxide assumes a positive charge state, then the slow diffusion of gold into the oxide could be responsible for the slow decrease of the effective surface state charge shift.

Because of the experimental difficulty mentioned earlier, and indeed because of the elusive nature of the interface region itself, concentration of gold cannot be precisely assigned to the silicon side and to the oxide side of the interface. The best quantitative description of the interface gold that can be presented here is the total number of interface atoms, which is taken as the sum of the gold atoms in the last oxide section (500Å) and the first silicon section (1500Å). The time dependence of this quantity is plotted in Fig. 5. Referring also to Fig. 4 shows that there are always more interface atoms than needed to explain the observed surface state charge variations, if all the gold atoms were charged. If it is assumed that the majority of total interface atoms after a few minutes is due to diffusion into the oxide, then from the slope of the linear portion and an assumed value of oxide solid solubility of approximately

$10^{18}/cm3^2$, a diffusion coefficient for the process of approximately $10^{-3}\mu^2/hr$ can be calculated. This is in agreement with Cagnina and Snow's value of $2x10^{-3}\mu^2/hr$ for the effective diffusion coefficient of gold in SiO_2 at 1000C. Thus, it is likely that the major increase in total interface gold atoms is due to gold entering the oxide following simple diffusion theory. The time dependence of the decrease of the surface state charge shift in Fig. 4 is of the same order as for diffusion of gold into the oxide. This suggests that gold diffusing into the oxide with a positive charge is responsible for the decrease of effective interface charge after the effect of negative interface gold in the silicon has saturated.

Diffusion of gold into the oxide from the outer surface is more complicated. Fig. 6 shows the concentration profiles for gold diffused into the oxide. For short diffusion times (up to a few hours) the concentration profiles reasonably match a simple complementary error function diffusion characteristic with a gold solid solubility of $3x10^{18}/cm^3$ and diffusion coefficient of $2x10^{-3}\mu^2/hr$. The slight increase at the interface for the two hour diffusion is possibly due to interface precipitation and some electrostatic binding. For longer diffusion times the gold concentration profile near the outer surface of the oxide continues to rise, reaching a value greater than $10^{19}/cm^3$ for the 100 hour diffusion. The observed behavior does not fit a simple surface rate limitation theory. The increased surface

concentration of gold could be due to formation of a gold compound at the surface since the surface oxide was visibly dulled after the long diffusions. Even for the long diffusion times, the average level of gold near the interface is only a few times $10^{18}/cm^3$, which is the value of the gold solubility inferred from short oxide diffusion times and from the experiments of diffusion from the silicon bulk.

The experiments of gold diffusion into the silicon back suggested that gold in the oxide should be positively charged. For gold diffused into the oxide then, the initial change in interface charge should be negative. This is indeed the case as shown by Fig. 7. For longer diffusion times, the gold in the silicon near the interface (which is expected to act like negative charge from the results of the experiments of gold diffused from the back) should reach a sufficient concentration to cancel the effect of the positive gold atoms in the oxide. It appears that this is also the case, as Q_{ss} in Fig. 6 starts to decrease after six hours.

From the diffusion data presented, the inference of Cagnina and Snow that the positive gold atoms in the oxide must reside close to the interface can be further justified. The diffusion constant of gold in silicon is about eight orders of magnitude higher than in the oxide. It is then reasonable that the initial change in Q_{ss}, reaching a maximum of $10^{12}/cm^2$ in 30 minutes for gold diffused from the silicon back (Fig. 4) is due to gold near the inter-

face in the silicon alone. That only the atoms in the oxide near the interface appear to be electrically charged has been shown for sodium[4].

For samples having gold diffused from the oxide, the MOS capacitance minimum shift agrees with the measured silicon bulk concentration as it did in the backside diffusion case.

Since gold diffused into the oxide or diffused into the back of the sample affects interface charge significantly, it might also be expected to affect interface state density. A sensitive indication is the MOS conductance[5]. Conductance measurements were taken on both oxide and bulk diffused gold samples, and typical results are shown in Fig. 8.

To insure reproducible data, two precautions had to be observed for gold diffused samples. The first consideration, which applies to experiments in general, that sample thermal cycling, especially the cooldown cycle, had to be carefully controlled. Early work with non-controlled sample cooldown resulted in conductance peak height variations by a factor of three. The second consideration was that sample bulk resistance had a dominating effect on the conductance data when the sample doping was such that the diffused bulk gold caused compensation. All raw conductance data was corrected for the sample bulk series resistance before comparison. The conductance curves obtained were, in general, identical for

gold diffused and no gold control samples. In some cases, the gold sample conductance differed from control sample curves. These deviations were all explained by effects other than gold-surface state interactions. The rise of the conductance peak for the 10 and 40 minute diffusion in the 0.6Ω cm case, Fig. 8b, is a result of the changing capacitance characteristic since it occurs only for samples showing a lowering of the MOS capacitance minimum. The peak conductance of a no gold sample having a resistivity chosen to give a match to the capacitance minimum of the gold sample was the same as the peak conductance of the gold sample. The conductance increase on the inversion side of the peak for the 40 minute curve of Figure 8b is an effect that occurs only for samples that have a drastic increase in depletion region length. The loss is just an effect of the decreased silicon capacitance and increased loss in inversion and thus not seen in the 0.1Ω cm case, Fig. 8a.

Some broadening and lowering of the conductance peak was observed for shorter time oxide diffused samples. This is believed due to nonuniform diffusion of the gold in the oxide since it disappeared after longer diffusion times. The capacitance curves also had a markedly decreased slope for the shorter diffusion times. After longer diffusion times though, both the capacitance and conductance curves matched the no gold characterisitics.

Since the MOS conductance of gold diffused samples was

identical to the conductance of no gold control samples, the effect of gold on interface state density must be small compared to the interface state density normally associated with the oxidized sample.

3. Conclusions

3.1 Major Results

The results of this study can be summarized as follows:

(1) Gold in the silicon near the interface seems to act as negative interface charge and can cancel residual Q_{ss}.

(2) Gold in the oxide seems to act as positive charge.

(3) The observed time dependence of ΔQ_{ss} in a diffusion experiment can be explained by a combination of (1) and (2).

(4) Gold diffused from the back of the silicon wafer has a constant concentration in the region approaching the interface, has a slight pile up at the interface and diffuses through the interface into the oxide.

(5) The pile up of gold in the silicon near the interface appears to be responsible for the observed negative interface charge.

(6) The constant concentration of gold in the bulk silicon agrees with the MOS capacitance minimum lowering within 40%.

(7) Gold diffused into the oxide initially follows simple diffusion behavior. Compound formation at the outer surface of the oxide greatly increases the surface concentration for long diffusion times. Gold near the in-

terface though, is within solid solubility limits.

(8) Gold in the oxide within 100Å of the interface can explain the observed variation in Q_{ss} from positive charge in the oxide.

(9) Basic gold concentration profiles observed when gold is diffused from the sample back match solutions to the two media diffusion problem for values of

Oxide Solid Solubility = $3 \times 10^{18}/cm^3$
Gold Diffusion Constant in the Oxide = $1 \times 10^{-3} \mu^2/hr$
Gold Segregration Coefficient at the Interface = 0.01

(10) Gold concentrations in the silicon when the gold is diffused through the oxide are about an order of magnitude higher than expected from the theory of gaseous diffusion through a membrane.

(11) Even though gold near the interface can cause changes in effective interface charge density as high as $10^{12}/cm^2$, the change in interface state density is much less than $10^{11}/cm^2$.

3.2 Application to Silicon Device Technology

The most interesting effect of gold on the interface system is the variations in Q_{ss} that can be produced by gold diffusion. This effect suggests the possibility of tailoring the gate characteristic of field effect devices to fill specific requirements. Since the gold distribution is sensitive to diffused layers, a study of the effects of gold versus device geometry could have technological importance.

The effect of gold on interface state densities should be ex-

amined in more detail. More sensitive measurement techniques would enable the measurement of the gold induced states and would contribute to a more exact theoretical understanding of the gold effects.

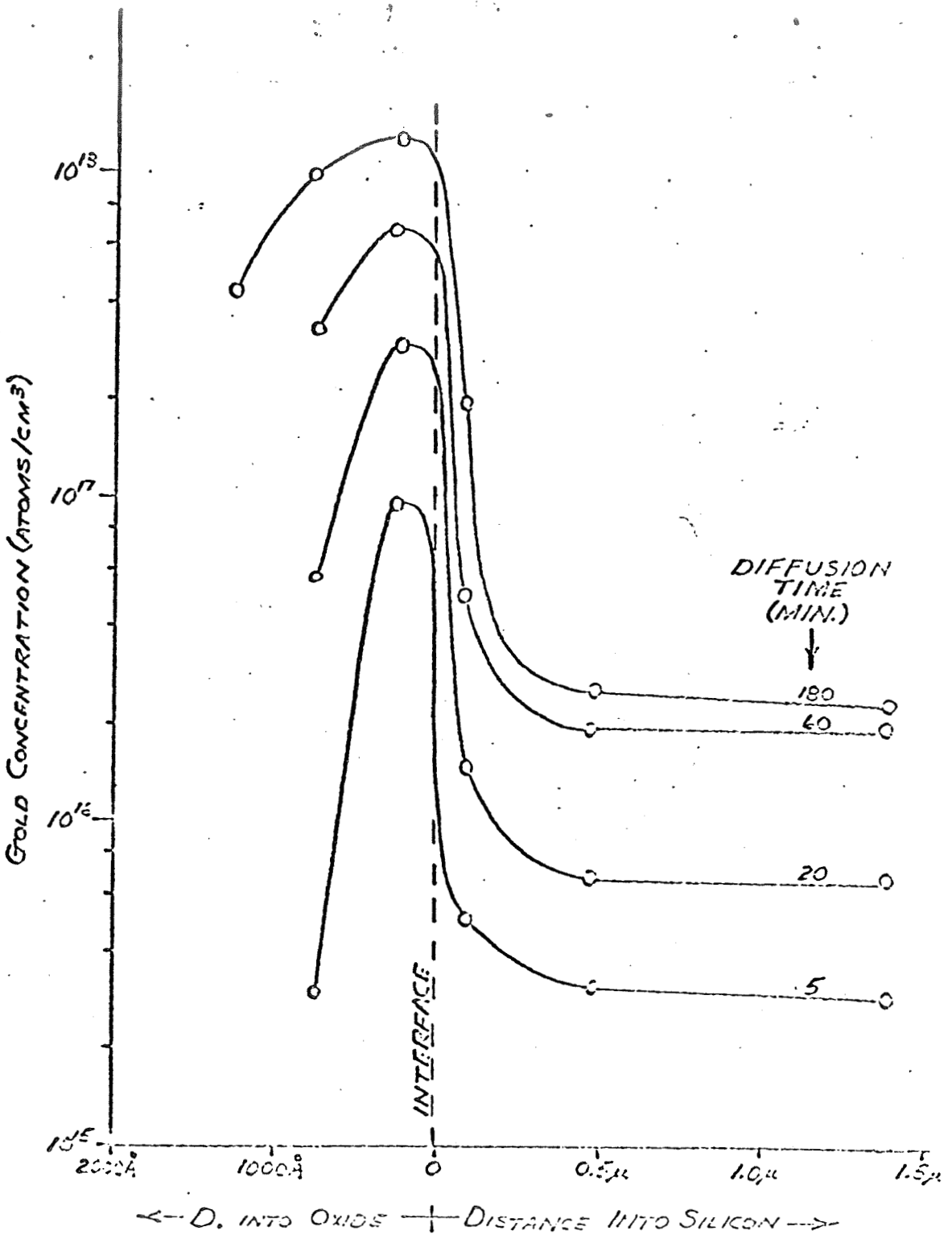

Figure 1. Gold Concentration Profiles for Backside Diffusions.

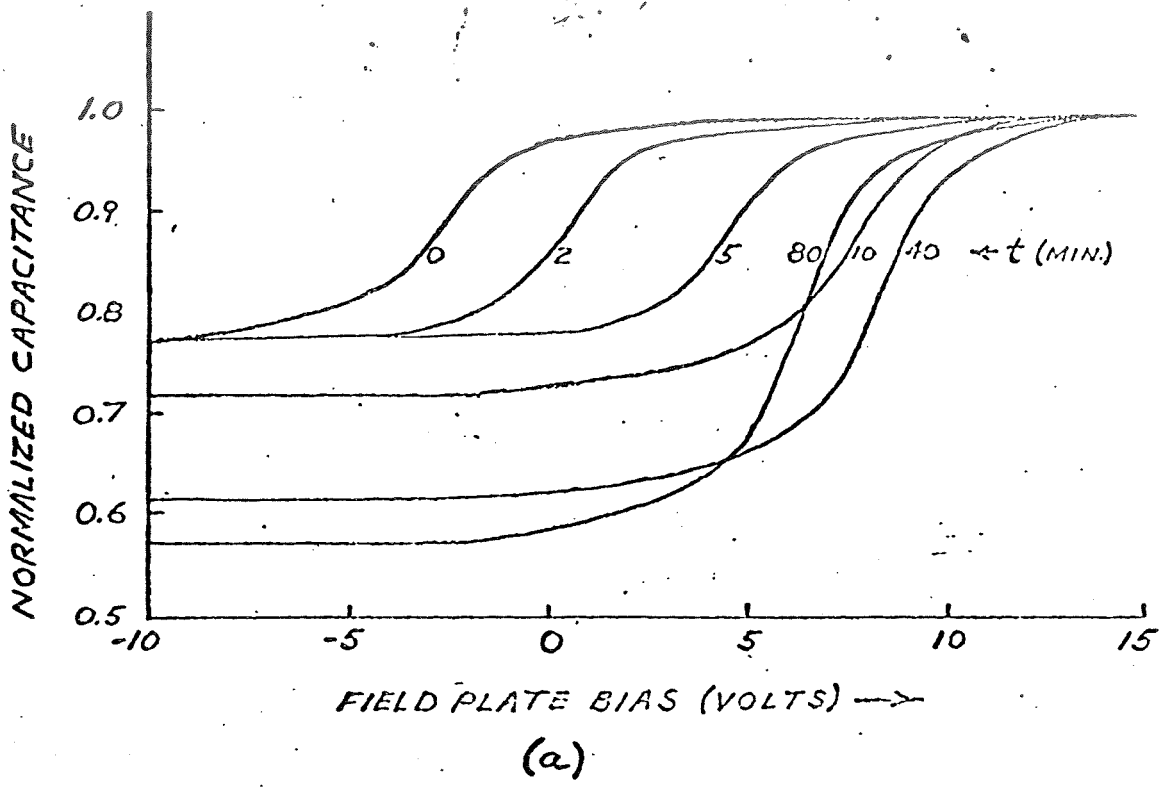

(a)

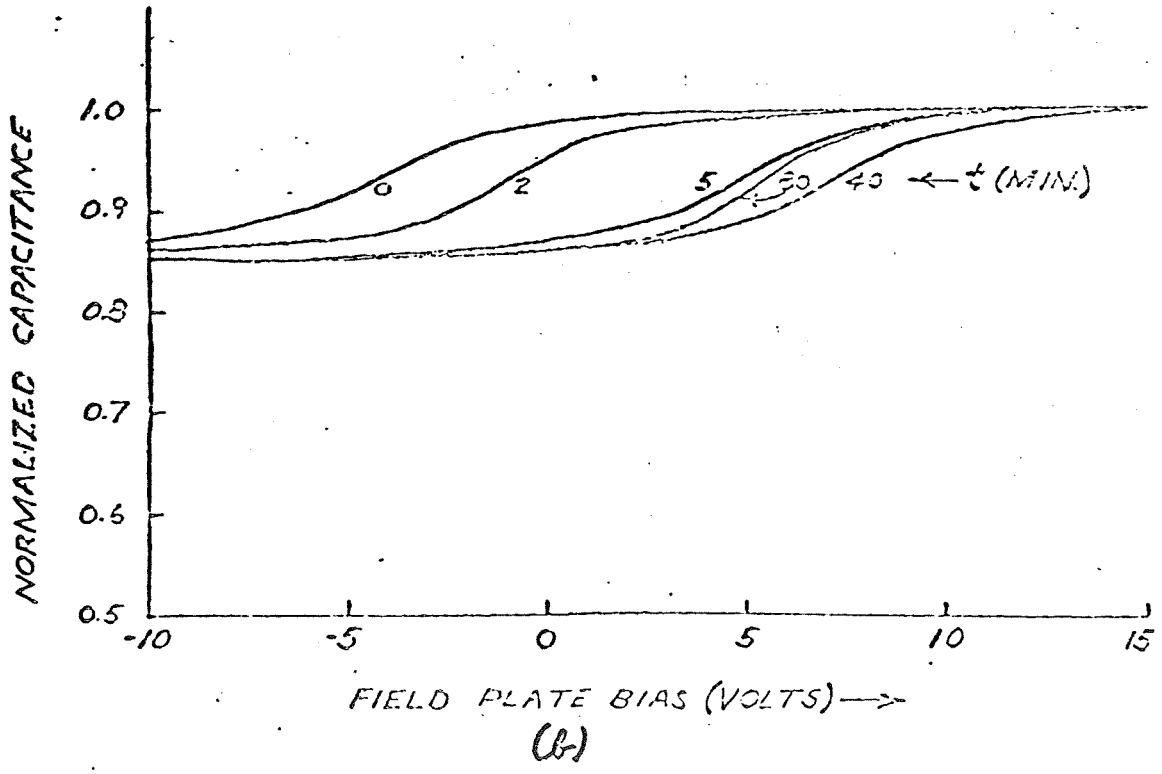

(b)

Figure 2. MOS Capacitance Curves for Various Gold Diffusion Times, (a) ρ_{Bulk}=0.6Ω-cm, (b) ρ_{Bulk}=0.09Ω-cm.

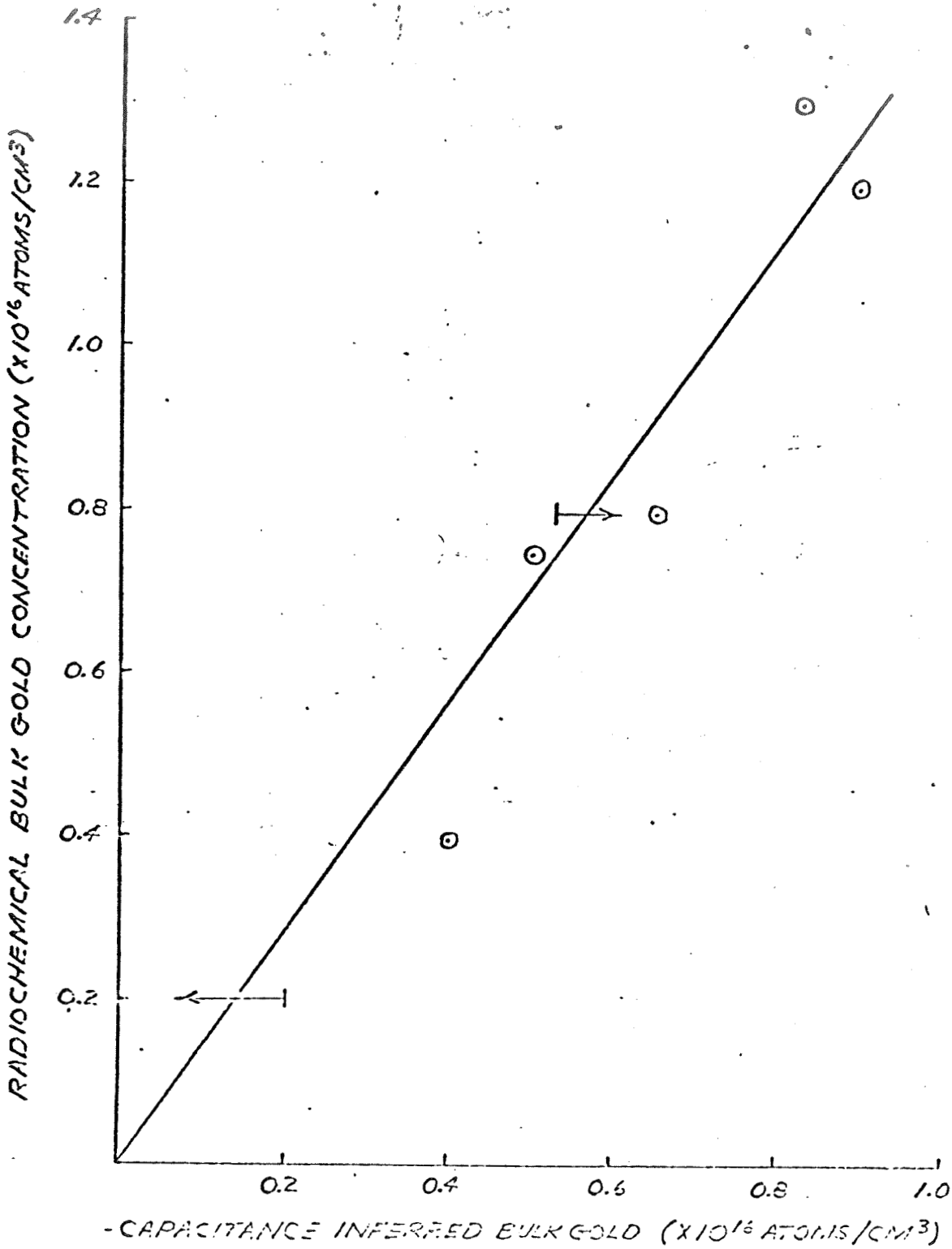

Figure 3. Comparison of Actual Bulk Gold With the Value Inferred from the MOS Capacitance.

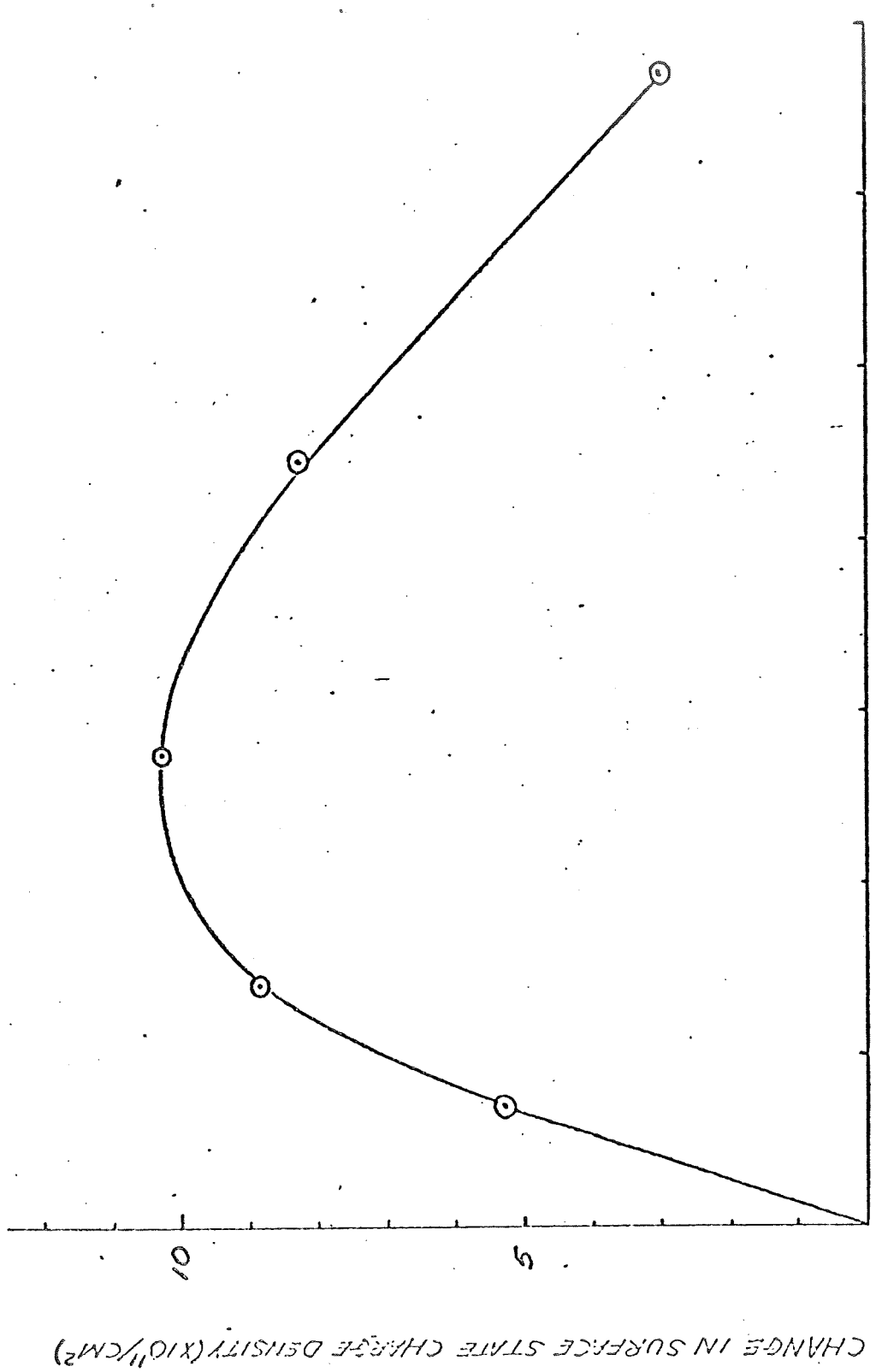

Figure 4. Variation of N_{ss} With Time for Backside Diffused Gold.

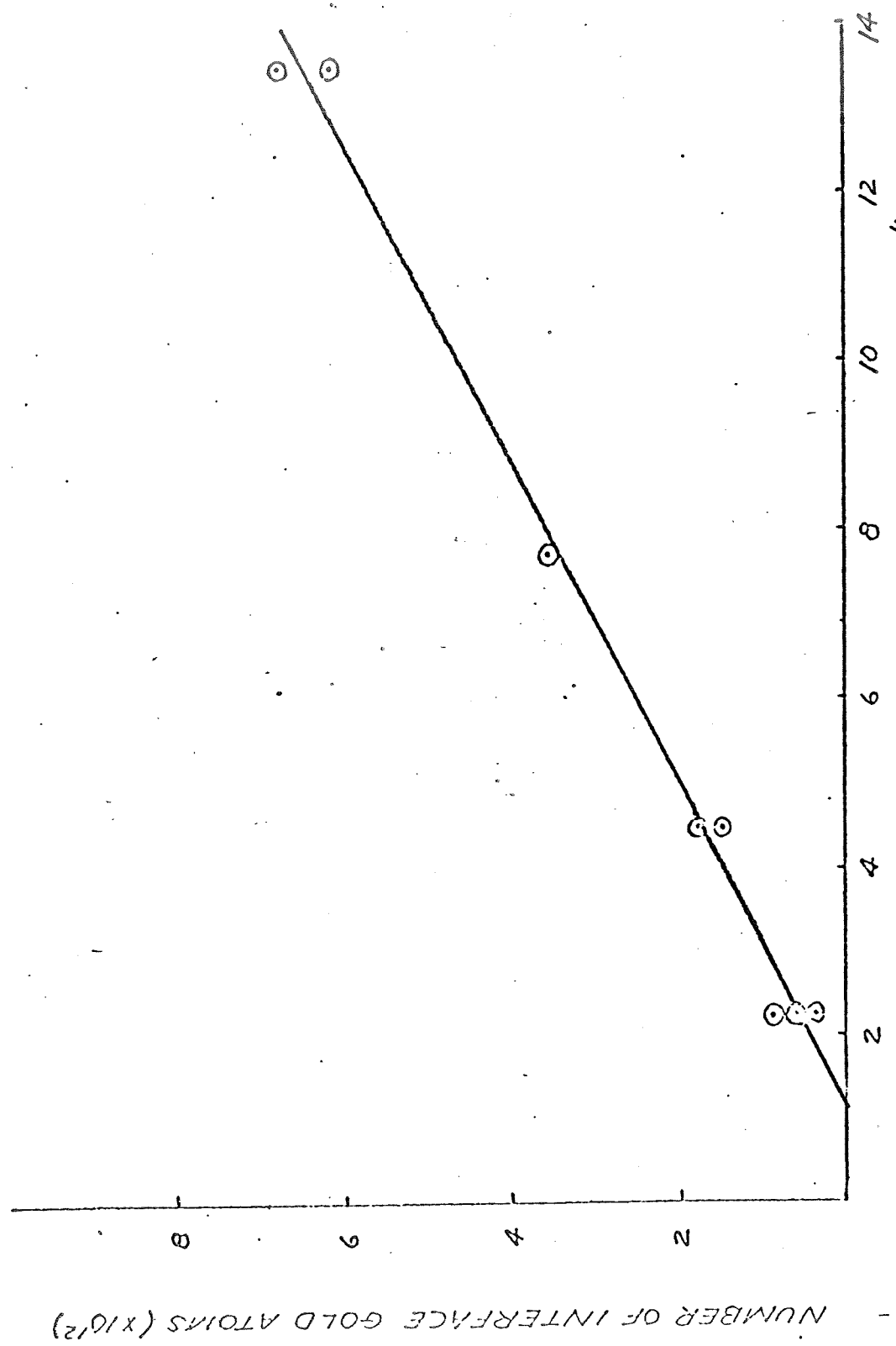

Figure 5. Time Dependence of Total Interface Gold Atoms.

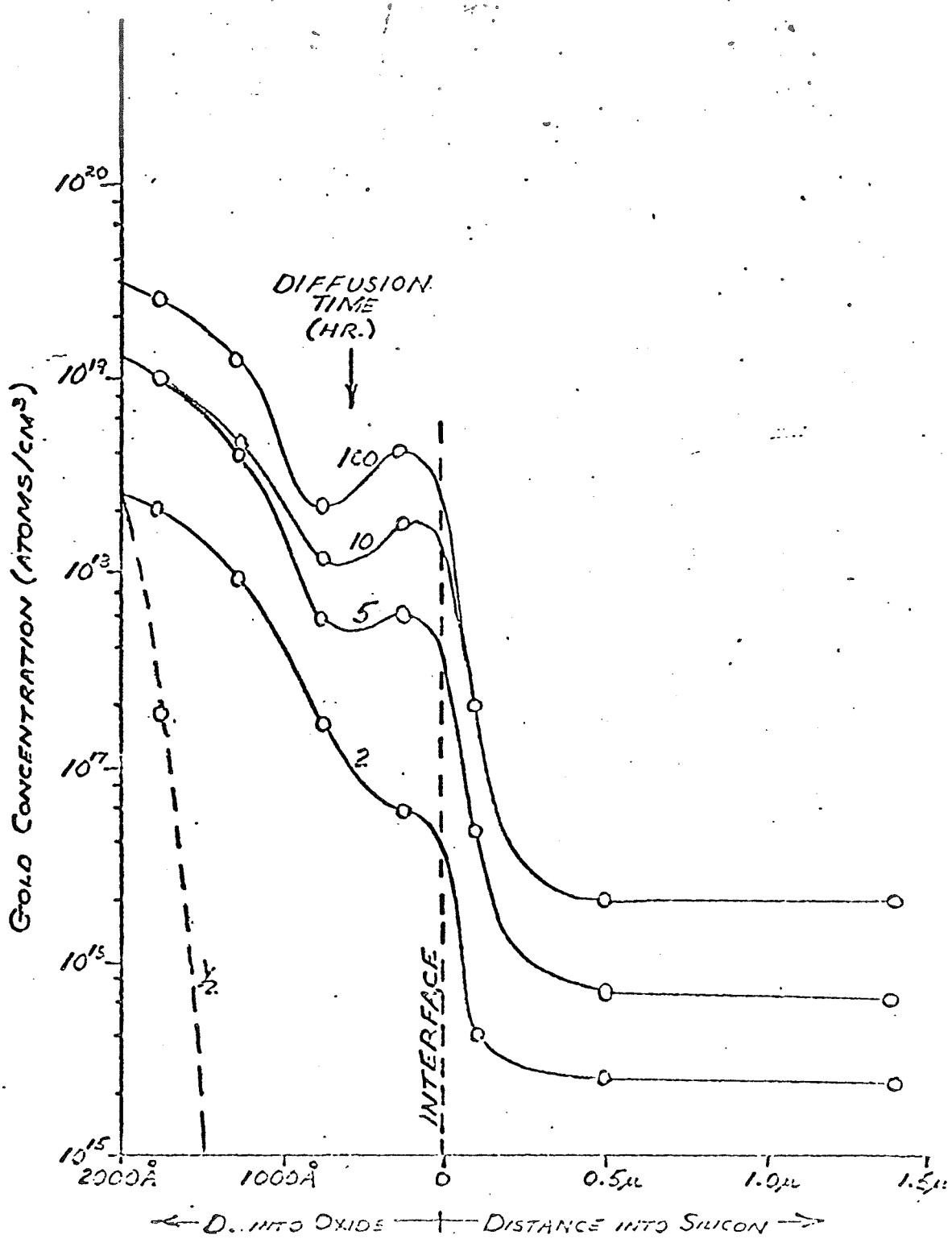

Figure 6. Gold Concentration Profiles for Oxide Diffusions.

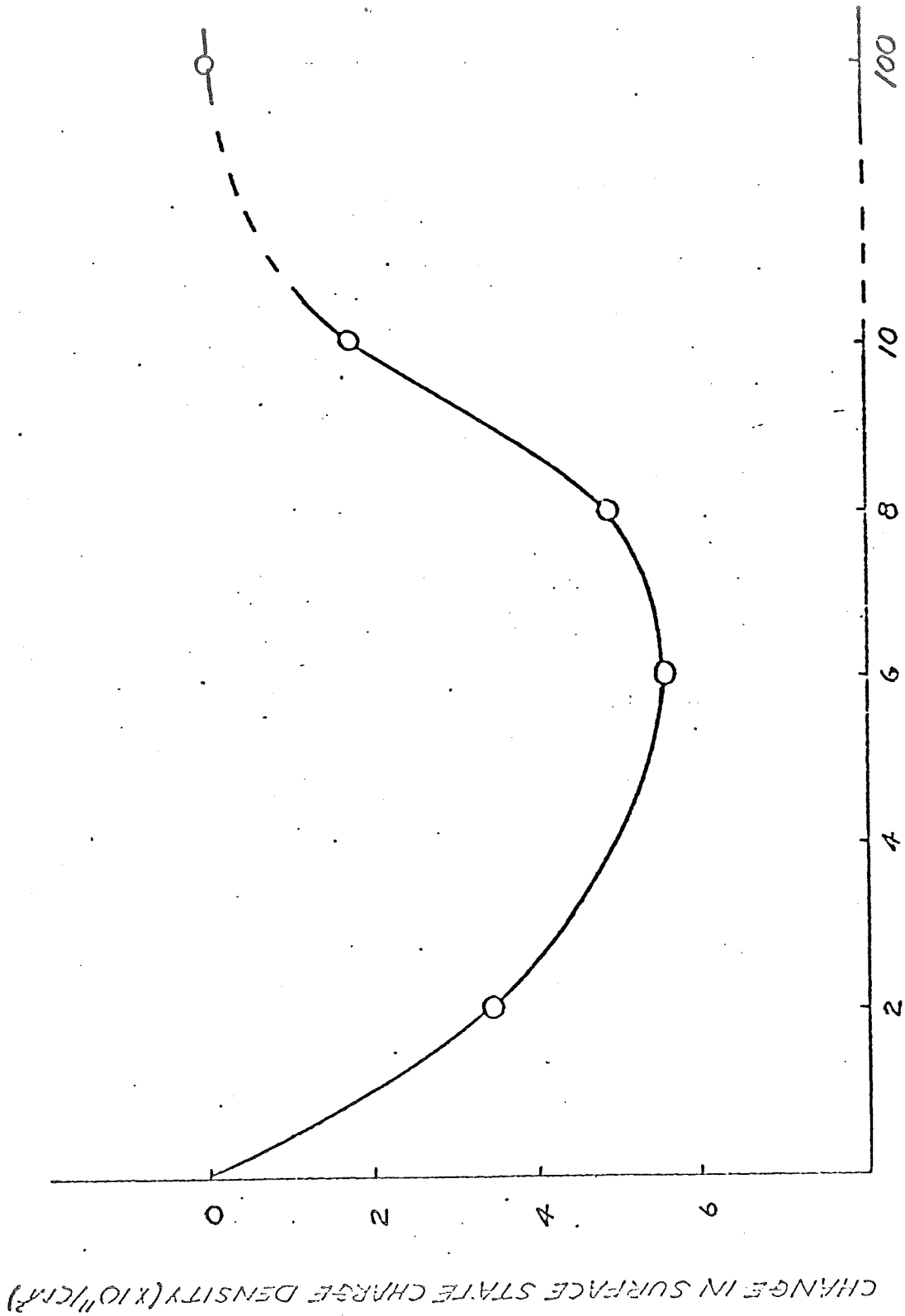

Figure 7. Variation of N_{ss} With Time for Oxide Diffused Gold.

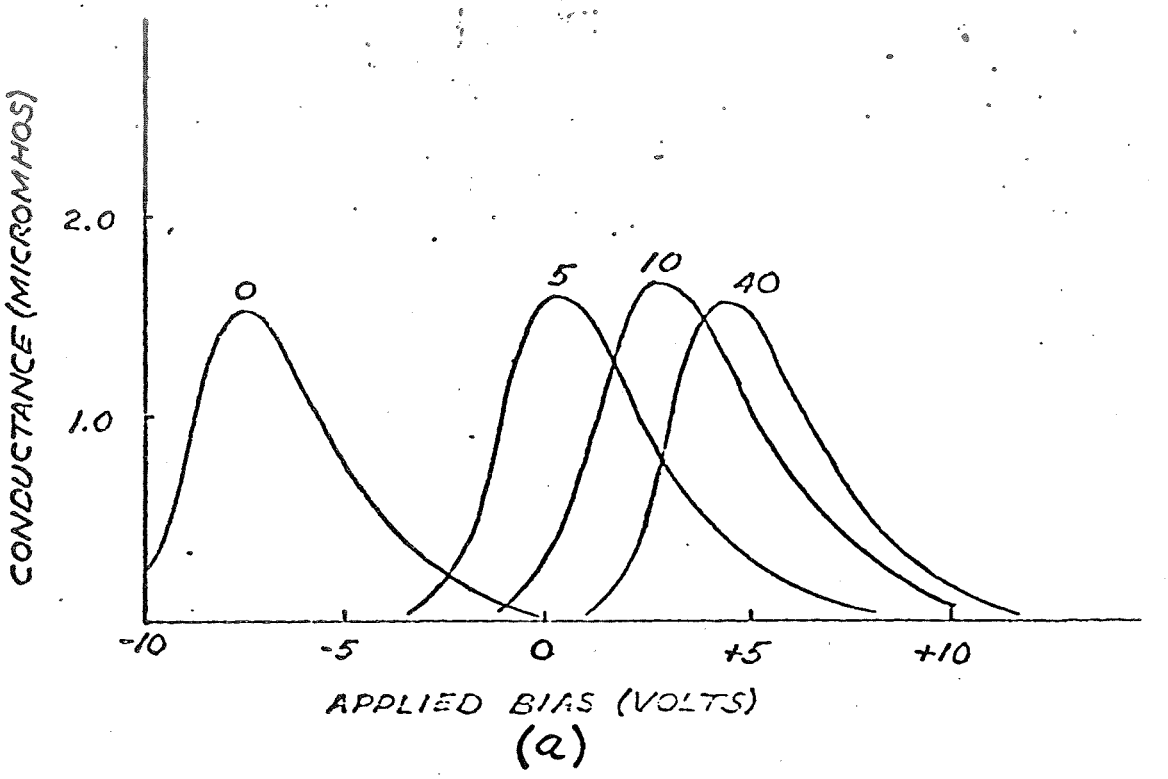

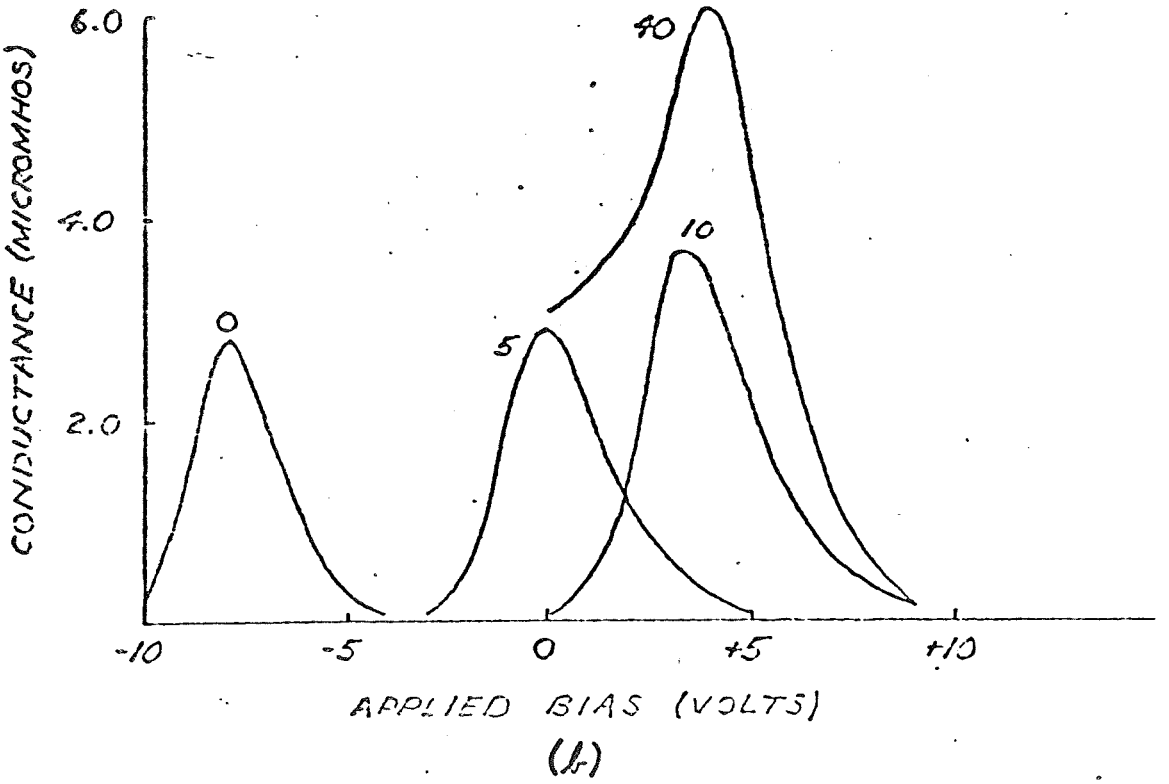

Figure 8. MOS Conductance for Various Gold Diffusion Times, (a) ρ_{Bulk}=0.09Ω-cm (b) ρ_{Bulk}=0.6Ω-cm.

II. WATER CONTAMINATION IN OXIDE

1. Introduction and Background

1.1 Statement of the Problem

It was proposed to study the diffusion of water in thermally-grown oxide films on silicon under conditions approximating those of device use. Diffusions were done with tritiated water vapor at water vapor pressures below one atmosphere and at diffusion temperatures of 50 - 250°C for diffusion times up to several hours. Samples were sectioned to obtain hydrogen profiles as functions of the diffusion parameters.

Water and sodium interactions during diffusion in the oxide film were studied. An attempt was made to correlate the distributions found radiochemically with charge measured by MOS technique.

1.1a Purpose of the Study

Water has long been considered to be a serious contaminant in the oxide passivating layer on silicon planar devices. It is impossible to eliminate it in the manufacture of the devices or, except by hermetic sealing, in the use of the devices. The next best thing is to find out what the water is doing in the oxide so that at least the behavior is predictable, or to find out enough to be able to counteract the contamination effects. No radiochemical measurements on

water in the oxide have been made previously under conditions approximating device operating conditions.

Furthermore, it appears from previous studies that electrical instability caused by contaminants is not the isolated actions of the individual contaminants. Rather, it appears that water and sodium, the most ubiquitous, and therefore the most troublesome, contaminants somehow interact to produce their observed electrical effects. Thus, it was desirable simultaneously to study water and sodium movements in the oxide.

At this point a brief review will be given of relevant previous studies. A review will first be given of experiments with water diffusion in bulk silica glass. This will be followed by discussion of water in an oxide film on silicon. A discussion will then be given of sodium in the oxide and previous indications of sodium-water interactions either in an oxide or in bulk glass. Finally, a brief review will be given on the oxygen analysis techniques.

1.2 Previous Studies on Water Movement and its Effects in Bulk Silica Glass

Moulson and Roberts[6] used infrared absorption measurements to follow water in-diffusion and out-diffusion in plates of silica glass. They found that the 2.7 micron IR absorption, which has generally been attributed to resonance absorption by Si-OH bonds, was present only in glass containing 'water', and the amount of

absorption was taken to be proportional to 'water' content of the glass.

Diffusion coefficients and solubilities were measured from 600° to 1200°C with water vapor pressures near atmospheric. Samples were profiled by successive grindings and remeasurements of IR absorption. Diffusion coefficients were found to increase with temperature, and solubilities to decrease with temperature as expected. Total water content of the glass increased as the square root of the diffusion time as expected for a diffusion-controlled process. Furthermore, solubility varied as the square root of the water vapor pressure, which indicated a breakup of the water molecule into two parts (presumed to be Si-OH groups) upon entering the silica.

Since IR absorption is inherently a rather insensitive method of measuring hydrogen distributions, Drury and Roberts[7] chose to follow the diffusing water with a tritium tracer. They confirmed much of the earlier work of Moulson and Roberts, but found some interesting anomolies. For example, the diffusion coefficient for water was not constant as had been indicated by the less sensitive IR measurements, but rather was quite concentration dependent at any given temperature. Furthermore, the concentration dependence of the diffusion coefficient was strongly dependent on the diffusion temperature, especially in the vicinity of 1000°C. Above 1000°C temperature dependence of diffusion coefficient was smaller than below 1000°C.

They also found that different batches of glass, although supposedly identical, gave different diffusion behavior and different water solubilities. Furthermore, the solubilities with the tritium were always higher than given by previous measurements with IR. If the tritium tracer technique was in proper calibration, the implication is that some of the water was in the silica in a form other than as Si-OH groups.

The problem of scatter among nominally identical batches of glass was at least partially resolved by the work of Roberts and Roberts[8], who found that diffusion and solubility of water in glass could be correlated with the thermal history of the glass. In particular, diffusion coefficients and solubilities depended on the fictive temperature (temperature at which the glass is in pseudoequilibrium with its environment) as well as diffusion temperature and water vapor pressure. The same effect was observed by Hetherington and Jack[9].

Study has been done on the form in which water exists in silica, and it is fairly certain that it exists as Si-OH groups. Presumably, an entering water molecule attacks an oxygen bridge between two silicon atoms to form two Si-OH groups. This is indicated by a number of pieces of evidence. The 2.7 micron IR absorption band, which is observed only in samples containing 'water' has been

identified by a number of investigators[7] as the stretching frequency of the Si-OH bond. Furthermore, the dependence of solubility of water on the square root of water vapor pressure[6, 7] indicates that the water molecule breaks into two parts upon entering the glass.

Also, Hetherington and Jack[9] have made a number of measurements on such things as viscosity of the glass, temperature coefficient of expansion, density and a number of other parameters which are indicative of the glass structure. All of these measurements indicate that glass containing 'water' has weaker three-dimensional bonding than glass not containing water. This would be expected since replacement of Si-O-Si groups by Si-OH groups would weaken the structure.

Bell, Hetherington and Jack[10] have shown that an equilibrium exists between hydrogen, water and silica. When hydrogen was diffused into silica, hydroxyl groups were formed just as with water. Furthermore, if the hydroxyl-containing silica were heated in vacuum, both hydrogen and water were given off, regardless of the way in which the hydroxyls had been initially introduced.

Lee[11] has done a study on the role of hydroxyl in diffusion of hydrogen in silica. He confirmed that either hydrogen or water will produce hydroxyl groups in the silica, though hydrogen diffusion rates were larger. Lee also noted that there are two types of hydroxyl

in the silica, one much more stable (difficult to out-diffuse) than the other, though both show the same characteristic IR absorption. The observation of two types of hydroxyl was confirmed by Hetherington, Jack, and Ramsey[12] who found that some hydroxyl groups were much more stable with respect to electrolysis than were others.

Roberts and Roberts[13] have recently used O^{18}-tagged water to compare diffusion of oxygen in water under the same conditions Drury and Roberts[7] had previously diffused tritium-tagged water. They found oxygen profiles by grinding the glass in layers, chemically releasing oxygen from the grindings, and analyzing it mass spectroscopically.

They found that the oxygen tracer diffused a much shorter distance than had the tritium under the same diffusion conditions. This showed that the water did not diffuse as molecules, since the profiles would then be identical. They suggested a model in which hydrogens and hydroxyls move as associated pairs. The water molecule reacts with a bridging oxygen to form two Si-OH groups. This configuration later regroups to give an oxygen bridge and the water molecule. The process then repeats itself at another site in the silica.

Only one of the Si-OH groups contains a tagged oxygen but both contain tagged hydrogen from the water. There is, therefore,

a 50% probability of passing on tagged oxygen and 100% of passing on tagged hydrogen. Thus, the oxygen tracer will diffuse a much shorter distance than the tritium tracer as observed.

Owen and Douglas[14] studied the electrical effects of water in fused silica. They found that metallic impurities, primarily sodium, determined the DC conductivity of the glass. Water had little effect on conductivity, but almost completely determined the dielectric properties of the glass.

1.3 Water in Oxide Films on Silicon

1.3a Difference Between Oxide and Fused Silica

Although the oxide films used in this study are a form of silica and are amorphous[15], there are a number of reasons for using caution in applying the material in Section 2.2 directly to the film. In a number of rather important respects the oxide film is different from the silica glass used in those studies.

In the first place, the oxide film is not a glass in the normal sense since it has never gone through a molten phase. It is formed at a temperature below its melting point. The structure may, therefore, possibly not relax to the same form as a glass which has been melted.

The diffusion process by which the film is grown, of necessity, leaves the film with gradients of silicon and oxygen[16]. Thus,

the film is oxygen-rich relative to silica near the air interface and silicon-rich near the silicon interface. These gradients, of course, set up chemical potential gradients which act in addition to a concentration gradient in controlling a diffusion process in the film. For example, the excess oxygen at the air interface could leave the surface with a slight negative polarization and hence attract positive charges to the surface.

The thermal growth process, furthermore, leaves the oxide under a high compressive stress[17]. The silicon substrate contracts considerably more than the oxide in cooling from oxidation temperature to room temperature. Since the oxide is firmly bonded to the silicon and is normally much thinner than the silicon, the oxide becomes compressed.

The existence of the silicon substrate itself is a difference between the oxide and the fused silica. The fact that the silicon is crystalline would be expected to have an influence on the structure of the oxide. It had been found that fused silica which had been formed by melting quartz crystals still retained some residual "channels" from the crystals[12]. It is reasonable to expect the oxide, which was never molten, to reflect some of the crystalline character of the silicon substrate. Indeed, a microchannel structure, possibly microcrystalline in nature, seems to exist in the oxide and is de-

pendent on the surface of the silicon before oxidation. This will be discussed more fully in Section 2.3c.

Finally, the oxide film is very thin (about 0.5 micron) relative to the fused silica samples. Therefore, it is reasonable to expect that the interfaces will have a much greater influence on diffusion processes in the oxide than in the bulk silica samples. This is especially significant in view of the observation of Drury and Roberts[7] that approximately the first micron on the surface of their samples diffused at 700° to 1200°C, contained an anomalously high amount of tritium tracer.

1.3b Previous Experiments with Water in Oxide Film

Investigations have indicated that water is a serious contaminant in oxide-passivated silicon devices. Kuper and Nicollian[18], for example, found that exposure of an oxidized junction to water vapor at atmospheric pressure and temperatures as low as 400°C for short periods (order of an hour) gave changes in reverse leakage of the diodes by several orders of magnitude and changes in capacitance of the junctions. Hydrogen gas gave the same sort of instabilities though other gases did not (this agrees well with the hydrogen-water-silica equilibrium found by Bell, Hetherington, and Jack[10]. Hydrations were reversible, and etch-off experiments indicated that the water species causing the instability was within 600Å of the silicon interface.

Nicollian and Goetzberger[19] correlated dielectric loss in an MOS capacitor with the density of fast interface states in the sample. They found that heat treatments between 200° and 400°C in a dry ambient increased the number of states and that treatments in a wet ambient decreased the number of states. Kooi[20] reported similar results.

Gray and Brown[21] correlated interface state density with the shift between room-temperature and liquid-nitrogen-temperature capacitance-voltage curves on a sample. They found[22] that interface state density was related to the amount of water in the ambient during oxidation of the silicon. Oxidations in drier oxygen or post-oxidation bakes in dry ambient (which presumably removed water from oxide) gave increased interface-stage densities.

Hofstein[23] concluded from his measurements that instabilities in oxide-passivated MOS devices were almost entirely the result of water contamination in the oxide. He concluded from electrical measurements that the instabilities were due to the movement of positive ions. The mobility of the ions, determined in an electrical drift measurement, indicated that the mobile species was the H^+ ion.

Ligenza and Spitzer[24, 25] studied the exchange of oxygen between O^{16}-oxide and O^{18}-enriched water, and vice versa.

Diffusions were done at high temperature and pressure, and exchanges were on the order of 30 or 40%. They found oxygen profiles by successive etching and remeasurement of the IR absorption of their samples. The absorption wavelength of the Si-O bond is slightly longer for O^{18} than for O^{16}. They found a fairly flat oxygen profile rather than the normal diffusion profile. Lee[11] has attributed this to the extreme conditions of temperature and pressure under which the diffusions were done and times which were long compared with normal diffusion times under such conditions.

Burkhardt[26] and Burgess and Fowkes[27] have reported studies of oxides grown in tritiated steam at 1000°C. Their profiles were peaked at the interfaces and fairly flat in the bulk of the oxide. Both of these investigators tried to drift the hydrogen in an electric field with no consequent redistribution of tritium.

Hofstein[28], on the other hand, has recently presented tritium tracer data which shows tritium redistribution under bias-temperature stress. Hofstein, however, introduced tritiated water into an already-grown oxide by boiling it in tritiated water for a few minutes. The obvious conclusion is that the water is incorporated differently into the oxide at high temperatures (oxidation) than at low temperature. This may be related to the earlier observation of two types of hydroxyl in silica glass.

1.3c Evidence for Micropore Structure in Oxide

As mentioned in Section 2.3a, there is evidence of micropore structure in a thermally grown oxide film.

Ing, Morrison and Sandor[29], working with stripped films, found that permeation rates were orders higher than expected for silica. They attributed this to pores in the oxide. Electron micrographs of the oxides showed no pores, however, to a resolution of 50 Å. It was concluded that pores were no larger than a few atomic diameters in size.

They found that the extent of porosity was correlated with the cleanliness of the silicon surface before oxidation. Poorer preoxidation cleaning led to a greater porosity in the film. Foreign particles on the silicon tended to cause crystallites at the surface of the oxide. Revesz[15] has also noted that imperfections in the silicon surface tend to produce crystallites in the oxide surface. D'Asaro[30] noted that sodium tends to cause crystallization in an oxide film. It has been observed that sodium always peaks at the air interface of the oxide[31]. Thus, the incidence of crystallites and, hence, the degree of porosity would tend to be greater at the surface of the oxide.

Lopez[32] has produced further evidence for a porous structure in the oxide. Etching experiments indicated the presence of fast-etching regions, assumed to be pores or incipient pores. Phosphorus diffusion through the oxide was also much faster than expected,

and indicated a pore structure. Dielectric breakdown was found to be localized in certain spots. Revesz[15] has similarly found conduction in the oxide to be localized.

Hofstein[28] has reported anomalously fast sodium and water diffusion through an oxide film at a temperature of 100° C. He attributed the fast diffusion to structural tunnels in the oxide.

It has been observed in sodium radiotracer experiments that sodium precipitated in regions of low dielectric strength[33]. Also, the high surface concentration of sodium at the oxide surface after a sodium diffusion could be lowered by an acid soak[31], possibly indicating that part of the sodium at the surface was residing in pores and could be leached by the acid.

Revesz and Zaininger[34] have suggested that the large linear region on the oxidation rate curve for silicon can be attributed to diffusion of oxidant through structural tunnels. They have presented a discussion of channel formation in the oxide. The formation of channels is associatec with a nonrandom distribution of bond angles or bond lengths in a certain preferred direction.

1.4 Previous Work on Sodium Diffusion and Water-Sodium Interaction

It has been known for several years that sodium and other alkali ions are involved in instability mechanisms in oxide-passivated

devices. The relationship between sodium and electrical instability was demonstrated by Snow, etal. Bias-temperature tests with MOS capacitors indicated instabilities in sodium-contaminated devices but not in uncontaminated controls.

Yon, Ko and Kuper[31], using a combination of neutron activation analysis and radiotracer, traced actual sodium levels in contaminated and uncontaminated samples. Amounts of sodium inferred from electrical measurements were found to be well correlated with amounts measured radiochemically. Movement of sodium was traced under a variety of diffusion and drift conditions.

A number of examples of interaction between water and sodium in silica can be found in the literature. A recent investigation by Burgess, et al[35] indicated that sodium was transported through an oxide film on silicon to a greater extent when the diffusion was done in a wet ambient than when it was done in a dry ambient. After the wet diffusion sodium was found to be more peaked at the silicon interface.

It seems also that the presence of sodium increases water transport in the oxide. Revesz and Zaininger[34] found that sodium contamination increased oxidation rates in steam oxidation of silicon. Since water is the oxidant in a steam oxidation, the sodium contamination had the effect of increasing water transport in the growing oxide.

Hofstein[28], working with sodium and tritium tracers, found that sodium could cause the release of a proton from absorbed surface water. Aluminum, like sodium, can also affect the drift of protons. Garino Canina and Priqueler[36] found that protons could be drifted in fused silica in an electric field only if alumina were present in the silica.

A discussion of glass corrosion by Charles[37] could help elucidate sodium-water interactions in diffusion. It was found that fused silica containing sodium end groups corroded in water vapor at a much greater rate than did pure silica. Charles proposed a set of reactions to explain this behavior.

The sodium end group first reacts with a water molecule by the reaction.

$$\left[\begin{array}{c} | \\ -\mathrm{Si}- \\ | \end{array}\mathrm{O}\text{-}\mathrm{Na}\right] + \mathrm{H_2O} \rightarrow \begin{array}{c} | \\ -\mathrm{SiOH} \\ | \end{array} + \mathrm{Na^+} + \mathrm{OH^-} \qquad (2\text{-}1)$$

The hydroxyl released in reaction (2-1) then reacts with an oxygen bridge to form a silanol and a reactive oxygen end structure by the reaction

$$\left[\begin{array}{c} | \\ -\mathrm{Si}- \\ | \end{array}\mathrm{O}\text{-}\mathrm{Si}\text{-}\right] + \mathrm{OH^-} \rightarrow \begin{array}{c} | \\ \mathrm{SiOH} \\ | \end{array} + \begin{array}{c} | \\ -\mathrm{Si}- \\ | \end{array}\mathrm{O}\text{-} \qquad (2\text{-}2)$$

Another water molecule then reacts with the reactive oxygen to form another silanol by the reaction

$$\left[\begin{array}{c}\\ -\mathrm{Si}-\mathrm{O}-\\ \\ \end{array}\right] + H_2O \rightarrow \begin{array}{c}\\ -\mathrm{SiOH}\\ \\ \end{array} + OH^- \qquad (2\text{-}3)$$

This set of reactions has several consequences. First, the reactions produce excess hydroxyl which raises the pH of the glass and hence the corrosion rate, i. e. the reaction catalyzes itself. Second, the reactions convert oxygen bridges to pairs of silanol groups; this gives a more open structure to the glass[9] and would be expected to increase diffusion rates of both water and sodium. Third, the reactions release the sodium from the glass structure, which should make the sodium more mobile.

1.5 Oxygen Analysis Technique

It would be desirable to find distributions within the oxide of both hydrogen and oxygen from diffused water. This could help elucidate diffusion mechanism and diffusing species.

In such a measurement it is necessary to determine oxygen in an oxide matrix, i. e. to differentiate between the oxygen used in growing the oxide and that carried in by the diffusing water. It is obvious that different isotopes must be used for the two types of oxygen. Unlike the case of hydrogen, no suitable radioactive isotope is available to tag the oxygen of diffusing water. The longest-lived

radioisotope, O^{15}, has a half-life of only 124 seconds, unsuitable as a diffusion tracer.

Since no suitable radioactive isotope is available, it is necessary to use a stable oxygen isotope to tag the water. The oxide is grown in ordinary oxygen (primarily O^{16}) so that either O^{17} or O^{18} may be used to tag the water. The problem, then, is to find a technique for determining O^{17} or O^{18} in the presence of O^{16} to a sensitivity of $\sim 10^{12}$ atoms or $\sim 10^{18}$ atoms/cc. A further complication is the amount of O^{17} or O^{18} normally in the oxide. This problem is discussed in Section 4.2.

There are several ways to determine either O^{18} or O^{17}. Ligenza and Spitzer[24, 25] traced O^{18} by the shift of an IR absorption peak. This technique will detect O^{18} in concentrations much less than 10%. In principle, this method could also be used with O^{17}, but sensitivity would be even lower than with O^{18}.

It is also possible to determine O^{17} in the presence of O^{16} and O^{18} by nuclear magnetic resonance, since only O^{17} has a net nuclear moment. However, according to Evans[38], the required sample size is on the order of 10^{18} atoms, which is orders of magnitude too insensitive.

A mass spectrometer technique is also capable of separating the oxygen isotopes. However, in this case the sample must be put into a form compatible with the spectrometer inlet system and must

be sectioned dry. It cannot be etched in a conventional manner, since the etch solution would contain several orders of magnitude more O^{17} or O^{18} than the sample would be expected to contain. Thus, etching would completely lose the desired information. The method is also destructive.

A number of nuclear methods have been proposed for determining O^{18} or O^{17}. An O^{18} determination technique proposed by Conditt and Holt[39] uses radioactivation by the reaction $O^{18}(p,n)F^{18}$ followed by sectioning and counting of F^{18}. Accelerator protons at 2.7 MeV were used. Hunt and Miller[40] used recoil protons from an (n,p) reaction in polyethylene as a proton source for this reaction with a reactor as a fast neutron source. They found, however, that reproducibility was poor.

A particularly interesting O^{18}-determination technique was described by Choudhury, et al.[41]. In this technique, a beam of monoenergetic protons is allowed to impinge on the surface of the sample, at a known angle. The protons produce alphas by the reaction $O^{18}(p,\alpha)N^{15}$, and the alphas are detected at a known angle to the surface and their energy distribution analyzed. Alpha energy distribution can be uniquely related to the depth distribution of O^{18} in the oxide. With a suitable standard, the measurement can be made quantitative.

Amsel and Samuel[42] have reported using this method to determine O^{18} tracer in anodically-grown Al_2O_3 films on aluminum. Palmer[43] used the technique to study diffusion of oxygen in quartz crystals.

A similar method, with an O^{17} tracer, has been reported by Ollerhead, Almqvist, and Kuehner[44]. In this case, a beam of ~5 MeV He^3 ions was used, and a (He^3, α) reaction took place. Again, the alpha spectrum could be uniquely related to the O^{17} depth profile. This method seems to offer no advantage over the O^{18} tracer method. This technique requires a more expensive isotope and requires the use of a very expensive accelerator; furthermore, the resolution is poorer than with the O^{18} method, according to the authors.

The most promising of these techniques, then, appears to be the $O^{18}(p, \alpha)N^{15}$ reaction of Choudhury, et al. Equipment to carry out oxygen counting by this technique was assembled, but no further work was performed using this technique.

2. Water Diffusion Experiment

2.1. Sample Preparation

Silicon substrates used for this investigation were either 1 or 10 ohm-cm, n-type, 111 orientation. The wafers were obtained from Semimetals, Inc., already lapped and polished. The wafers were one-inch diameter and about 8-mils thick.

Wafers were cleaned before oxidation by degreasing in hot, electronic-grade trichloroethylene and then rinsing in a stream of deionized distilled water (2-4 megohm-cm resistivity). The samples were then dried with a vacuum pencil and placed directly into the oxidation furnace.

The oxidations were done in a resistance-heated furnace with a quartz tube. Samples were oxidized on a quartz boat at 1200°C. The oxidizing ambient was oxygen which had been bubbled through deionized distilled water at 95°C. Oxygen flow rate was 1.15 liters per minute. Oxides were grown to a thickness of approximately 5400 Å.

After oxidation the furnace temperature was dropped to 1000°C, and a dry nitrogen ambient was introduced. The samples were then baked for 30 minutes in this ambient. After the bake, the samples were cooled in the furnace ambient at the mouth of the furnace tube before removing the wafers from the boat.

2.2 Low-Temperature Water Diffusion Technique

Water was diffused in the oxide films by holding the sample at a known temperature for a known length of time in an ambient of pure water vapor at a known pressure. Each of the three diffusion parameters--temperature, time, and water vapor pressure--were independently varied in order to find the dependence of the diffusion on each of the parameters.

Out-diffusion measurements were made in order to test how firmly the 'water' was bound into the oxide. Also, as-grown oxides, which contained large concentrations of water, were diffused in order to find the effect on the diffusion of the water present in the oxide from the oxidation process. Multiple samples were run for several diffusion conditions to test reproducibility.

Diffusions were done at temperatures ranging from 50 to 250°C, times ranging from 15 minutes to 8 hours, and water pressures ranging from 25 to 400 mm of mercury.

A diagram of the apparatus used in these experiments is shown in Figure 1. The apparatus, with the exception of the diffusion cell, was built of stainless steel. The water was held in a small stainless-steel vial which was hard-soldered to the end of a tube. The tubing system was assembled with Swagelok tubing connectors. The valves were Nupro bellows-sealed valves. The tubing at the cell end of the apparatus was welded to a stainless steel flange; a Viton O-ring was used to seal the flange to the diffusion cell.

The diffusion cell itself was a cylindrical piece of aluminum into which three slots have been milled. The samples to be hydrated were dropped into these slots and held tightly against the aluminum by means of Teflon strips at the edges of the wafers. Aluminum was used for the cell because of its good thermal conductivity.

Before final assembly of the hydration apparatus, all components were thoroughly cleaned with electronic-grade trichloroethylene and acetone and with deionized distilled water. After assembly the system was checked for tightness with a helium leak-checker; the leak rate was too small to be detectable ($<10^{-10}$ cc/sec).

A different cell was used in some of the earlier diffusions, but hydration profiles for the two cells agreed within experimental errors of ~20%.

The sample cell was maintained at temperature by means of a small oven, made up of a hot-plate heating element and a ceramic enclosure. A chromel-alumel thermocouple in the base of the cell measured cell temperature; a reference thermocouple was kept in a Dewar of ice water. The thermocouple output was monitored by a 10-mv Brown recorder which had been provided with a pair of contacts--one on the pen carriage and another which could be moved along the recorder scale. These contacts were used in conjunction with an electronic relay to control power to the cell heater. The controller operated in a simple on-off mode, but temperature control was within 0.5°C. Thermocouple outputs beyond the 10 mv range of the recorder were measured by providing a bucking potential for the thermocouple.

The thermocouple-controller combination was calibrated against a thermometer and water bath at low temperatures and against

several known melting points at higher temperatures. The calibration curve agreed with NBS calibration values for a chromel-alumel thermocouple.

A second thermocouple was temporarily placed near the top of the cell in a place normally occupied by one of the samples in order to check how well the monitor thermocouple in the base of the cell measured the actual sample temperature. It was found that the sample temperature lagged the temperature of the monitor thermocouple by several degrees during heat-up or cool-down, but the two thermocouples agreed within $< 0.2^{\circ}C$ after a minute or two at any temperature.

Heat-up time was longer for higher diffusion temperatures, but was always on the order of several minutes. No water vapor was admitted to the diffusion cell, however, until the cell was at diffusion temperature, so the long heat-up time caused no timing inaccuracy.

Cool-down times were much shorter than heat-up times. By immersing the cell in a beaker of cold water, it could be cooled from $200^{\circ}C$ to $50^{\circ}C$ in a few seconds. Thus, measured diffusion times were accurate within a few seconds.

Water vapor pressures were established by adjusting the temperature of the water source vial. Standard water vapor pressure-temperature tables were used to pick the temperature corresponding to the desired vapor pressure. In order to ensure that the vapor

pressure in the apparatus was properly correlated with the source temperature, the tubing and valves were wrapped with a heating tape and kept at a temperature well above the source temperature to prevent condensation. A sufficiently large quantity of water was used in the source so that there was always liquid in the vial.

Since the source vial was fixed in place and could not be moved into and out of a water bath, an apparatus was constructed as a movable thermostat for the source vial. This consisted of a Dewar flask, outfitted as shown in Figure 1. The Dewar was connected to a Lauda model K-2 constant temperature circulator and effectively acted as a moveable extension for the circulator bath.

With this arrangement, temperature was found to be within about 0.2°C of the circulator bath temperature. Actual bath temperature was controlled within 0.1°C. This temperature error corresponds to an error in vapor pressure of less than 1% over the range of vapor pressure which were used in this study.

Samples to be hydrated were cleaned by degreasing in hot trichloroethylene and then rinsing several times in deionized distilled water. The samples were then placed in the hydration cell as previously described.

The heating tape on the apparatus tubing and the constant temperature circulator were brought to temperature. The source vial was then cooled in liquid nitrogen to lower the water vapor pressure.

The entire apparatus was then evacuated with a mechanical pump. After pumping for at least 15 minutes, the source valve (valve 1 in Figure 1) was closed and the source thermostat assembly substituted for the liquid nitrogen. The oven was then placed around the hydration cell and the cell brought to diffusion temperature. The valve to the vacuum line (valve 2) was then closed and the source valve opened to allow water vapor to fill the entire system.

Diffusion timing was started when the source valve was opened. It was calculated that at a fore-pump vacuum (a few microns pressure) it would take no more than a few seconds for the water vapor pressure in the cell to equal the vapor pressure at the water source. This was also checked experimentally. A glass plate was temporarily put in place of the diffusion cell and the apparatus evacuated. When the source valve was opened, water began immediately condensing on the glass plate.

At the end of the diffusion time, the oven was removed from the hydration cell and the cell quickly cooled. When the cell had been cooled to a few degrees above the source temperature, the source vial was again immersed in liquid nitrogen to condense the water vapor back into the source vial. The source valve was then closed, the cell cooled to room temperature, the apparatus brought to atmospheric pressure, and the samples removed.

2.3. Hydrogen Tracing Techniques

Two methods have been used for tracing water in silica---infrared absorption by Si-OH groups in the silica and tritium tagging of the hydrogen. The tritium tracer is a much more sensitive technique and has been used in this study. The water source vial contained 0.5 cc of tritiated water with a specific activity of about 200 millicuries per gram.

The choice was then made on the method of developing a profile of tritium in the oxide. In sectioning the oxide, either the removed section or the oxide remaining on the wafer could be counted after each section is removed. The wafer counting technique would give a somewhat higher counting efficiency, but the technique is complicated by the fact that the range of the tritium betas is several times larger than the 5000 Å thickness of the oxide. Thus, betas would simultaneously be counted from all depths in the oxide.

The thinness of the oxide and of the removed sections, consequently, make it difficult to obtain a true differential tritium profile from the integral profile for several reasons: (1) It is necessary to determine relatively small changes in relatively large count rates. (2) A peak can be easily overlooked in an integral distribution curve. (3) The beta spectrum is changing as it penetrates the oxide. This gives changing absorption properties with distance in the oxide. The

problem is even more serious in the vicinity of the silicon interface, where back-scatter of betas from the silicon substrate contributes a further distortion to the beta spectrum and to the number of betas. It was, therefore, decided to count the removed sections.

The sectioning technique chosen was hydrofluoric acid etching. This method has the disadvantage of producing a relatively large sample to be assayed (about 2 cc's), but the advantages are considerable: (1) It is fast. (2) Removed sections are immediately available for tritium assay. (3) Sections of any desired thickness can be removed accurately, reproducibly, and in a planar fashion.

Once it was determined that the tritium to be assayed would be contained in about two cc's of solution, the most reasonable counting technique was liquid scintillation counting. All other counting systems suffer either from large beta self-absorption in the sample or from severely restricted sample size. In either case, counting efficiency is poor.

Liquid scintillation counting has a number of advantages as a counting technique: (1) The active material is in intimate contact with the detector, even for large samples. This avoids any absorption between the sample and the detector. (2) The counting is done in a 4-pi geometry, i. e. all sample betas are emitted into the detector. (3) The scintillation technique allows a large fraction of the background counts to be rejected on the basis of pulse height selection.

It was necessary to etch the samples in the smallest possible quantity of acid because liquid scintillation counting efficiency is adversely affected by large quantities of aqueous material in the solution. Consequently, an apparatus was constructed to allow etching the sample with minimal quantities of acid and rinse water. The apparatus consisted of a polystyrene cylinder with a depression on top of it to retain the sample. A Teflon top, which screwed down on top of the sample, had a vertical hole which exposed 2.85 cm^2 in the center of the sample to be etched. This, in effect, formed a small Teflon beaker with the sample forming the bottom of the beaker.

Acid and rinse water were alternately put onto the sample with syringes. After etching or rinsing, the acid or water was drawn into a counting vial by vacuum. This was done by placing the counting vial into a suction flask and sucking the acid or water through a small Teflon tube from the sample to the vial.

Etch timing was started when acid was put onto the sample and stopped when the acid was removed and rinse water put onto the sample. Timing was accurate to about one second, which gave about a 3% uncertainty in the shortest etch times (30 seconds).

It was found that etching could easily be done with 0.5 cc of acid, and the rinse with one cc of water. The rinse water was added and removed in three or four smaller aliquots to increase rinse

efficiency. Acid and rinse water were combined in the same counting vial to give a total sample of 1.5 cc of aqueous material.

Several checks were made on the quantitativeness of the transfer from the sample to the counting vial. A second rinse was given to samples in some cases and the rinse counted to check for activity left behind by the first rinse. No activity was found in these rinses. In another test, tritium-tagged acid was pipetted onto a sample which contained no tritium. The acid was transferred and the sample rinsed in the usual manner. It was found that transferred activity matched the activity of the same quantity of acid pipetted directly into a counting vial, within pipetting and counting errors of less than 5%.

Originally, it was intended to use the Teflon top of the etching apparatus as an etching mask for the sample. It was found, however, that acid sometimes leaked under the Teflon and etched some of the oxide which should have been masked. This problem was solved by sealing the edge of the mask with Apiezon wax. The wax was applied with a small brush from a trichloroethylene solution. With this seal there was always a sharp interface between bare silicon and oxide of the originial thickness when the sample was removed from the apparatus.

Since the oxide around the edges was only masked and was not removed, it could possibly still have been a source of error. The

acid etched sideways under the mask at the same rate as it etched downward toward the silicon, and the side etching was a source of additional activity. It was calculated, however, that this constituted less than 1% additional activity in any section. This was also shown experimentally by the fact that profiles were not changed when the extra oxide was removed before sectioning.

Etching with this apparatus had several advantages: (1) Total etch-rinse volume was small. (2) Only an area in the center of the wafer front was sectioned, without the necessity of masking and removing unwanted oxide before beginning the sectioning. (3) The sample area was constant and well defined. (4) Etch timing was precise. (5) The vacuum removal of acid and rinse left the sample surface dry. This allowed a quick check of oxide interference color against the etch time.

In any scintillation counting technique, the radiation to be detected is converted into visible light photons in some suitable medium. The light photons are monitored by a photomultiplier tube which is coupled to an appropriate amplifier, pulse height analyzer, and counting circuitry.

The radiation-to-light transducer and the photomultiplier are linear devices. The output pulses from the amplifier bear a functional (usually linear) relation to the input pulses from the photomultiplier.

Thus, the pulse height analyzer can select an interval of pulse sizes corresponding to a certain energy interval in the input radiation spectrum. The pulse height analyzer, thus, allows one to reject background pulses outside of this energy interval without reducing counting efficiency.

The most common transducer in scintillation counting is a crystal of some scintillating material. Such a transducer gives high counting efficiency for penetrating radiation such as gamma rays and high-energy beta particles. However, for the low energy beta particles of tritium (17.6 KeV maximum energy), the crystal has disadvantages. Most betas will probably be absorbed in getting out of the source and into the detector. Furthermore, only a fraction of the particles will be emitted in the direction of the detector.

The liquid scintillation technique overcomes these problems by mixing the sample with the scintillating medium in a suitable vial. The scintillating medium in this case is a phosphor dissolved in some suitable solvent. The sample to be assayed is dissolved in, emulsified with, or suspended in the scintillating medium.

The energy transfer process occurs in several steps. The beta particle interacts with the solvent molecules, the solvent molecules interact with phosphor molecules, and the phosphor molecules finally emit visible photons. The photons must then be brought out

of the counting vial and into the photomultiplier. Energy may be lost in any of these steps. The loss mechanisms collectively are referred to as "quenching".

Water, unfortunately, is a strong quenching agent. The problem of assaying aqueous samples is further compounded by the fact that water-miscible solvents are quite inefficient. For example, the popular dioxane naphthalene-PPO-POPOP mixture gave only about 5 or 6% counting efficiency with the etch samples.

Hayes and his coworkers made an extensive study of solvents and phosphors for liquid scintillation counting. They found that the most efficient solvent is xylene[45] and that PBD is the most efficient phosphor[46]. Unlike most liquid scintillation phosphors, PBD works most efficiently without a secondary phosphor, or wavelength shifter.[47] Optimum concentration was found to be 10 grams of PBD per liter of xylene[46].

The problem of developing an efficient counting solution then became the problem of developing a stable mixture of xylene and water. One method which had been suggested by Patterson and Greene[48] was an emulsion of xylene and water. They stabilized their emulsions with a detergent called Triton X-100 (Rohm and Haas) and reported about 10% tritium counting efficiency for solutions which were up to 23% aqueous. This technique was tried, and results were comparable to those of Patterson and Greene for tritiated water.

However, tritiated HF gave nonreproducible counting efficiencies, even after the acid had been neutralized.

Another solubilizing agent was found, however, which gave satisfactory results. This was Colosolve CS-3 (now marketed by Beckman as Biosolve BS-3). The solubilizer formed a clear, stable solution with the aqueous component and the xylene-PBD scintillating mixture. Several hundred different samples were tested with various ratios of components. Also, since it was found that the unneutralized acid caused solution instability, different HF concentrations and various neutralizing agents were tested.

The solution finally chosen was a compromise between cost and counting efficiency. Slight increases in efficiency could be obtained by using greater phosphor concentration or by using purer xylene, but it was felt that the slight increase in efficiency did not justify the extra cost. The final mixture was as follows: 1.5 cc of sample (0.5 cc of 15:1 HF and 1cc of water) neutralized with an excess of calcium carbonate, 3 cc of CS-3, and 15 cc of technical grade xylene containing PBD at a concentration of 10 grams per liter.

This solution gave counting efficiency of about 25% with background of about 25 counts per minute. This allows the determination of 2×10^{17} hydrogen atoms per cc in 1000 Å of oxide to a one-sigma confidence level of 10% in a one-hour count. The count rate of a

sample was found to be stable within counting statistics for at least a period of several days.

Most of the tritium counting in this study was done with a Picker Ansitron 11 liquid scintillation counter.

2.4 Data Handling

A standard (15:1 HF containing a known amount of tritium) and a blank were counted with each batch of liquid scintillation samples. The standard and the blank were made up at the same time as the samples to be counted. The tritiated water used in making up the acid standard was obtained from Tracerlab, Inc., and its specific activity was specified within three percent.

In cases where water rinses were counted, a second standard usually was made up with tagged water. The counting efficiency for the water was usually one or two percent higher than for the neutralized acid.

The standards and the blank usually were counted both before and after counting the other samples in order to insure that counting efficiency and background were not changing during the counting run.

The count on the standard sample was used to determine the counting efficiency for each batch of samples. This technique allowed elimination of errors caused by long-term drift of the liquid scintillation counter and by slightly different formulations of the counting

solution. The efficiency was found to constant from one batch of samples to another.

Etch rate for each sample was calculated by dividing oxide thickness by total etch time. Etch rates were constant from sample to sample in the absence of room temperature changes. Section thicknesses were calculated from etch times, with oxide interference colors as a check. The section area was the area exposed by the etching mask.

A computer program was written to reduce the hydration data. The program calculated an efficiency and background rate and calculated an absolute disintegration rate for each counting sample. The disintegration rate then was converted into a number of hydrogen atoms.

The section volume was calculated and hydrogen concentration was calculated. A statistical error on the counting was then computed. This counting error was converted to equivalent error in hydrogen concentration in the section. Long enough counts were usually taken to keep count errors below 5%.

The program output the information on section thicknesses, concentrations, and errors. Information on rinses was tabulated separately. The program then computed total amounts of hydrogen in the oxide and on the surface. Finally, a rough semilog plot of

the profile was printed to allow a look at the profiles before hand-plotting.

Although it was desired to follow the diffusion of 'water', the tritium tracer does not of necessity follow water, even though that was the chemical form to which the oxide was exposed. All that can really be said with certainty is that the tracer was following hydrogen. The tracer technique is incapable of differentiating H_2O from H_2, Si-OH, H^+ or any of the other chemical forms that hydrogen could take in the oxide.

A second limitation concerns the "isotope effect" associated with any tracer experiment. Since the tracer atom has a different atomic mass from the stable atom which it is tracing, it will also diffuse at a different rate; the ratio of diffusion rates will be inversely proportional to the square root of the mass ratio of the two atoms.

This effect has been ignored in this work for two reasons. First, the amount of isotope effect cannot be calculated unless the diffusing species is known. The effect would be rather small for a diffusing water molecule ($\sqrt{20/18}$) but would be large for a hydrogen ion ($\sqrt{3}$).

Second, the isotope effect makes the conclusions of this work somewhat more conservative. As discusses in the remainder of this chapter, the tritium was found to diffuse much faster than expected. Normal hydrogen, of course, diffuses faster still.

2.5 Results of the Hydrations

As mentioned previously, hydration profiles were produced for a variety of hydration conditions. A typical profile is shown in Figure 2. Thicknesses of etched sections are shown by the dashed lines at the bottom of the graph, and counting errors are shown by vertical error bars on the data points. Concentration equivalent of background is shown by the dashed line in Figure 2.

The profile is characterized by three regions: (1) a sharp gradient of hydrogen at the air interface; (2) a relatively flat hydrogen profile in the bulk of the oxide; (3) a slight hydrogen build-up at the silicon interface. The sharp hydrogen spike at the air interface is present in all the hydrogen profiles, the hydrogen peak at the silicon interface in some.

Profiles were found to be reproducible from one sample to another under most hydration conditions. The reproducibility of the data is illustrated in Figure 3. These four samples were hydrated simultaneously in the hydration cell. The results show that the data is consistent to within 20%

Hydrations were done at 200°C and 25 mm Hg water vapor pressure for times ranging from 0.25 to 8 hours. The family of profiles thus obtained are shown in Figure 4 and 5.

The profiles are roughly exponential in the bulk oxide and are

thus approximated by the dashed lines in Figure 4. Profiles in bulk oxide tend to fill and flatten with increasing hydration time.

The only hydration data available for comparison are those of Hofstein. He found hydrogen throughout the oxides at concentrations of $\sim 10^{18}$/cc after soaking his samples for 15 minutes in tritiated water at 100°C.

The profiles correspond to a very fast penetration. Extrapolation of bulk silica hydration from 600°C [6] would yield a diffusion length of ~1000 Å for one hour at 200°C, whereas the 'water' completely penetrates the 5400 Å oxide in less time than this at 200° C. Also, the profile is not the complementary error function expected for a constant-concentration boundary condition. (A calculated error function profile for a one-hour diffusion is shown in Figure 4 for comparison).

Rather, the data are consistent with the grain-boundary diffusion model of Fisher[50] and are analyzed on this basis in a following section. This type of diffusion path would be expected to be most noticeable at low temperatures where bulk diffusion is quite slow.

Profiles for 15-min hydrations are very nonreproducible and frequently show anomalous peaking near the silicon. Three 15-minute profiles are shown in Figure 5. Profiles are somewhat more reproducible for 30-minute hydrations and are very reproducible for

hydration times of an hour or more, as was demonstrated in Figure 3. The anomalous peaking is also observed for low hydration temperature and will be discussed further.

Total oxide hydrogen content is shown as a function of hydration time in Figure 6. The graph shows an initial rapid penetration which corresponds to the anomalous peaking. Then the amount of oxide hydrogen appears to drop, which would imply that a net amount of hydrogen out-diffused between 15 and 30 minutes in the hydration. However, there is a great deal of scatter in the oxide hydrogen content after 15- or 30-minute hydrations and the apparent decrease in hydrogen content of the oxide may be an experimental error. In any case, the initial nonreproducible peaking suggests that the 'water' is interacting with an oxide defect structure which quickly saturates.

The dashed theory curve in Figure 6 is the behavior predicted by the micropore diffusion model discussed later.

Hydrations were done for 2 hours at 25 mm pressure for hydration temperatures between 50° and 250°C. The set of profiles from these hydrations are shown in Figure 7.

The effect of varying hydration temperature is similar to the effect of varying hydration time. Low temperature gave anomalous peaking which disappeared at higher temperatures just as in the case of time variation. Increasing temperature, similarly, gave filling

and flattening of profiles in the bulk oxide.

The 50°C profile shows a large peak as did the 15-minute hydrations profiles. In the 100°C profile, the peak is much smaller, and for hydration temperatures of 150°C and higher, the peak is absent.

It would appear, therefore, that there is a very rapid buildup of hydrogen in the region a short distance back from the silicon. It is interesting to recall that Burkhardt[26], on the basis of tritiated-steam oxidations, hypothesized a reaction intermediate 600-800 Å from the silicon. It is possible that this region is oxygen deficient and that water initially reacts in this region to compensate the oxygen deficiency.

The loss of the peak at higher temperature or longer time would then correspond to an oxidation in this region followed by a diffusion of hydrogen gas out of the oxide. It is important to bear in mind that the tritium tracer in no way differentiates the various chemical forms in which the hydrogen may exist in the oxide. The postulated water-hydrogen-silica reaction has been observed in bulk silica.[19]

An activation energy was obtained for the diffusion coefficient by plotting log of total oxide hydrogen versus reciprocal temperature. The plot is shown in Figure 8. The circles correspond to integration of the solid profiles in Figure 7. The triangles correspond to

the dashed extrapolations in Figure 7, which ignore the anomalous peaking. It can be seen that ignoring the peaking causes all the points to follow an Arhennius relation.

The activation energy was estimated from the relation

$$N\alpha \sqrt{D}\, \alpha e^{-E_a/2kT}$$

where N is the total hydrogen content of the oxide, D is the diffusion coefficient, E_a is the activation energy, k is Boltzmann's constant, and T is the temperature. This relationship would be correct for an error function profile and is assumed to roughly correct for these profiles. This method estimated an activation energy of about 0.25 eV.

The activation energy may similarly be estimated by measuring the advance of the diffusion profile at a constant concentration level as a function of diffusion temperature at constant diffusion time. In this case

$$x\alpha \sqrt{D}\, \alpha e^{-E_a/2kT}$$

where x is the distance at which the profile crosses the given concentration level (3×10^{18}/cc was used). This method gives an activation energy of about 0.3 eV in agreement with the other method of estimation.

The estimated activation energy is very low compared with activation energies order 1 eV[26] normally quoted either for

hydration of bulk silica or for outdiffusion of hydrogen from steam-grown oxides. This low activation energy supports the micropore diffusion mechanism.

A set of hydrations were done for four hours at 200°C with water vapor pressures from 25 to 400 mm Hg. The family of profiles resulting from these hydrations are shown in Figure 9.

It can be seen that the effect of pressure increase was to shift the profile uniformly upward. All profiles have roughly the same shape.

Pressure dependence of the hydrations is shown in Figure 10. Log of total oxide hydrogen content is plotted versus log of hydration pressure. The dependence is very nearly $P^{1/2}$ which implies that the water molecules break into two parts upon entering the oxide, as is the case for high-temperature diffusion of water in bulk silica.

This observation, then, precludes the possibility of water entering and diffusing in the oxide as molecules. The water must react with the oxide in some manner to produce two fragments. It is likely that the fragments are Si-OH groups as in high-temperature water diffusions.

Profiles in Figures 4, 7, and 9 indicate that peak concentration at the air interface increases with hydration time, temperature, and pressure. The width (penetration) of the spike does not seem to change.

Approximate concentration in the oxide at the air interface was obtained by plotting concentration profiles for the first few sections on semilog paper with an expanded thickness scale and smoothly extrapolating back to zero thickness. These extrapolated surface concentrations are shown in Figure 11 as functions of t and T.

The surface concentration has the same sort of time and temperature dependences as does total oxide hydrogen. The time dependence curve shows a rapid buildup followed by a decrease followed by an increase again to a saturation. The temperature dependence shows an initial slow buildup with T which becomes faster at higher T. It is possible that the peaking of surface hydrogen concentration at small t and the weak dependence at small T may be associated with the back diffusion of hydrogen postulated previously.

Pressure dependence of interface hydrogen concentration is shown in Figure 12. The open circles represent the concentration in the oxide at the air interface; the solid circles represent the concentration at the silicon interface. It may be seen that the pressure dependence in both cases is approximately $P^{1/2}$.

The concentration at the air interface may be compared with literature values for a similar situation. The dashed line in Figure 12 represents the solubility of water (expressed as OH/cc) in fused silica at 600°C as determined by Moulson and Roberts[6]. C_o

determined from the present experiments would be expected to be near maximum solubility of water at 200°C which appears consistent with the silica solubility data.

Perhaps a more valid comparison is with Burkhardt's[26] data for steam oxidation of silicon. His C_o value is represented by the triangle in Figure 12. The agreement here is good, since solubility of water in silica[6] is probably about twice as high at 200°C as at 1000°C where Burkhardt did his oxidations.

Although the interface concentration agrees well with other data, it does not seem to be the correct C_o for the bulk oxide profiles. Figure 4, for example, indicates that the profiles are developing from $C_o \approx 6 \times 10^{18}$ (indicated by extrapolation of bulk profiles). If the C_o obtained from the surface peak were the C_o determining the bulk profiles, then the peak should penetrate several thousand angstroms from bulk diffusion for a diffusion time of several hours.

Attempts were made to remove the surface spike by various washes before sectioning. Neither an overnight soak in concentrated HCl nor an overnight wash in running water caused a decrease in surface concentration. A light surface etch followed by a water wash lowered the amount of hydrogen in the first section, but this was presumably only because the light etch removed the very high

concentration surface layer which would normally be contained in the first section.

It was thought possible that the outer 1000 A of oxide was different from the remainder of the oxide. This could, for example, be attributed to light surface damage in the silicon substrate prior to oxidation. It was considered possible that, if the first 1000 Å were etched off before hydration, no spike would form at the surface. The result of this test, in Figure 13, was contrary to such an expectation. It appears that the outer 1000 Å of oxide either has no special characteristic or else that its special characteristics are regenerated in a short time at 200° C. The same result was obtained for the same etch-off experiment before a one-hour hydration.

An outdiffusion experiment was done to further characterize the hydration mechanism. Three samples were hydrated simultaneously for four hours at 200°C and 25 mm. One of the three oxides was etched as a control. It agreed well with previously obtained profiles under the same hydration conditions. This is profile A in Figure 14.

The first 1250 Å of the second hydrated oxide was sectioned and counted. This is profile C in Figure 14. It may be seen that the surface region of this sample showed excellent agreement with the same region of the control oxide, and there is every reason to believe

that the remainder of the oxide had a rather flat profile as does the remainder of profile A.

The partially sectioned sample and the unetched third sample were then vacuum baked for four hours at 200°C. The sample which had not been etched before baking had profile B in Figure 14 after baking. Roughly half of the hydrogen content of the oxide had outdiffused, and peaking was somewhat more pronounced at both interfaces.

The amount of outdiffusion is much greater than predicted from outdiffusion measurements on tritiated-steam grown oxides.[26, 27] Extrapolation of those outdiffusion results would predict a negligible outdiffusion in a few hours at 200°C. The obvious conclusion is that the water which was diffused into the oxide at 200°C was much less firmly bound into the oxide than is water introduced by oxidation. This supports the micropore diffusion mechanism which has been postulated for these hydrations.

The sample which had a flat profile before baking had profile D after baking. The surface spike reformed during the vacuum bake, and the peak also became much greater at the silicon interface. Furthermore, the dip in the profile just inside the oxide suggests that hydrogen was preferentially segregated from this region into the surface region.

It seems then that the spike at the air interface cannot simply be the result of slow diffusion in this region, for such a mechanism could not explain the reformation of the spike from outdiffusion of a sample with a flat profile. There is obviously some difference between the interface region and the rest of the oxide which causes the 'water' to preferentially segregate near the surface. This could be either an electrical binding effect or an enhanced solubility at the surface.

Since the water seems to be completely inactive electrically, the effect would appear to be due to enhanced solubility in the surface region. In line with the pore diffusion model, this would suggest a greater porosity in the surface than in the bulk oxide.

On the basis of previous experiments it was anticipated that water diffusing through the oxide film would either act as a positively charged species and make the silicon surface more n-type or else cause annihilation of interface states. Neither of these contentions was found to be correct in the present low temperature range.

Samples were measured before and after hydration using evaporated aluminum contacts. Surface potential changes were determined by measuring voltage shift of the flat-band point on a capacitance-voltage characteristic for the sample. Interface state density was measured by the Gray-Brown technique which determines

interface state density from the difference between the flat-band voltage (V_{fb}) at room temperature and V_{fb} at liquid nitrogen temperature. Measurements were made with a Boonton model 71A one-megahertz capacitance meter equipped with an x-y recorder.

Measured interface state densities seemed to be unaffected by hydrations at 200°C or below, even with 5×10^{18} H/cc at the silicon interface. Hydration in wet nitrogen in a furnace at 800°C, however, gave significant annihilation in agreement with other investigators. Presumably 200°C for four hours at 25 mm pressure is insufficient to cause measurable interface state annihilation.

Measured values of V_{fb} indicate that the silicon surface not only does not become more n-type from a hydration, but actually becomes less n-type, as if the water were carrying in a negative charge. Measurements made with untritiated water indicate that V_{fb} shifted steadily in the positive direction as hydration proceeded, generally saturating a few volts more positive than before hydration (1 volt = 4×10^{10} charges/cm^2). Some typical data are shown in Table 1.

TABLE 1

Effect of Hydration on Flatband Voltage

0	15	30	60 min.	Conditions
7.0V	6.0	5.4	4.8	250°C, 400 mm
4.4	2.1	2.0	2.0	325°C, 300 mm
6.6	5.2	4.7	4.6	310°C, 300 mm

This behavior was observed consistently and seemed independent of the initial value of V_{fb}. Samples with initial V_{fb} from -4 to -20 volts showed a positive shift of V_{fb}.

A similar behavior was observed by Yon[33] for sodium diffusions under conditions similar to those used in this study. Such results have also been observed for sodium diffusions and for sodium-water diffusions in this study and will be discussed in the next chapter.

2.6 Models for Hydration Data

Micropore Diffusion Model

Fast penetration, low activation energy, and profile shapes observed in this study suggest that 'water' diffuses via micropores in the oxide. Evidence of this pore structure in the oxide observed by other investigators was summarized in Section 1.3c.

A micropore in an amorphous solid, as discussed by Revesz,[15] is the inverse of a dislocation line in a crystal. That is, the pore is a line of greater order in a completely disordered structure while the dislocation line is a line of less order in an ordered system. Either the pore or the dislocation line will, however, act as a region of higher diffusivity than its surroundings, and mathematical treatments of the two cases are identical.

A treatment which has been given to diffusion in grain boundaries between crystlline grains is to consider the grain boundary to be made up of a series of dislocation lines. The spacing of the dislocation lines is related to the misorientation of the two crystalline grains, a greater misorientation causing a greater density of dislocation lines.

The porous oxide, similarly, may be considered to have such lines of high diffusity channels. The treatment will then be to consider the series of channels to form a thin slab of high diffusivity material. A diagram of such an arrangement, proposed by Fisher[49] is shown in Figure 15.

Following Fisher's model, a concentration of diffusant is established on the surface ($y = 0$) of a sample. The sample has zero initial concentration. Material is then allowed to diffuse both in the bulk sample and in the high diffusivity slab. The slab is considered sufficiently thin that concentration is uniform across its width.

Diffusion far from the sample surface (far meaning far for bulk diffusion) may be considered as diffusion in the slab followed by diffusion from the slab into the surrounding bulk material. If the diffusivity in the slab is much higher than in the surrounding material, the flow out of the slab will be in the x-direction.

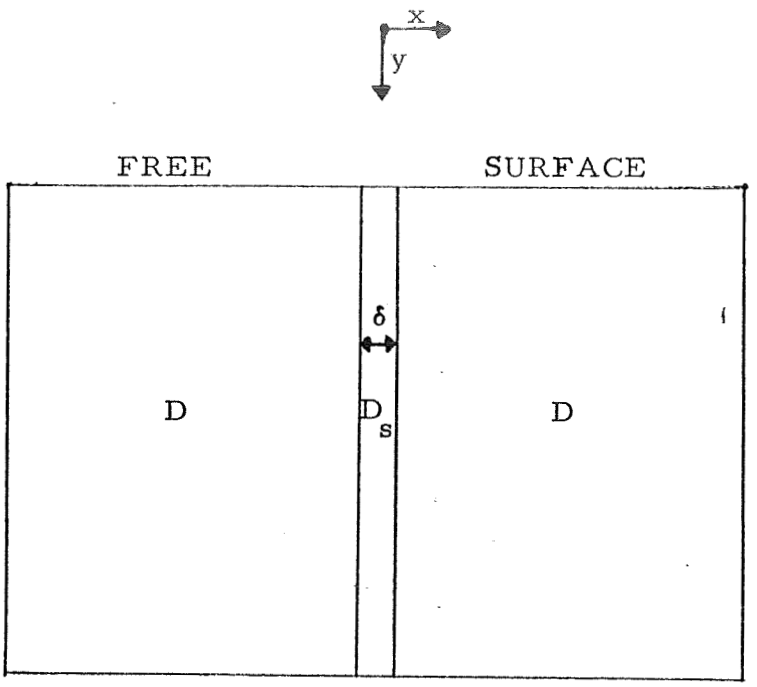

Figure 15

Coordinate System for
Micropore Diffusion Model

If a material balance is made about an element in the slab, Fick's second law gives

$$\frac{\partial C}{\partial t} = \left[D_s \frac{\partial^2 C}{\partial y^2} + \frac{2D}{\delta} \frac{\partial C}{\partial x} \right]_{x = o} \qquad (2\text{-}1)$$

where C = concentration of diffusant

D_s = diffusivity in slab

D = diffusivity in bulk material

δ = thickness of slab.

The first term represents normal diffusion into the slab; the second term represents leakage from the sides of the slab into the bulk material.

Concentration in the bulk material (away from the slab) will obey Fick's law, i. e.,

$$\frac{\partial C}{\partial t} = D\nabla^2 C \tag{2-2}$$

If Eqs. (2[1) and (2-2) are multiplied by δ^2/D and changes of variables made as follows:

$$\begin{aligned} t_1 &= \frac{Dt}{\delta^2} \\ x_1 &= \frac{x}{\delta} \\ Y_1 &= \frac{Y}{\delta(D_s/D)^{1/2}} \end{aligned} \tag{2-3}$$

then Eqs. (2-1) and (2-2) become

$$\frac{\partial C}{\partial t_1} = \left[\frac{\partial^2 C}{\partial y_1^2} + 2 \frac{\partial C}{\partial x_1} \right]_{x_1 = 0} \tag{2-4}$$

$$\frac{\partial C}{\partial t_1} = \frac{\partial^2 C}{\partial x^2} \tag{2-5}$$

The problem is to solve Eqs. (2-4) and(2-5) simultaneously. Fisher did this first by a numerical technique. On the basis of his numerical analysis he noted that the concentration in the slab built up very rapidly to its equilibrium value and could, to a good approxi-

mation, be assumed constant from $t = 0$. This approximation allowed a separation of variables and gave the concentration in the slab, Φ, as a function of y only. The concentration at any point away from the slab was then given by a solution of (2-5) with a concentration Φ at the face of the slab, i.e.

$$C(x, y, t) = \Phi(y) \operatorname{erfc}\left(\frac{x_1}{2t_1^{1/2}}\right) \tag{2-6}$$

In order to find the function Φ, (2-6) is substituted into (2-4) and the condition $\frac{\partial C}{\partial t} = 0$ imposed. This leads to the differential equation

$$\frac{d^2\Phi}{dy_1^2} - \frac{2\dot{\Phi}}{\pi^{1/2} t_1^{1/2}} = 0 \tag{2-7}$$

With the boundary condition $C = C_o$ at $y = 0$, Eq. (2-7) has the solution

$$\Phi = C_o e^{-K_1 Y_1} \tag{2-9}$$

where

$$K_1 = \frac{2^{1/2}}{(\pi t_1)^{1/4}} \tag{2-10}$$

Substituting (2-9) into (2-6) the concentration is given by

$$C = C_o e^{-K_1 Y_1} \operatorname{erfc}\left(\frac{x_1}{2t_1^{1/2}}\right) . \tag{2-11}$$

In order to see how a sectioned profile would look, the concentration in (2-11) is integrated over all x and over the thickness of a section, i.e.,

$$N = \int_{Y_1}^{Y_1+\Delta Y_1} \int_{-\infty}^{\infty} C dx_1 dy_1$$

$$= C_o \int_{Y_1}^{Y_1+\Delta Y_1} e^{-K_1 Y_1} \operatorname{erfc}\left(\frac{x_1}{2t_1^{1/2}}\right) dx_1 dy_1$$

$$N = K_2 t_1^{1/2} e^{-K_1 Y_1} \qquad (2\text{-}12)$$

where N is the amount of diffusant in the section and K_2 is a constant of proportionality.

From Eq. (2-12) it can be observed that a profile obtained by sectioning would be exponential if the pore diffusion mechanism were dominant (as opposed to $\sim e^{-x^2}$ for bulk diffusion). Such a profile, of course, would be a straight line on a semilog plot. The profiles in Figures 4 and 7 can, indeed, be well approximated by straight lines in the bulk oxide away from the interfaces.

More refined treatments of the problem[51] give a slightly stronger dependence on y ($y^{-4/3}$ or $y^{-6/5}$). This difference in dependence would probably not be seen in these profiles.

It may be further observed from Eq. (2-10) that the slope of the profiles should have a $t^{-1/4}$ dependence. The profiles in Figure

4 have been approximated by straight lines. The slopes of these lines are plotted vs $t^{-1/4}$ in Figure 16, and the slopes appear to have a $t^{-1/4}$ dependence.

According to the Fisher model, initial buildup of oxide hydrogen should be very rapid. At long times, the exponential factor in Eq. (2-12) approaches unity and the time dependence of hydrogen buildup should approach $t^{1/2}$. This behavior is represented by the dashed curve in Figure 10.

Another observation is that, in a grain boundary, only the product δD_s can be determined. Similarly, in the micropore problem, only the product of pore diffusivity and pore number can be calculated, and no estimate of pore number can be obtained except by knowing the pore diffusivity.

Bulk-Diffusion in Oxide

This interpretation assumes that extrapolation of high-temperature data underestimates the diffusion coefficient at 200°C by more than an order of magnitude. If the diffusion length were much larger than the oxide thickness, and diffusion were conventional then

$$C(Y,t) = C_o \operatorname{erfc}\left(\frac{Y}{2\sqrt{Dt}}\right) \simeq 1 - \frac{Y}{\sqrt{\pi Dt}} \simeq \exp - \frac{Y}{\sqrt{\pi Dt}}$$

and the profiles would look exponential. This interpretation is not favored because the profiles for shorter times do not show the neg-

ative curvature characteristic of the complementary error function. Also observed fast penetration anomalies at small T or t are not consistent with this model.

Another interpretation is that diffusion is conventional, but that blocking at the silicon interface causes a filling and flattening of the error function profile near the silicon. The profile still looks like an error function profile (negative curvature) for a diffusion length on the order of one-fifth of the oxide thickness (as estimated from extrapolated data for a one-hour diffusion at 200°C). The diffusion length must be of the order of oxide thickness before the profile looks exponential. As in the last interpretation, the anomalous penetration would not be explained.

3. Interaction of Water with Sodium

As explained in the last chapter, water was found to have little or no electrical effect in diffusion through the oxide, even with concentrations of 5×10^{18} hydrogen atoms/cc near the silicon. As explained in Section 1.3, however, water has been frequently implicated in instability of MOS structures. It was, therefore, considered possible that water causes instability, not directly, but by enhancing the effect of sodium in the oxide. Consequently, a study was done on interactions of sodium and water in diffusions and their associated electrical effects.

A dilute, Na^{22}-tagged NaCl solution was made upfor sample contamination. The $Na^{22}Cl$, which had been obtained carrier-free from Tracerlab, Inc., was diluted about 140. with stable NaCl and made up to 15 cc in electronic grade methanol. This gave a sodium concentration of about one PPM.

Samples were contaminated by dipping them into the solution. The methanol gave more uniform wetting and drying than a water solution. The samples were air-dried on a Teflon sheet.

The contaminated samples were then sandwiched between two bare silicon wafers as cover plates to prevent the sodium from evaporating during diffusion. The sample sandwich was placed on a boat and pushed into a furnace for diffusion; both the boat and the furnace tube were quartz. Because of the low level of intentional contamination used in this study, the boat and furnace tube had been carefully cleaned to prevent unintentional contamination. Cleaning consisted of an etch in concentrated HF followed by washing in deionized distilled water. Cover plates were also cleaned thoroughly.

A thermocouple in the boat monitored the sample temperature as the boat and sample heated. Timing was started when the sample was within $15^{o}C$ of the specified diffusion temperature. Unlike the hydrations, the contamination was present on the samples at the start of the heatup and was diffusing as the sample heated. The

choice of procedure was a compromise between starting to time the diffusion immediately upon placing the samples into the furnace (which would give an incorrectly short diffusion time) and starting to time when the sample reached diffusion temperature (which would give an incorrectly long diffusion time).

Yon[33] determined that diffusion of sodium contamination under these conditions is controlled by a surface-rate limitation. He found the rate constant to have an activation energy of 0.38 eV for one-minute diffusions. With this activation energy, it was calculated that the rate constant 15° below diffusion temperature was only about 7% less than the rate constant at temperature for a 600° diffusion and about 4% low for an 800°C diffusion. Heat up time to the -15° point was about 30 seconds, and time from the -15° point to proper diffusion temperature was about one minute.

Either of two ambients was used for the diffusions. The dry oxides were diffused in a dry-nitrogen ambient. The wet oxides were diffused in a wet-nitrogen ambient which was produced by passing nitrogen through a water bubbler at 95°C.

3.1 Sodium Profiles from Diffusion

The sodium profiles obtained for NaCl diffusions at 600°C and for diffusions at 800°C were sufficiently different that they will be discussed separately.

3.1a Profiles from 600°C Diffusions

Sodium-contaminated samples were diffused at 600°C in both wet and dry ambients. Diffusions were done for 1, 15, and 60 minutes. The resulting profiles are shown in Figure 17 for the dry diffusions and in Figure 18 for the wet diffusions.

The dry diffusion profiles were not greatly affected by the length of diffusion time. Also, the profile falls rather steeply even after a one-hour diffusion, and there is little sign of its flattening (diffusion length for one-hour diffusion at 600°C is more than 200 microns[14]). This suggests that the sodium concentration gradient is not the controlling factor in the gradient of electrochemical potential across the oxide. It appears that the sodium is attracted toward the outer surface of the oxide. The attraction could be electrostatic (since some sodium exists in the oxide as Na^+) or it could result from chemical gradients across the film (such as an oxygen gradient).

The sloping profiles seem to contradict results of other investigations. For example, Yon[33] found a flat profile in the bulk oxide for a one-minute NaCl diffusion at 300°C. However, the amount of NaCl he used for contamination was large relative to the amount used in this study. Presumably, the extra sodium overwhelmed any surface attraction to produce a flat profile in the bulk oxide.

Also, at these low concentrations a greater fraction of the

sodium appears to be ionized than in Yon's study. If electrostatic forces were attracting the sodium toward the surface, greater sodium ionizaeion would make the electrostatic forces more effective in determining the sodium distribution.

The wet diffusions show a more "normal" development of the profile with diffusion time. The profile in the bulk oxide has become fairly flat for the one-hour diffusion.

In addition to flattening in the bulk oxide, the wet-diffusion profils show significant sodium peaking at the silicon interface. This sodium peaking has generally been associated with charge production in the silicon[31], and it might be inferred that charge induced in the silicon would be greater for the wet diffusions than for the dry diffusions. This was found to be true.

It was found that sodium transport was considerably greater in the wet diffusions than in the dry. The one-hour wet and dry diffusion profiles are replotted for comparison in Figure 19. It can be seen that the wet-diffusion profile is well above the dry profile at all points. Total sodium is about five times as great in the wet case as in the dry. A similar water-enhancement of sodium transport has been reported recently.[35]

Since sodium diffusion has previously been shown to be surface rate limited,[31] sodium-water interaction at the surface must

overcome the surface rate limitation. The actual mechanism is probably similar to the reactions for glass corrosion discussed previously. The flatter profiles in the wet diffusion also seem to indicate a leveling of the electrochemical potential across the oxide.

3.1b Profiles from 800°C Diffusions

A set of samples were diffused both wet and dry at 800°C as at 600°C. The profiles obtained for the dry diffusions are shown in Figure 20 and those for the wet diffusions in Figure 21.

Unlike at 600°C, the dry-diffusion profile in the bulk is fairly flat in an hour and definitely peaking at the silicon for all diffusion times. However, there is still some slope to the one-hour profile, which possibly still indicates an attraction to the oxide surface.

In wet diffusions at 800°C, the amount of sodium in the oxide actually decreased as diffusion time increased.

In a one-minute diffusion sodium transport was greater for the wet-diffusion than for the dry, just as at 600°C. A leaching effect prevent the sodium buildup beyond this level.

It may be recalled that bare silicon cover plates were used to prevent evaporation of the sodium during diffusion. It was found that a significant thickness of oxide grew on the cover plate and took up much of the sodium which would otherwise have diffused into the sample.

Since the oxide on the cover grew thicker for longer diffusion time, the amount of sodium which it took up was also greater. Thus the amount available to diffuse into the sample was reduced for longer diffusions, and the amount of sodium in the sample decreased. This was confirmed by sectioning the oxide (~ 2000 Å thick). The sodium concentration in the oxide averaged about 2×10^{18}/cc which would roughly account for the "missing" sodium.

The thickness of the oxide grown on the silicon cover plates was indicative of a large sodium-enhancement of the oxidation rate. Only ~ 500 Å of oxide[15] should have grown on the bare wafers for a one-hour wet-oxidation at 800°C; in actuality, ~ 2000 Å were grown. Sodium-aided oxidation has previously been reported by Revesz and Zaininger[34].

That the enhanced oxidation rate was actually caused by the sodium could be substantiated by examining the cover plate (which was larger than the sample). The thickness of the oxide on the cover showed a gradual decrease from the 2000 Å immediately over the sample (where the sodium concentration was high) to ~ 500 Å, the expected oxide thickness, at the edge of the cover plate (where there was presumably no sodium). The outline of the sample could be seen on the cover plate after the diffusion.

Since the oxidation was done by water, water transport in

the oxide was apparently increased by sodium. Thus, water and sodium seem to have a cooperative effect which gives increased diffusion for both, again in line with the glass-corrosion previously discussed.

3.2 Electrical Effects of Diffused Sodium

To assess the electrical effects of the sodium, aluminum contacts were evaporated onto the samples before contamination, and V_{fb} was measured. The contacts were then etched off, the samples contaminated and diffused, and the contacts reapplied to remeasure V_{fb}.

The shift in V_{fb} was converted to an equivalent induced charge in the silicon. The induced charge is plotted against diffusion time in Figure 22 for the various diffusion conditions used. No data are shown for the 800°C diffusions since V_{fb} was beyond measureability in one minute. For convenience in comparison, Slabinski's[50] data for NaBr diffusion (dashed curves) are included in the figure. It can be seen that his data are in basic agreement with the results of the present study.

Charge production kinetics were much faster in wet diffusions than in dry diffusions of the sodium. At 600°C charge buildup in the dry diffusion was relatively slow as shown. In one hour the charge had built up to about 2×10^{12} per cm^2. In the wet diffusion this

charge level was reached in about one minute. The 15-minute wet-diffused sample was tested to a higher bias voltage than the other samples. Beyond 300 volts bias (1.2×10^{13} charges/cm^2) the oxide broke down with no indication of surface inversion.

The results for dry diffusions at 800°C are about as expected from previous results. The decrease in charge at long diffusion times has been attributed[33] to a compensation of sodium charge by anion (Cl^- in this case) charge. The wet diffusions, as mentioned, all gave charge production beyond measurability.

Measured and calculated flatband voltage shifts for the samples are given in Table 2. Shifts were calculated from the sodium profiles by the formula[51]:

$$\Delta V_{fb} = -\frac{1}{x_{ox} C_{ox}} \int_0^{x_{ox}} x \rho(x)\, dx \qquad (3\text{-}1)$$

where ΔV_{fb} = flatband voltage shift

x = distance from air interface

x_{ox} = oxide thickness

C_{ox} = oxide capacitance per unit area

$\rho(x)$ = change density in oxide.

For the sectioned profile, (3-1) was approximated by summing over the sodium charge in each section, i.e.,

$$\Delta V_{fb} = -\frac{1}{x_{ox} C_{ox}} \sum_{i=1}^{n} x_i \rho_i \Delta x_i \qquad (3\text{-}2)$$

where x_i = center of ith section

ρ_i = charge density in ith section

Δx_i = thickness of ith section

n = number of sections.

Eq. (3-2) was used to calculate ΔV_{fb} from observed sodium profiles under two conditions: (1) only sodium within 1000 Å of silicon was ionized (ΔV_{1000} in Table 2); (2) all sodium in oxide was ionized (ΔV_t in Table 2). For low sodium levels (600°C dry) in the oxide, ΔV_{meas} seems better correlated with ΔV_t than with ΔV_{1000}. This would seem to indicate that sodium is ionized in the entire oxide and not just near the silicon. However, the measured contamination level is near residual levels of 10^{16} to 10^{17} sodium atoms per cc and residual sodium in the oxide (not measured) could seriously affect the results.

As the sodium level in the oxide increased (800°C dry), ΔV_{meas} became less correlated with ΔV_t and more correlated with ΔV_{1000}, in agreement with previous results[31]. Since the sodium level was well above expected residual level in all the 800°C dry diffusions, it appears that when large amounts of sodium were

TABLE 2

Comparison of Measured and Calculated

Flatband Voltage Shifts for Sodium Diffusions

$600^{o}C$

	Dry			Wet		
Time	ΔV_{meas}*	ΔV_{1000}*	ΔV_{t}*	ΔV_{meas}	ΔV_{1000}	ΔV_{t}
1 Min.	9V	2	12	70	5	40
15	18	2	35	>300	80	200
60	48	6	36	>200	120	320

$800^{o}C$

	Dry			Wet		
	ΔV_{meas}	ΔV_{1000}	ΔV_{t}	ΔV_{meas}	ΔV_{1000}	ΔV_{t}
1 Min.	180	35	220	>200	100	370
15	140	60	360	>200	70	250
60	120	130	590	>200	40	160

*ΔV_{meas} = measured flatband voltage shift (1 volt corresponds to $\approx 4 \times 10^{10}$ electron charges/cm^2).

ΔV_{1000} = shift calculated from measured sodium within 1000 Å of silicon.

ΔV_{t} = shift calculated from measured sodium in entire oxide.

diffused into the oxide a smaller fraction of the sodium was ionized.

The other result of the electrical measurements was an enhancement of sodium effect in the wet diffusions. At 600°, this is probably because of the larger sodium transport in the wet diffusions than in the dry. In none of the wet diffusions, however, was ΔV_{meas} correlated with ΔV_{1000}. Water, therefore, at least seemed to cause a larger fraction of sodium to be ionized.

In some of the wet diffusions, however, even the entire amount of sodium in the oxide is insufficient to explain the measured flatband voltage shift. It appears that water is itself acting as a positive charge. This is rather surprising since water did not previously act as a charged species in a diffusion. At low temperatures, water acted uncharged or even slightly negatively charged as described previously. Also, samples hydrated at 800°C (for the wet diffusions) had flatband voltages comparable to unhydrated samples. Furthermore, wet oxidations produce only slightly more oxide charge than do dry oxidations[33].

It is possible that the presence of the sodium causes the hydrogen of the water to become charged. Since a great deal of water probably diffused in the wet diffusions, there would be enough hydrogen available. However, it is difficult to see how sodium could cause the hydrogen to become charged, except in an exchange

reaction; in an exchange reaction the sodium would be expected to lose its charge, and no net charge would be gained.

Another possibility is that the combined effects of sodium and water produce a disorder in the silicon/oxide interface which causes charge trapping and consequent surface inversion. Such disorder and increased interface charge has been shown by Revesz and Zaininger[52] to be increased by high oxidation rates and low oxidation temperatures. The presence of the sodium has the effect of enhancing oxide growth rate at a low oxidation temperature. In their investigation, Revesz and Zaininger found interface charge on the order of several times $10^{11}/cm^2$ for ordinary wet oxidations. With the sodium enhancement of oxidation rates it is possible that interface disorder and charge trapping could be much higher.

As previously mentioned, Yon[33] noted a decrease in measured interface charge when sodium was diffused for up to 10 hours at 300°C. At higher temperatures, the measured charge decreased and then increased. At high temperature, charge increase started immediately.

This effect has been confirmed in this work, as shown in Table 3. Diffusions of NaCl at 300°C gave charge decrease for either wet or dry diffusion. At 450°C, dry diffusion still gave a charge decrease. However, wet diffusion gave a charge decrease

followed by an increase. At 600°C, charge increase was immediate as previously discussed.

TABLE 3

Flatband Voltage Shifts For
Low-Temperature Sodium Diffusions

	Dry		Wet	
Time	300°C	450°C	300°C	450°C
1 Minute	0.2 V	0.9	4.3	1.2
15	0.7	0.1	2.9	4.9
60	2.5	4.0	3.2	-16.3

It appears that neither water, sodium, nor a combination of the two cause any significant interface charge for a diffusion at low temperatures. The observed decrease in interface charge is possible only an annealing effect.

3.3 Effect of Sodium Contamination on Low-Temperature Hydration

The enhanced oxidation rate noted in the presence of sodium implied that water was transported into and through the oxide faster in the presence of sodium than in a clean oxide. It was considered possible that the enhanced water transport could also be observed

for the low-temperature hydrations described in the last chapter.

To test this possibility, three oxidized and baked wafers were sodium contaminated and dry-diffused. The sodium-contaminated samples and two clean control samples were then simultaneously hydrated for two hours at 200°C and 25 mm pressure.

The samples were sectioned and counted as before. In addition, the sodium profiles obtained from the liquid scintillation counting were confirmed by gamma scintillation counting. The hydrogen and sodium profiles thus obtained are shown in Figure 23.

The lower hydrogen profile, obtained for the clean samples, agrees well with hydrogen profiles normally obtained under these hydration conditions. The hydrogen profiles in the contaminated samples, however, indicate increased 'water' transport in the oxide. Roughly an order of magnitude more water diffused into the contaminated oxides than into the clean oxides. This order of magnitude increase in water injection is with a low level of sodium contamination as indicated by the sodium profile in Figure 23.

It may be seen that the hydrogen profile for the sodium-contaminated oxides is shifted rather uniformly from the profile in the clean oxides and has a very similar shape. This would seem to indicate that the effect of the sodium is to make water entry into the oxide easier as well as possibly aiding transport across the film (i. e. a surface effect as well as a bulk effect).

Although sodium contamination aids water transport at both low and high temperatures, there seems to be no interaction to enhance the sodium's electrical effect at 200°C. At 200°C hydration of a sodium-contaminated sample produced no change in interface state density and gave the same slight positive shift of V_{fb} normally seen for the hydration of a clean sample. It appears that the sample must be heated beyond 200°C to get an interaction of sodium with water which enhances the sodium charge production in the silicon.

4. Conclusions

1. 'Water' penetrates quickly through the oxide film even for diffusions for short times (few minutes) or for low temperatures (near room temperature). Water is diffused to few times 10^{18}/cc hydrogen concentration in bulk oxide and several times higher at the air interface.
2. Diffusion is by a "micropore" structure in the oxide as supported by fast penetration, exponential profile, and low activation energy. Solubility is higher at the oxide surface, probably indicating greater porosity at the surface.
3. Since in-and out-diffusion is much faster than that for oxidizing water, this appears to suggest a different binding for 'water' injection at low and high temperatures. This con-

clusion is supported by the small effect of oxidation water on profile of water diffused at low temperature.

4. At temperatures up to 200°C, 'water' diffused to a hydrogen concentration of 5×10^{18} at the silicon has no measurable effect on interface state density and gives a slight decrease in fixed charge. This effect was the same in sodium-contaminated samples.

5. The combined effects of sodium and water are greater than expected from adding their individual effects. This is shown in several ways:

   a. Sodium diffuses several times faster in a wet oxide in a wet ambient than in a dry oxide in a dry ambient.

   b. Charge (MOS) produced by the sodium is much larger in the wet case than in the dry.

   c. Oxide is grown on samples diffused in a wet ambient at a great rate in the presence of sodium than in normal oxidations in the absence of sodium, indicating enhanced water transport with sodium contamination.

   d. Water diffusion (200°C) is increased about an order of magnitude in a sodium-contaminated oxide as compared with a clean oxide.

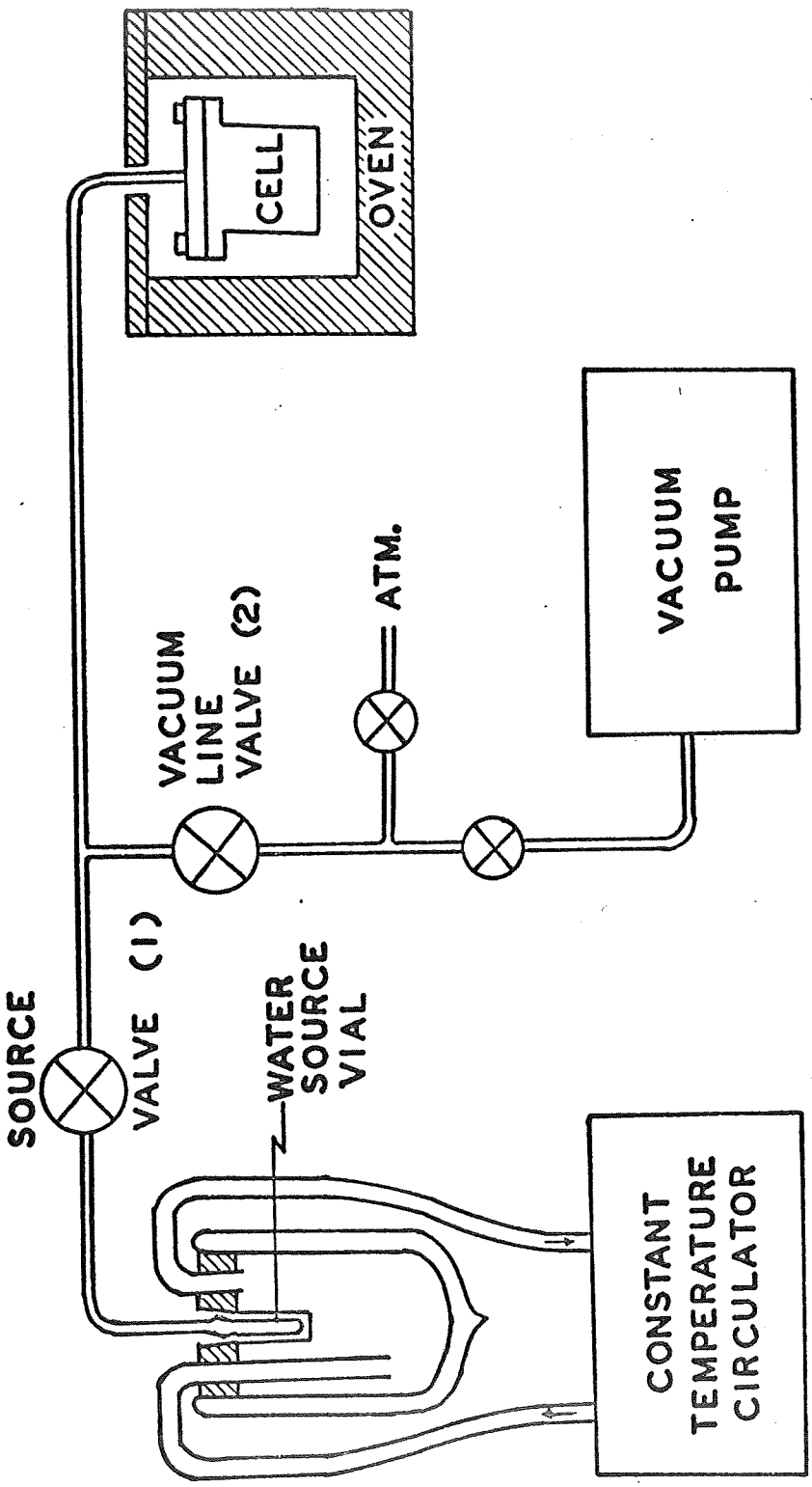

Figure 1

Hydration Apparatus

Figure 2

Typical Hydration Profile

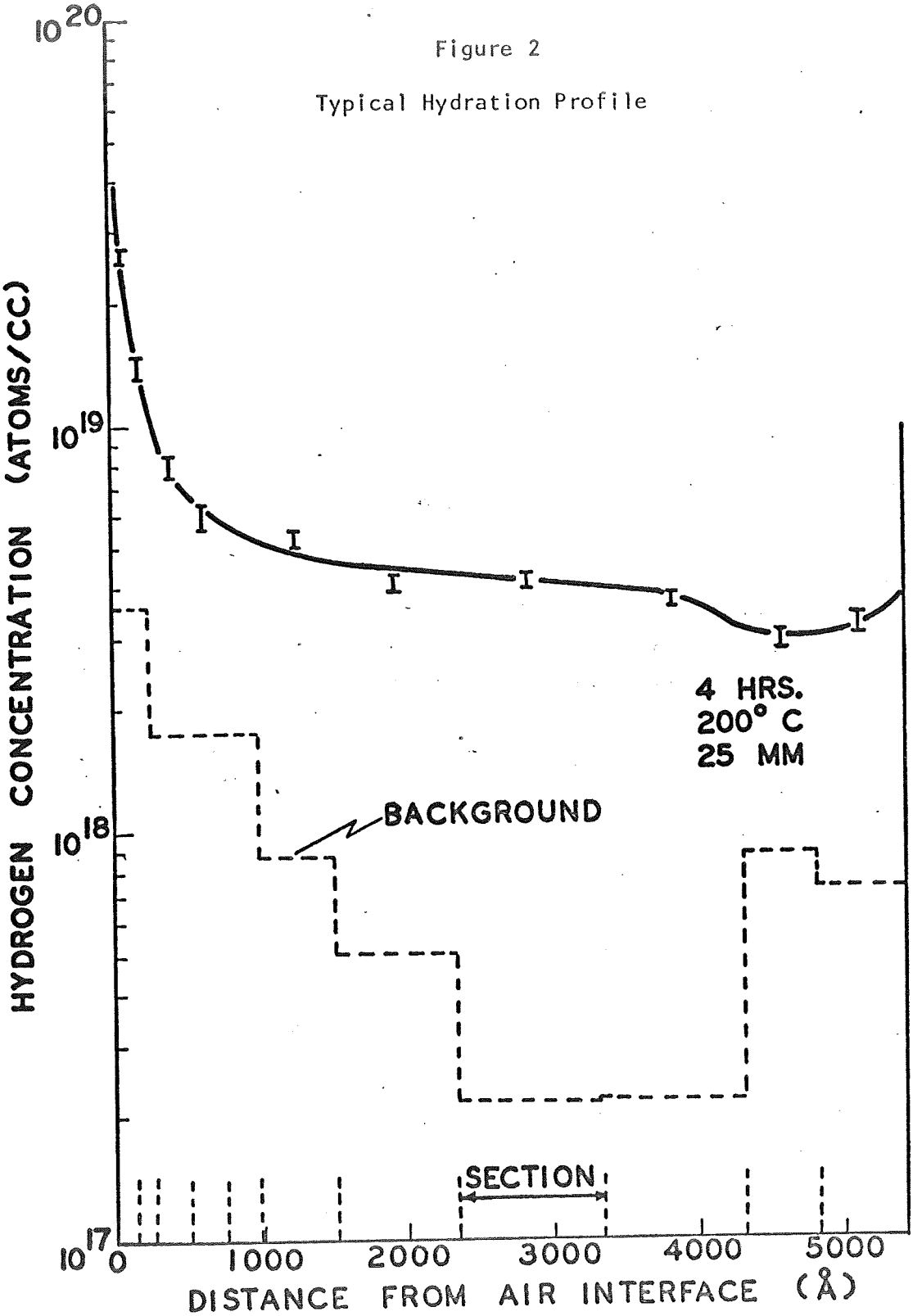

Figure 3

Reproducibility of Hydration Profile

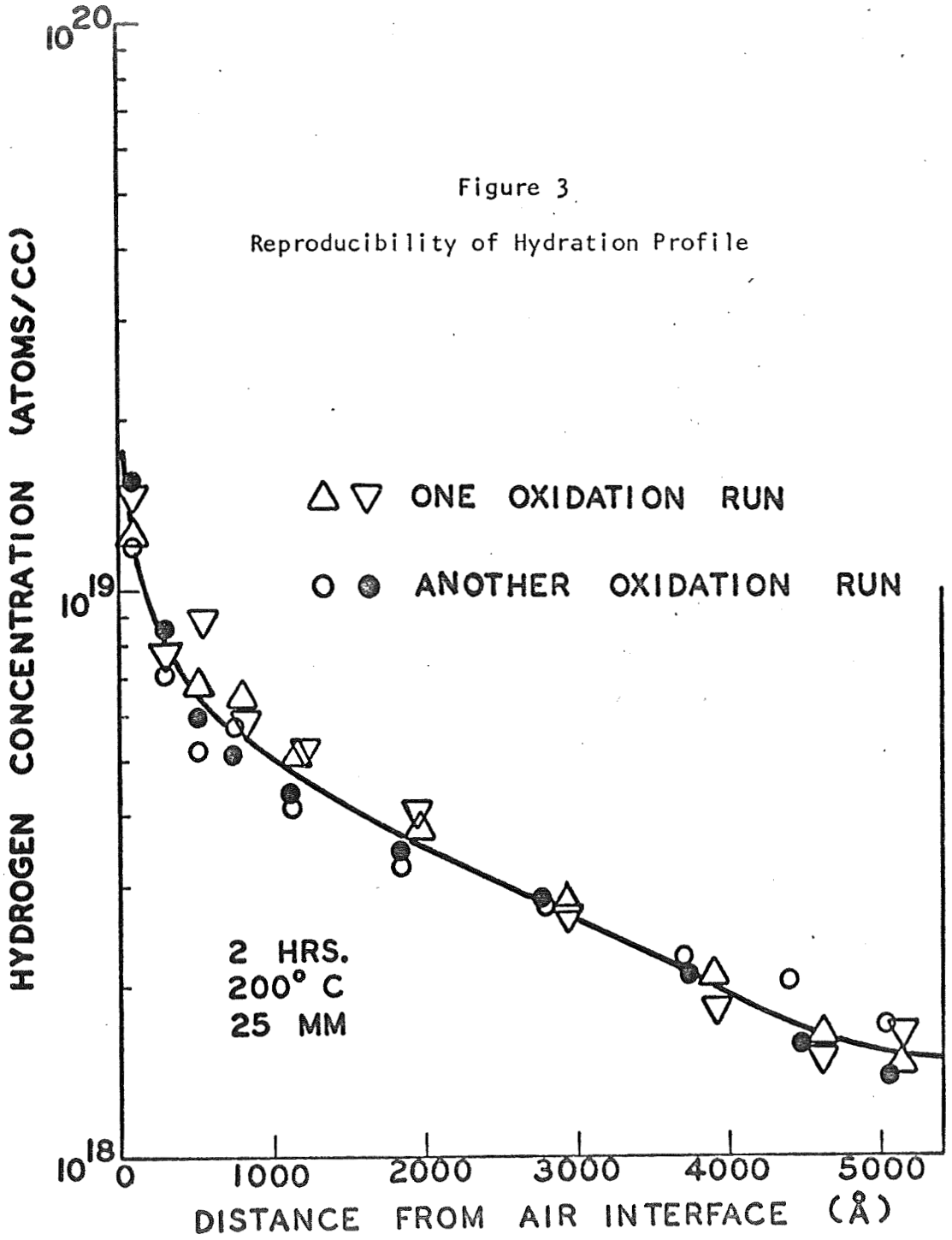

Figure 4

Time-Dependence of Hydration Profile

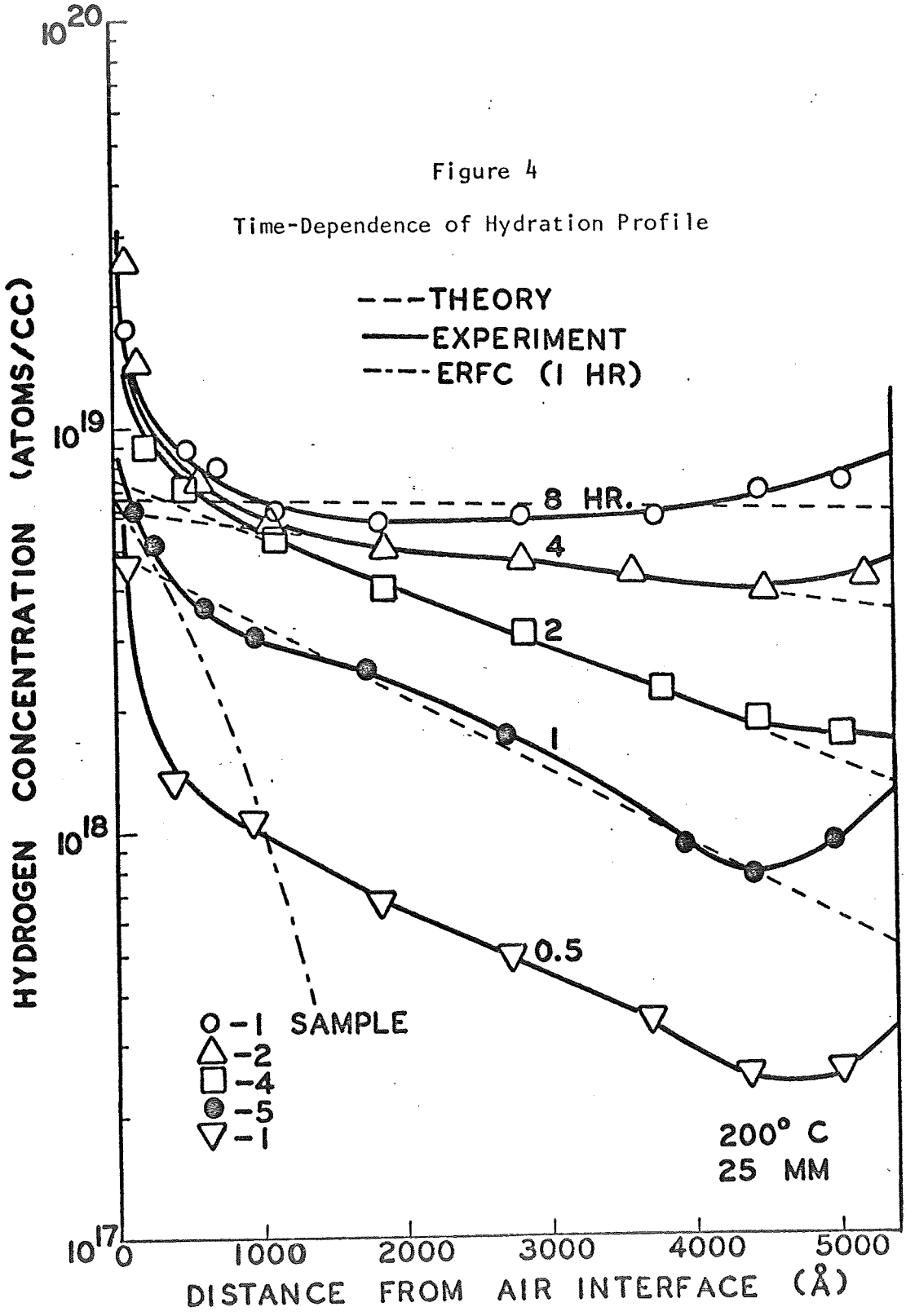

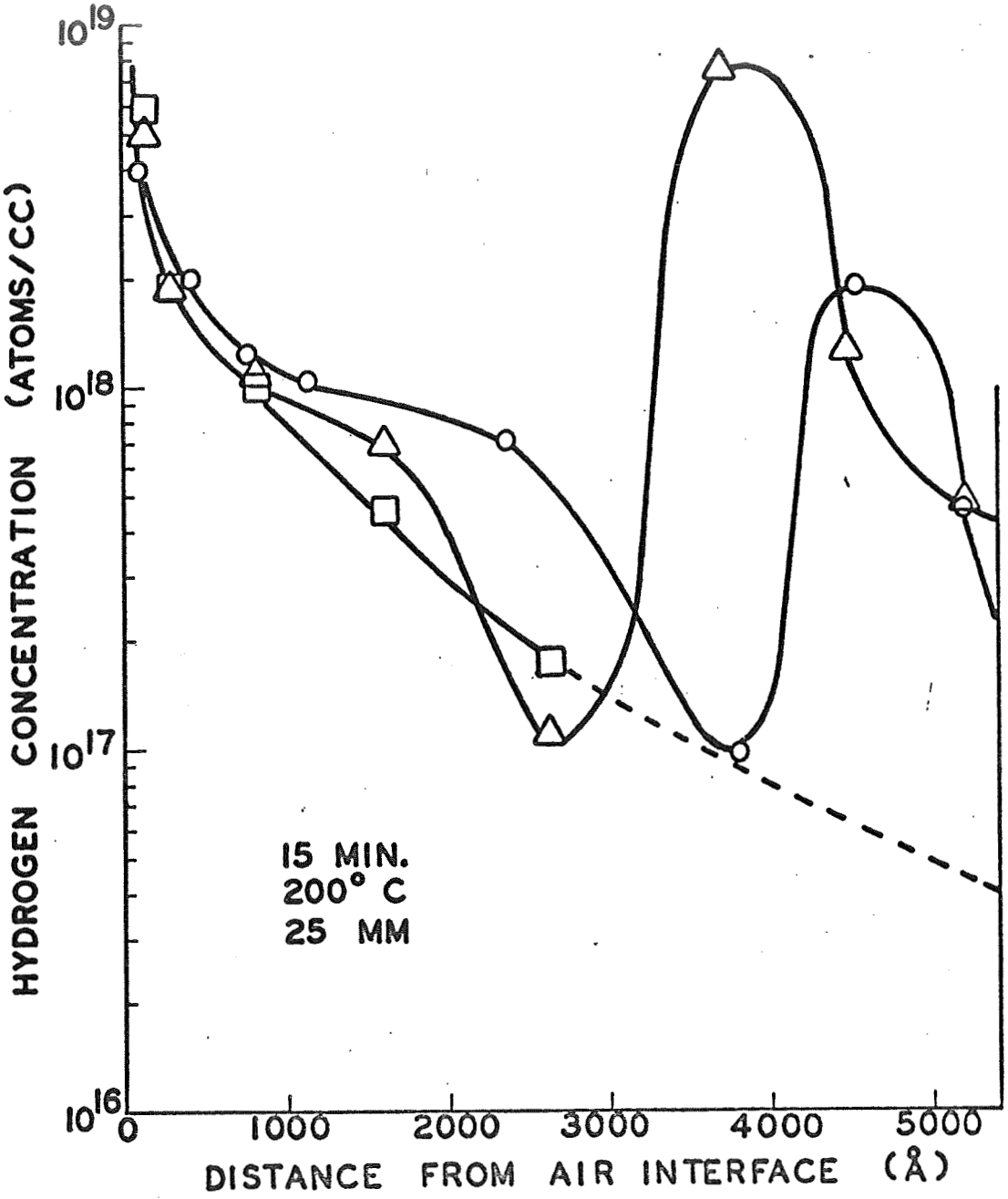

Figure 5

Profiles for 15-Minute Hydrations

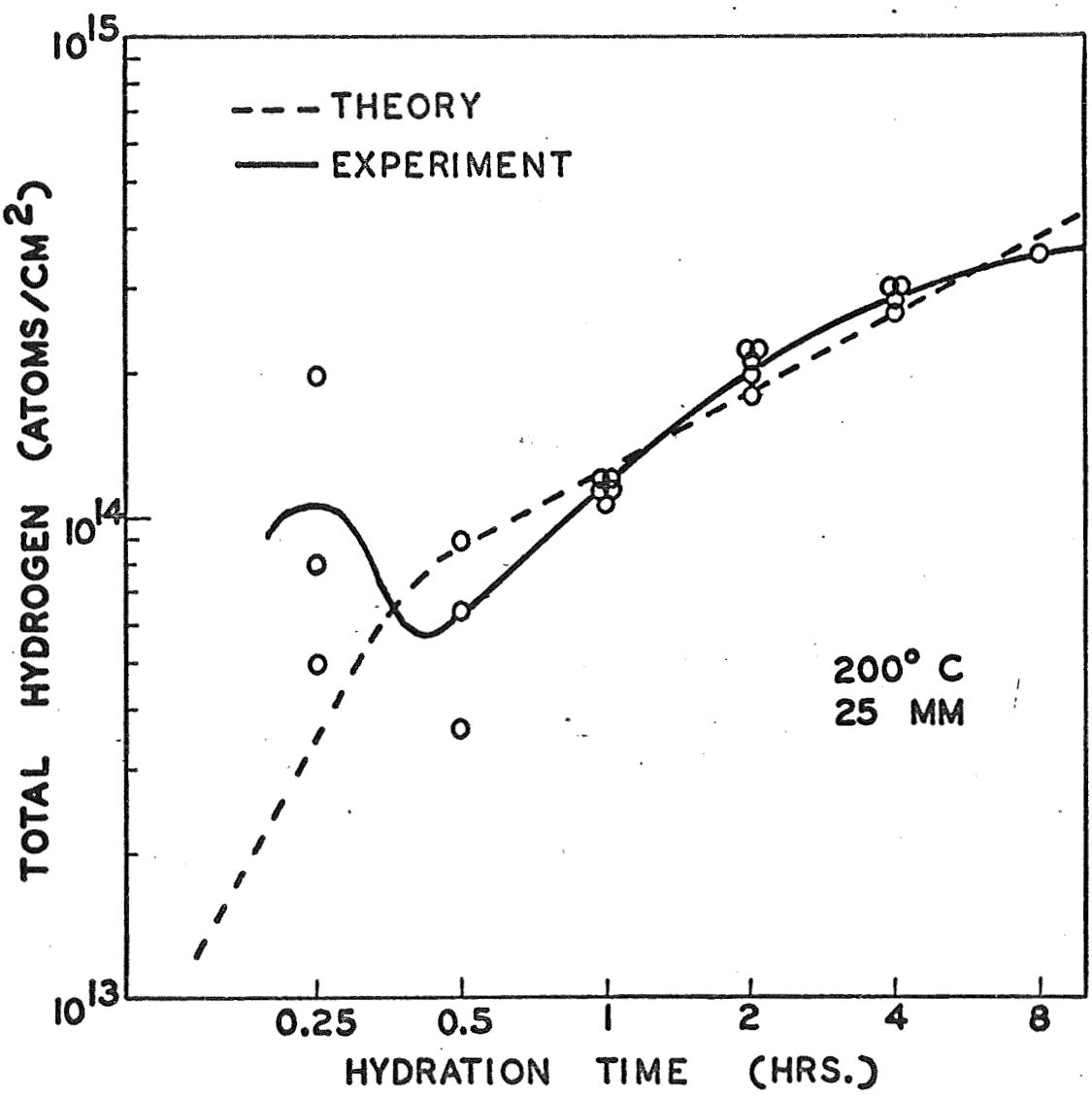

Figure 6

Total Hydrogen in Oxide as a Function of Hydration Time

Figure 7

Temperature-Dependence of Hydration Profiles

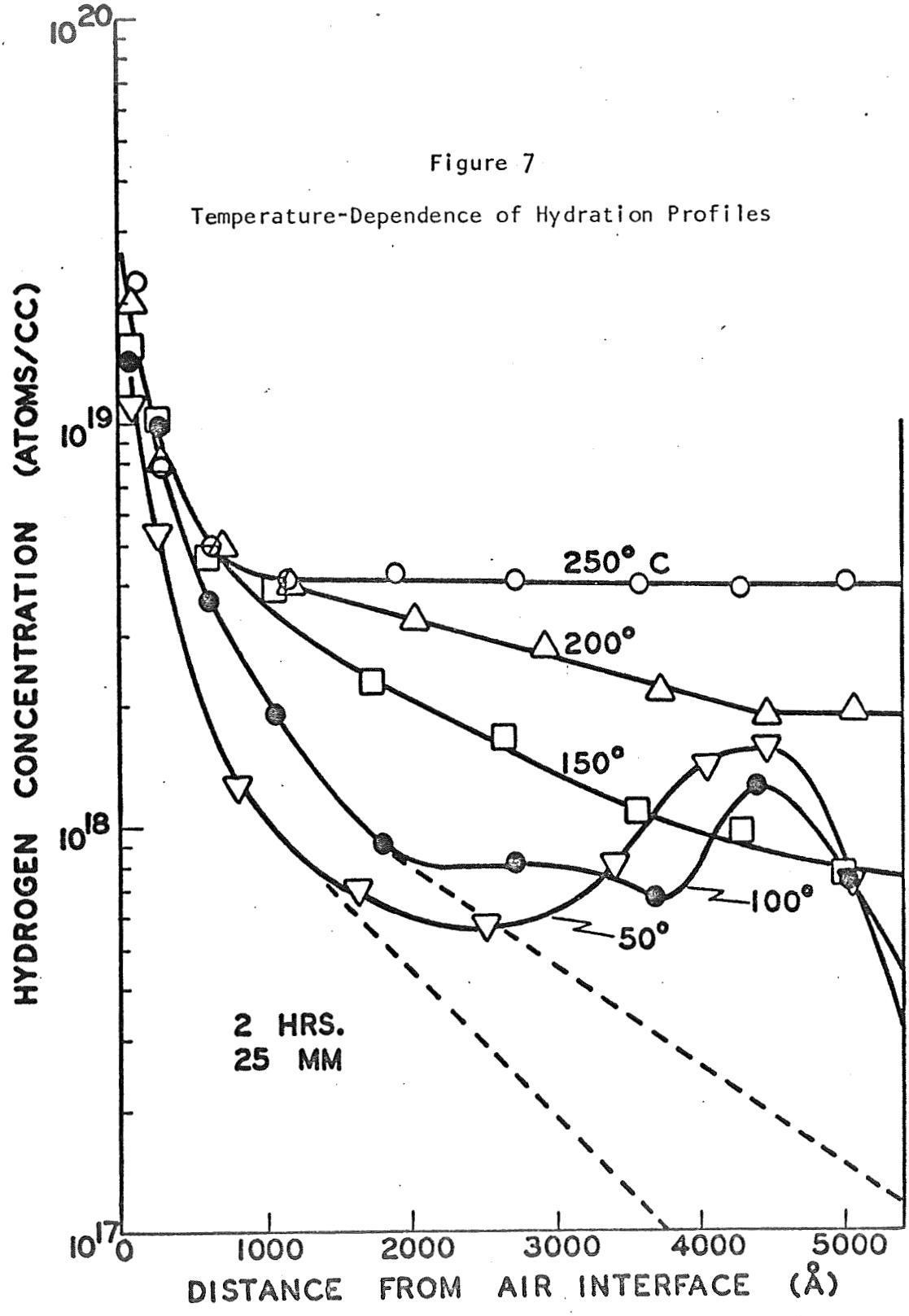

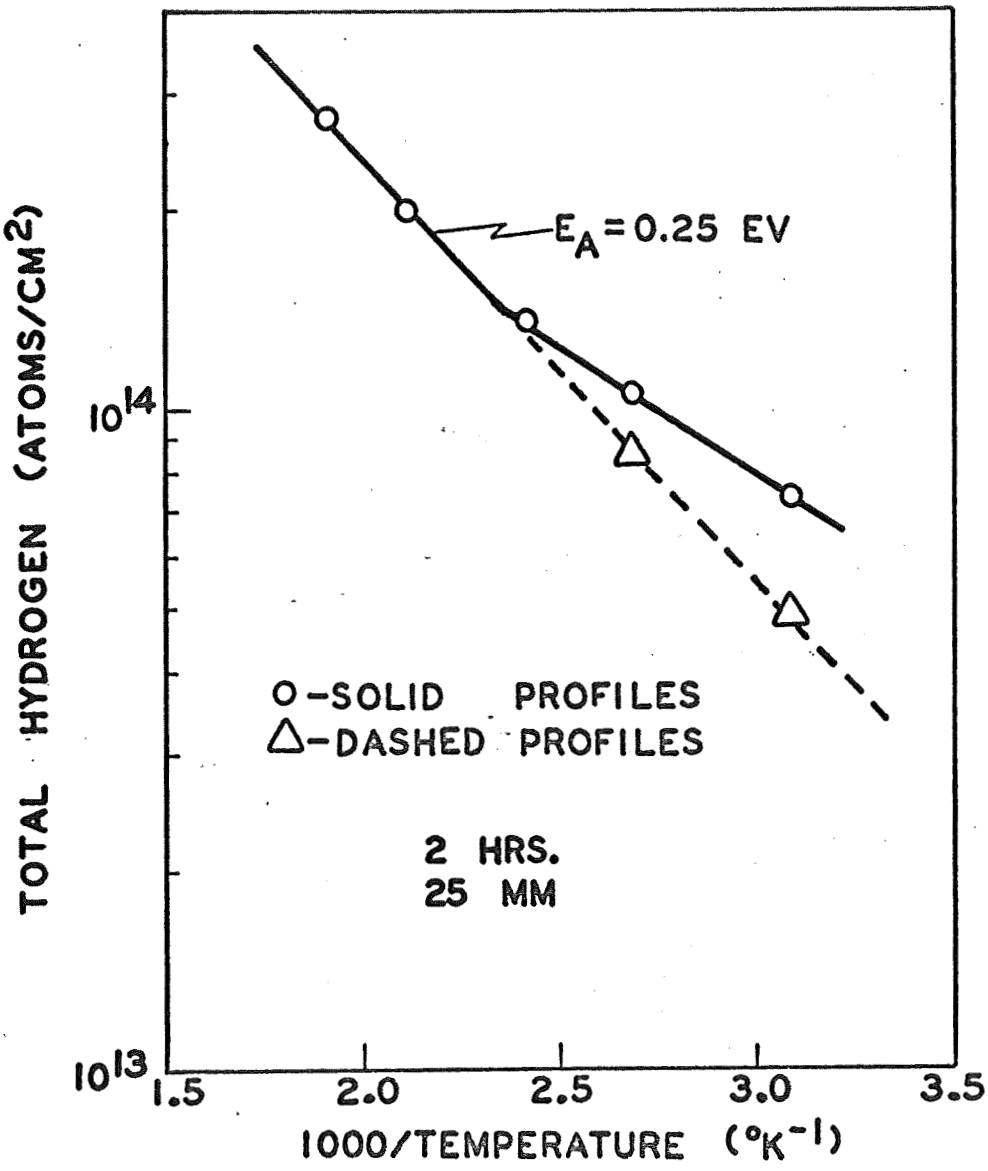

Figure 8

Total Hydrogen in Oxide as a Function of Hydration Temperature

Figure 9.

Pressure-Dependence of Hydration Profiles

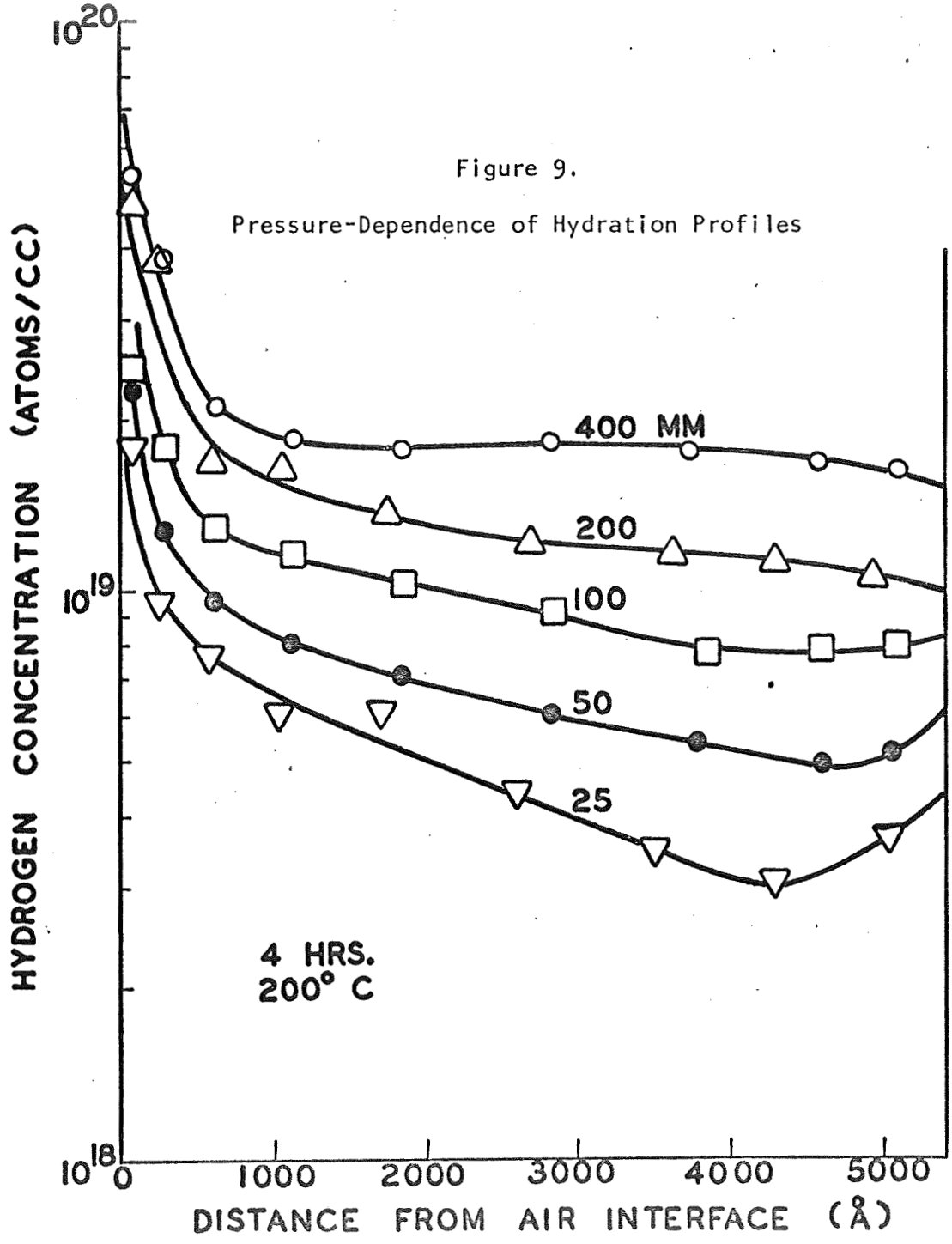

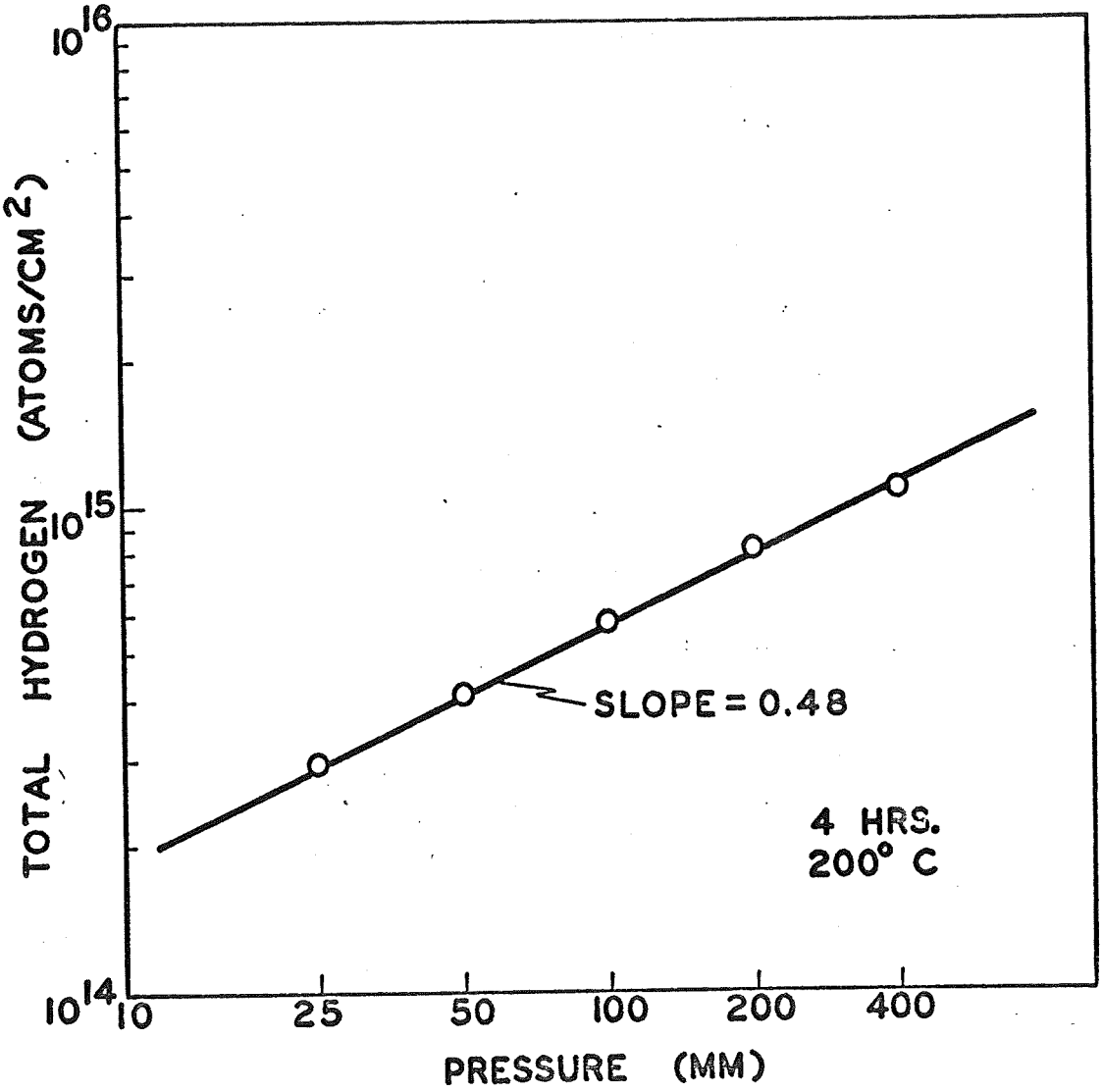

Figure 10

Total Hydrogen in Oxide as a Function of Hydration Pressure

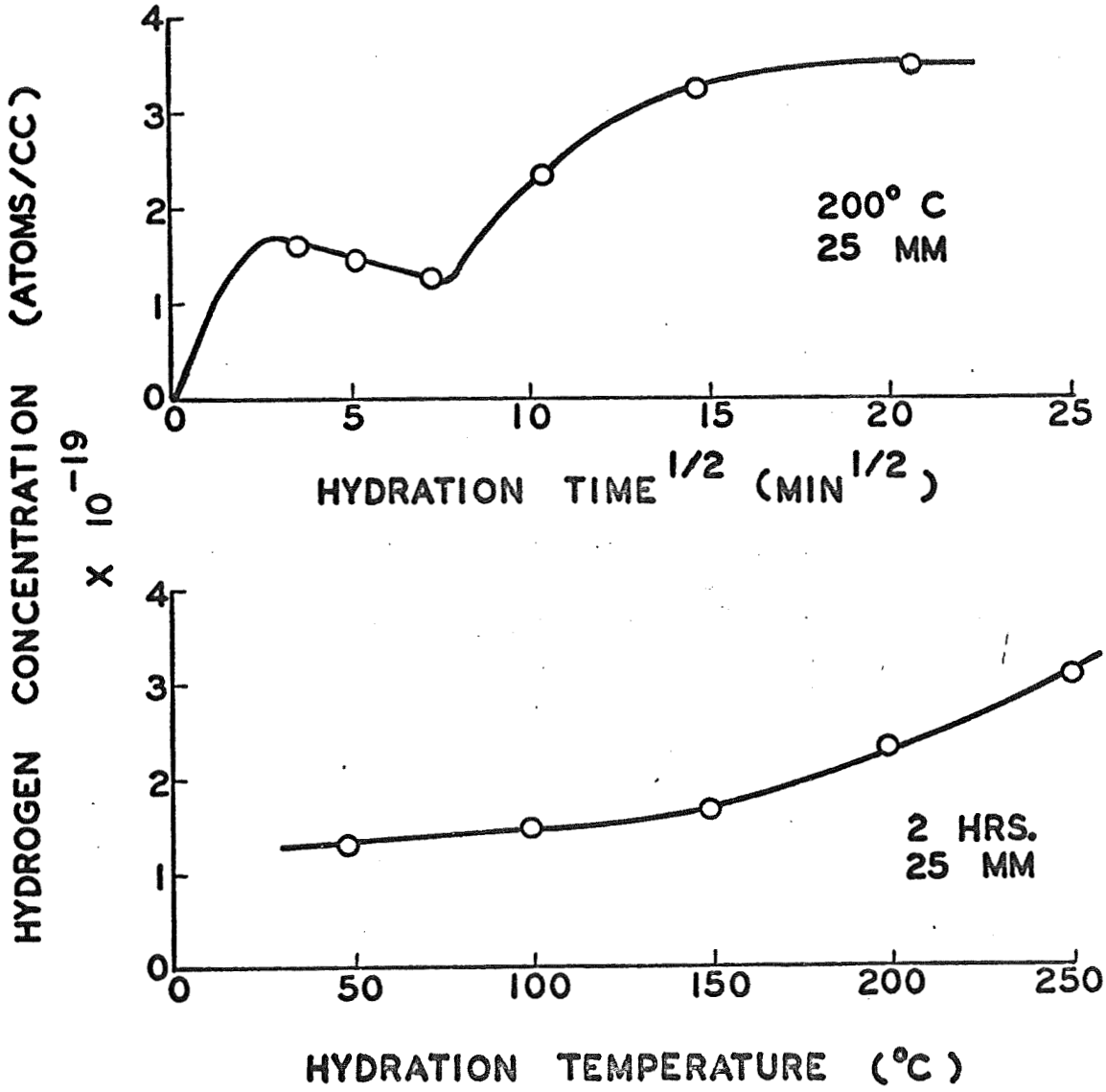

Figure 11

Hydrogen Concentration in Oxide at Air Interface as a Function of Hydration Time and of Hydration Temperature

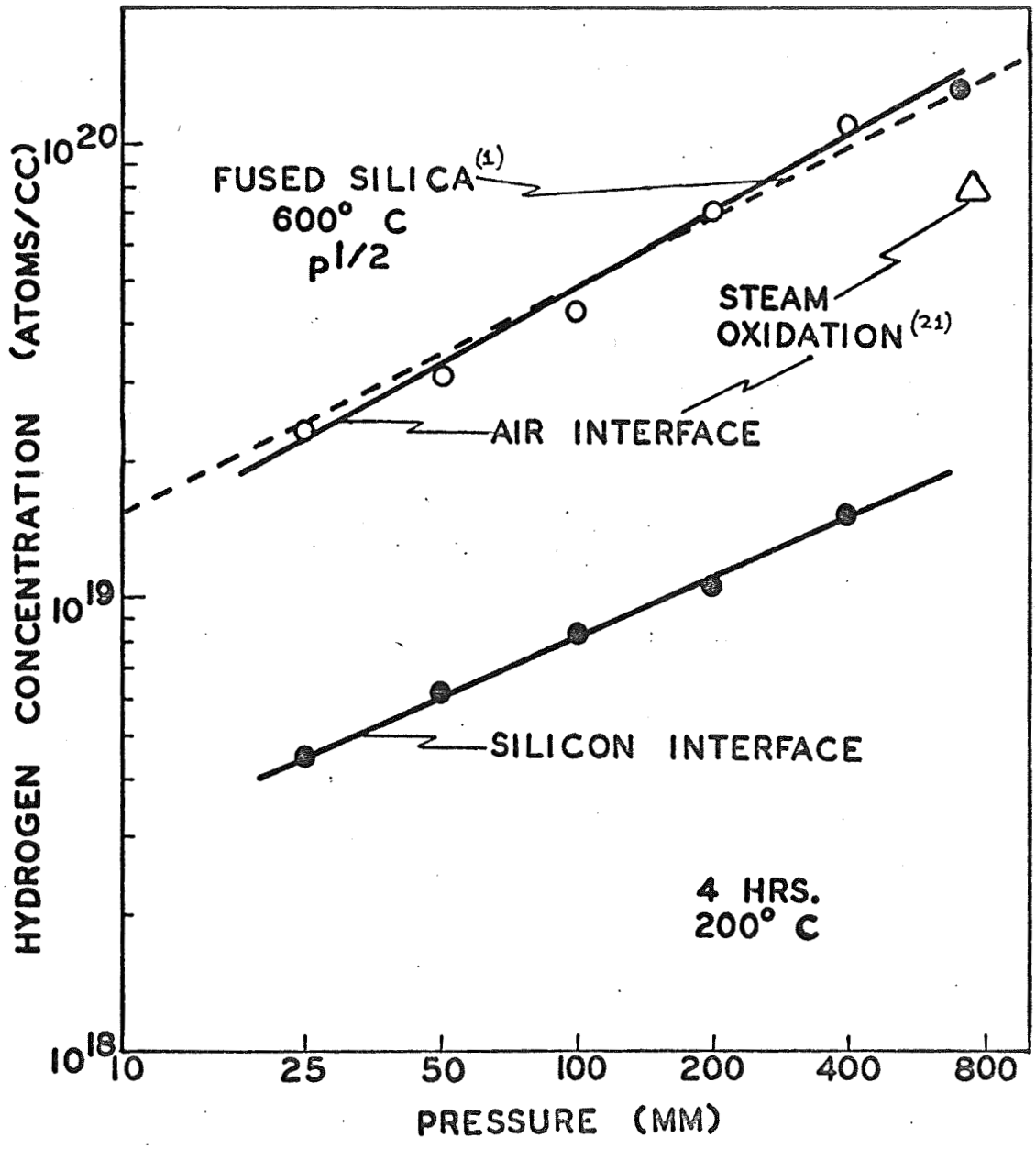

Figure 12

Interface Hydrogen Concentration as
a Function of Hydration Pressure

Figure 13

Effect of Removing Outer Region of
Oxide Before Hydration

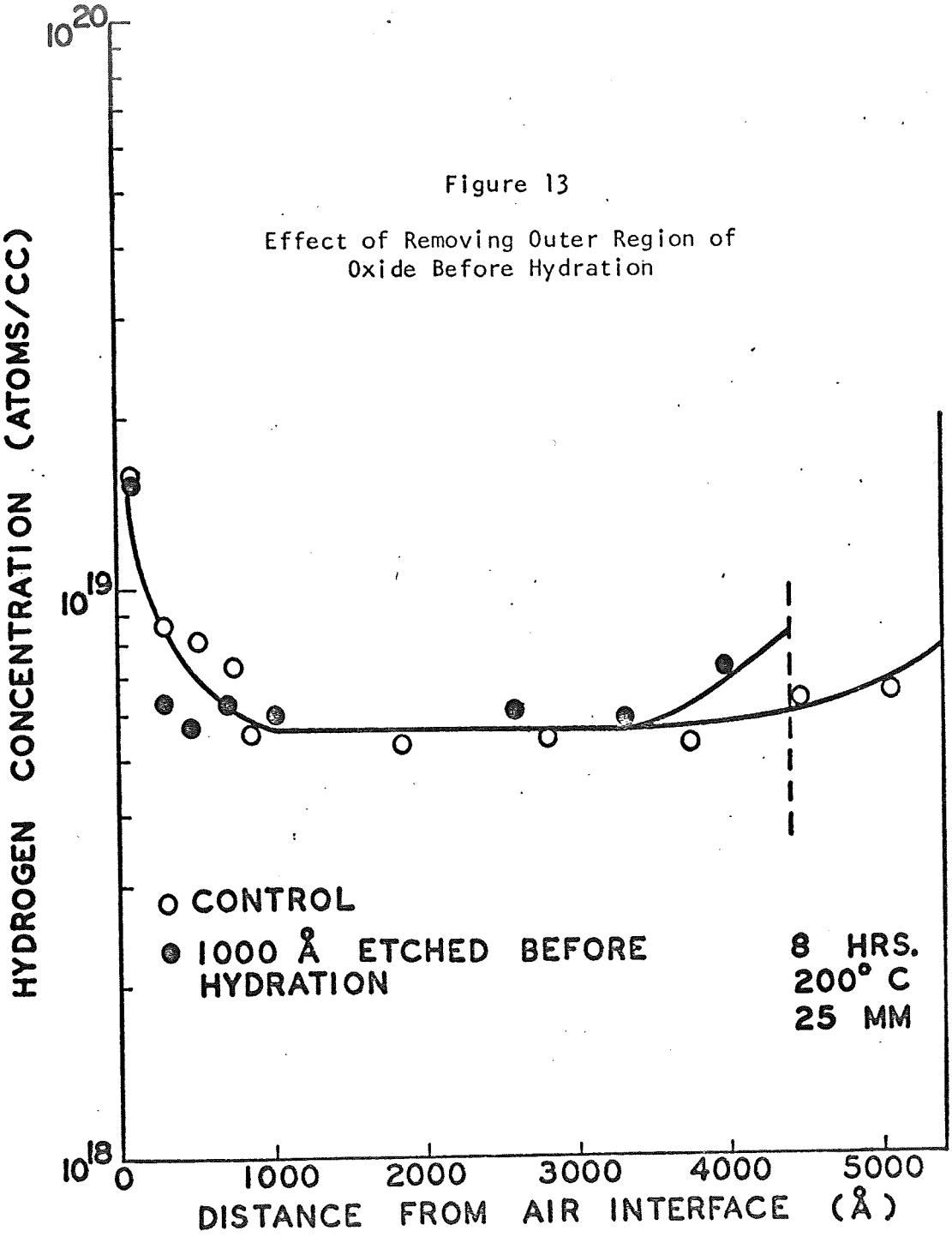

Figure 14

Outdiffusion Behavior of Hydrated Oxides

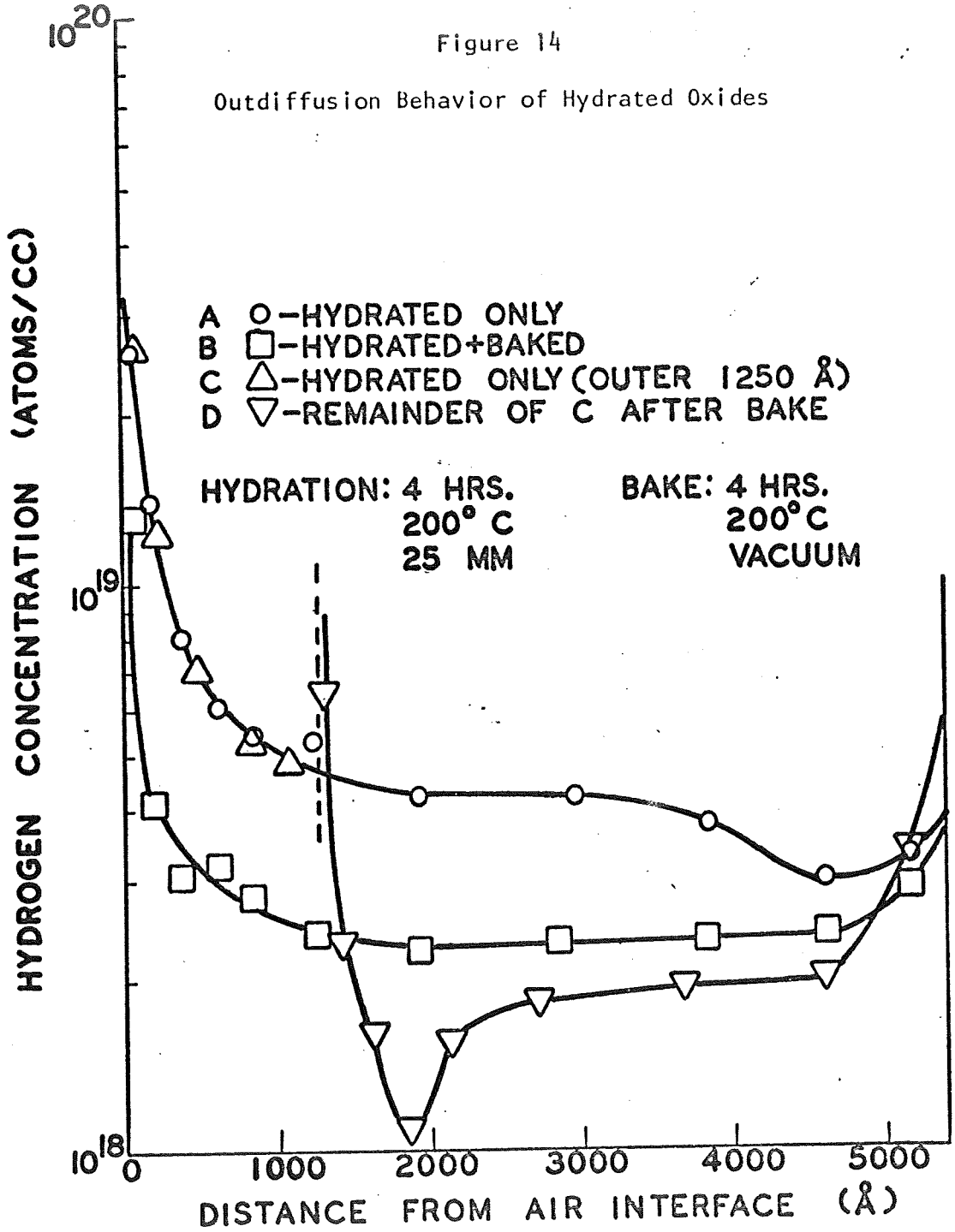

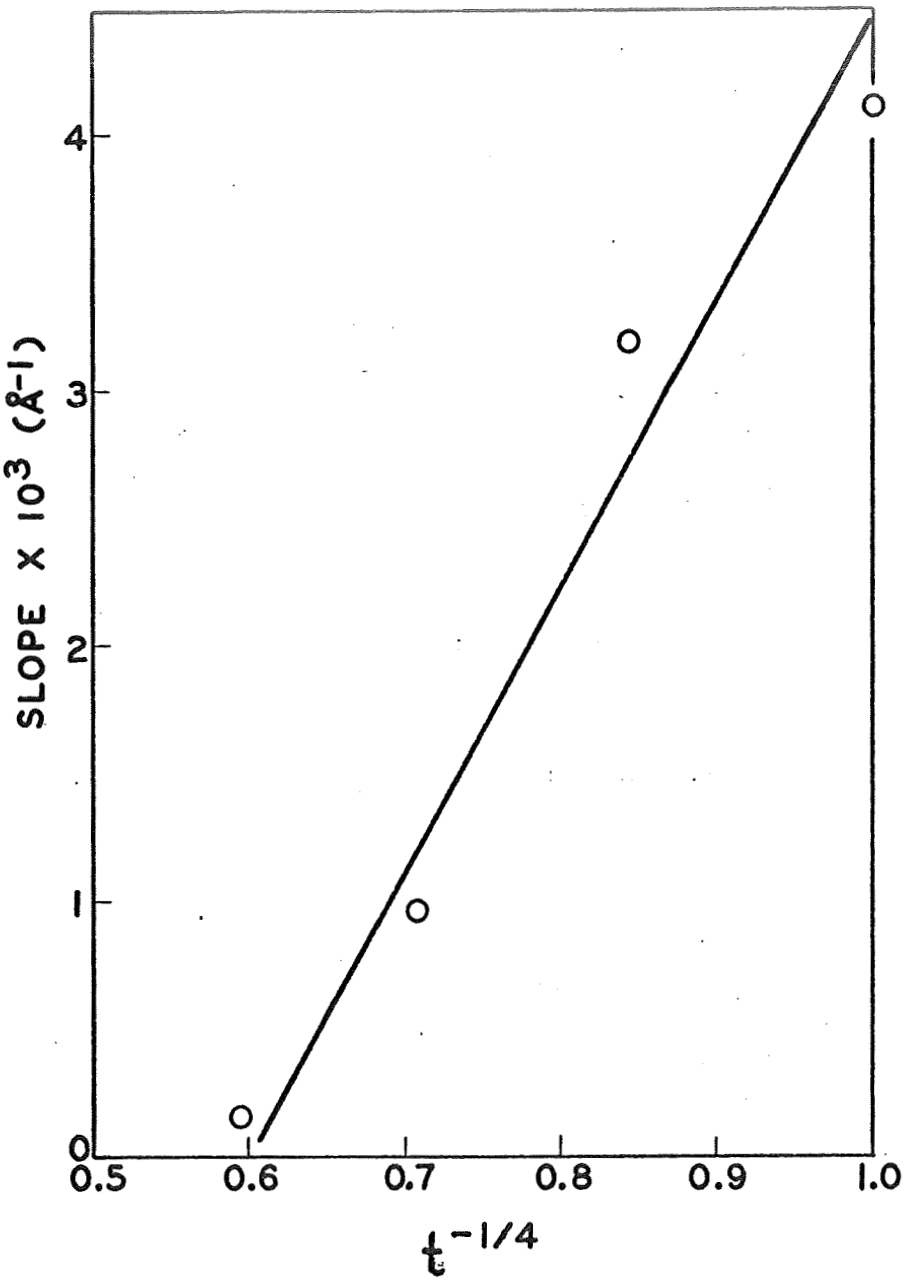

Figure 16

Time-Dependence of Hydration Profile Slopes

Figure 17

Sodium Profiles for Dry Diffusion of NaCl at 600°C

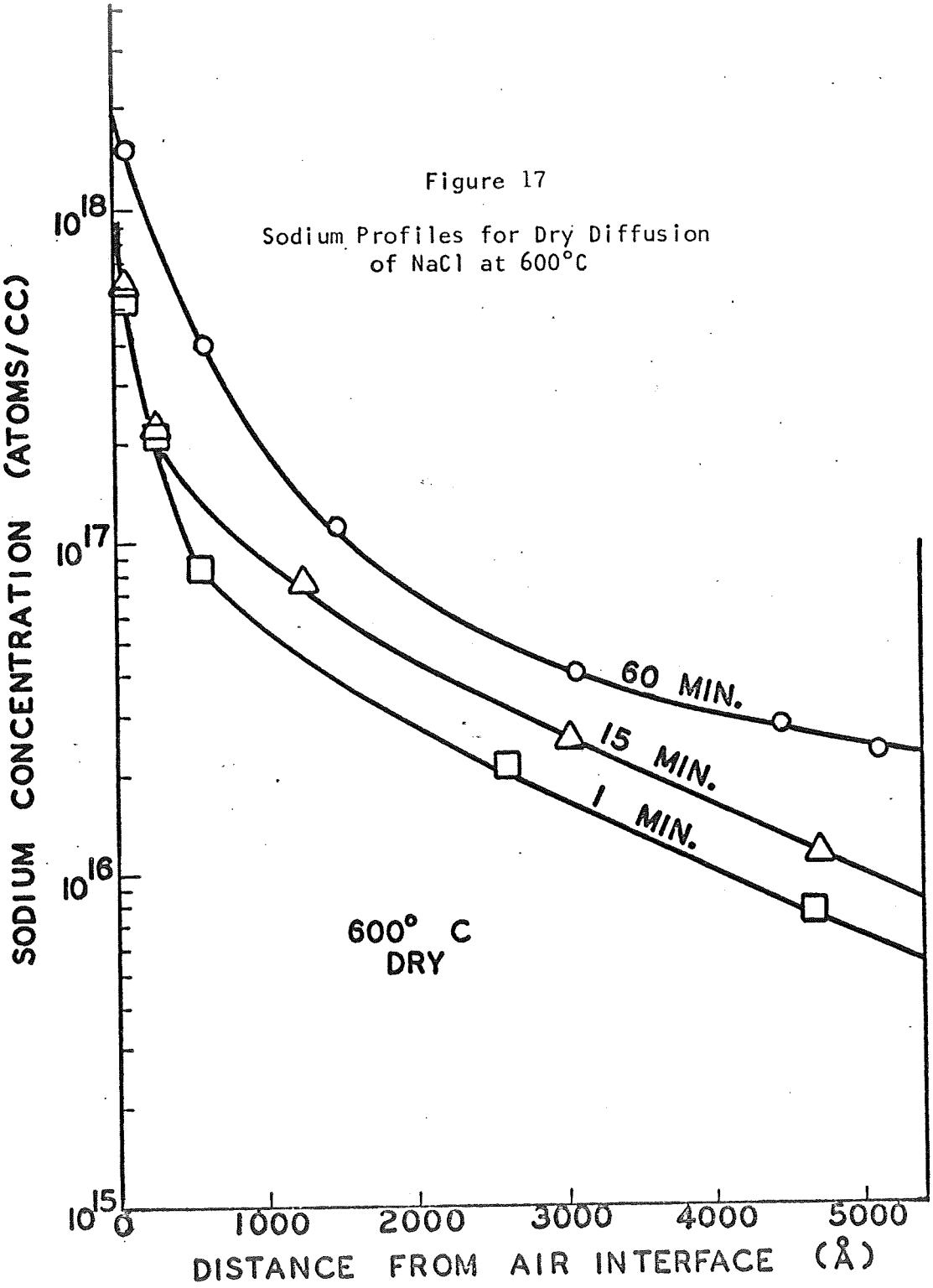

Figure 18

Sodium Profiles for Wet Diffusion
of NaCl at 600°C

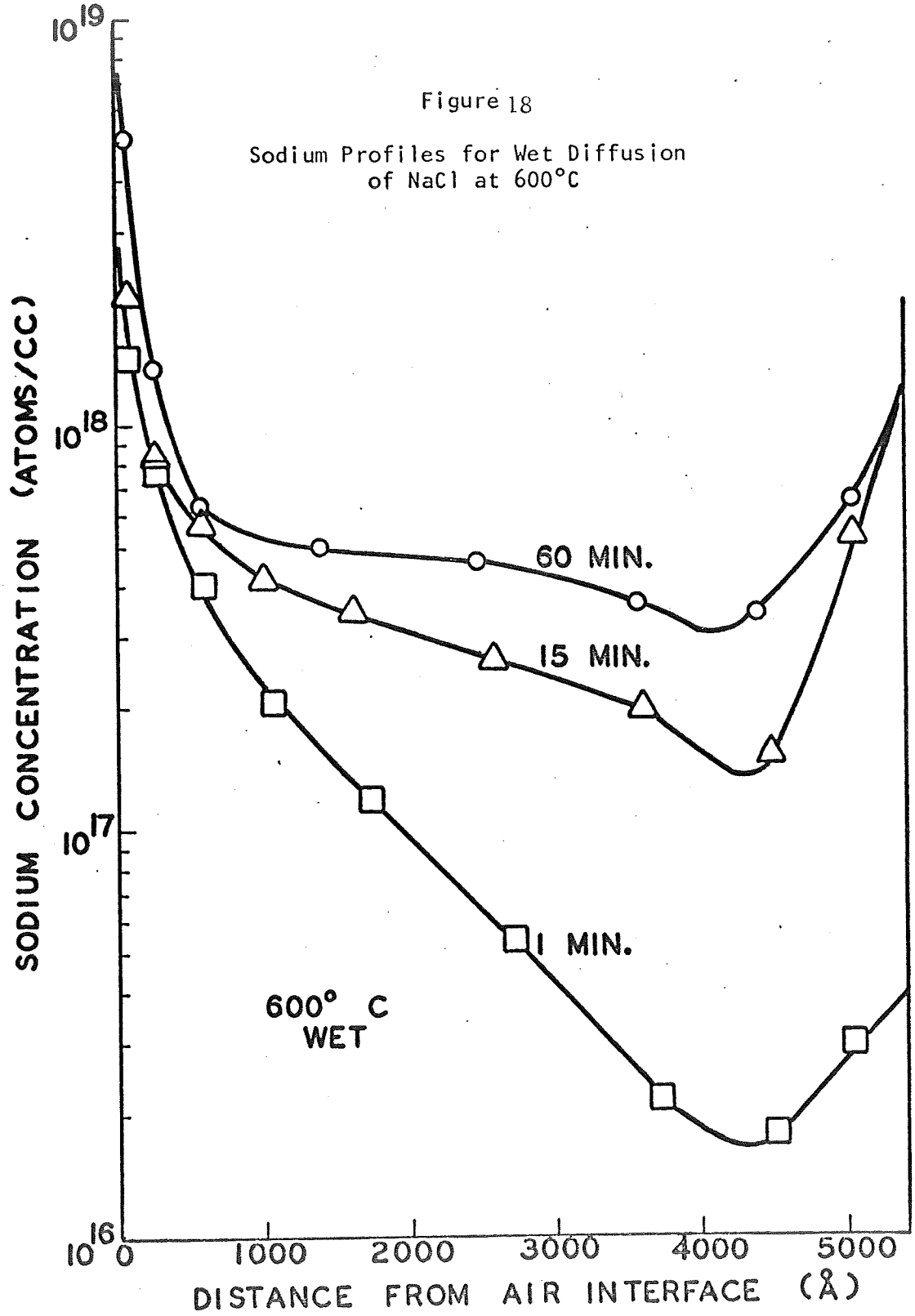

Figure 19

Comparison of Sodium Profiles for One-Hour Wet and Dry Diffusions of NaCl at 600°C

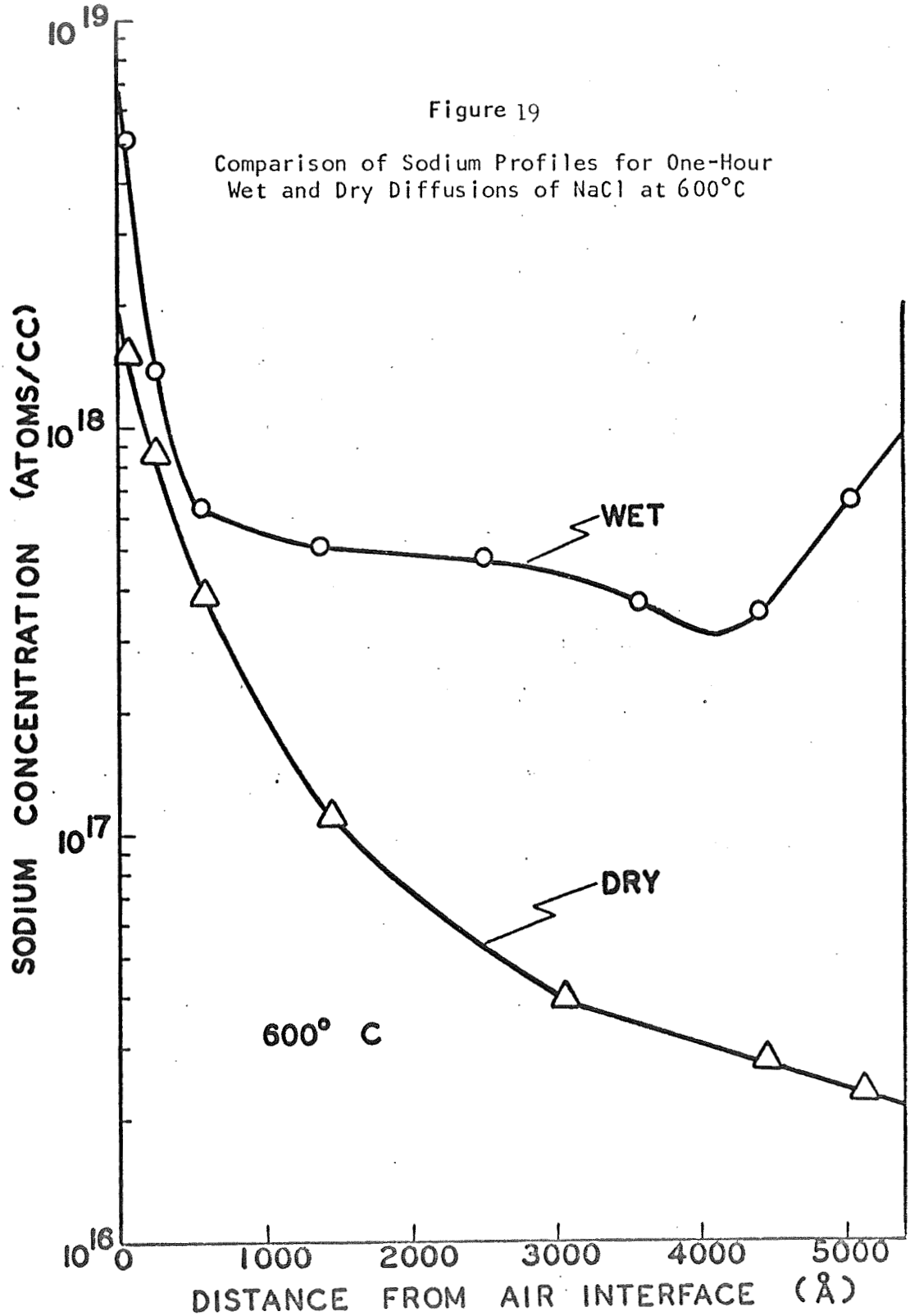

Figure 20

Sodium Profiles for Dry Diffusion
of NaCl at 800°C

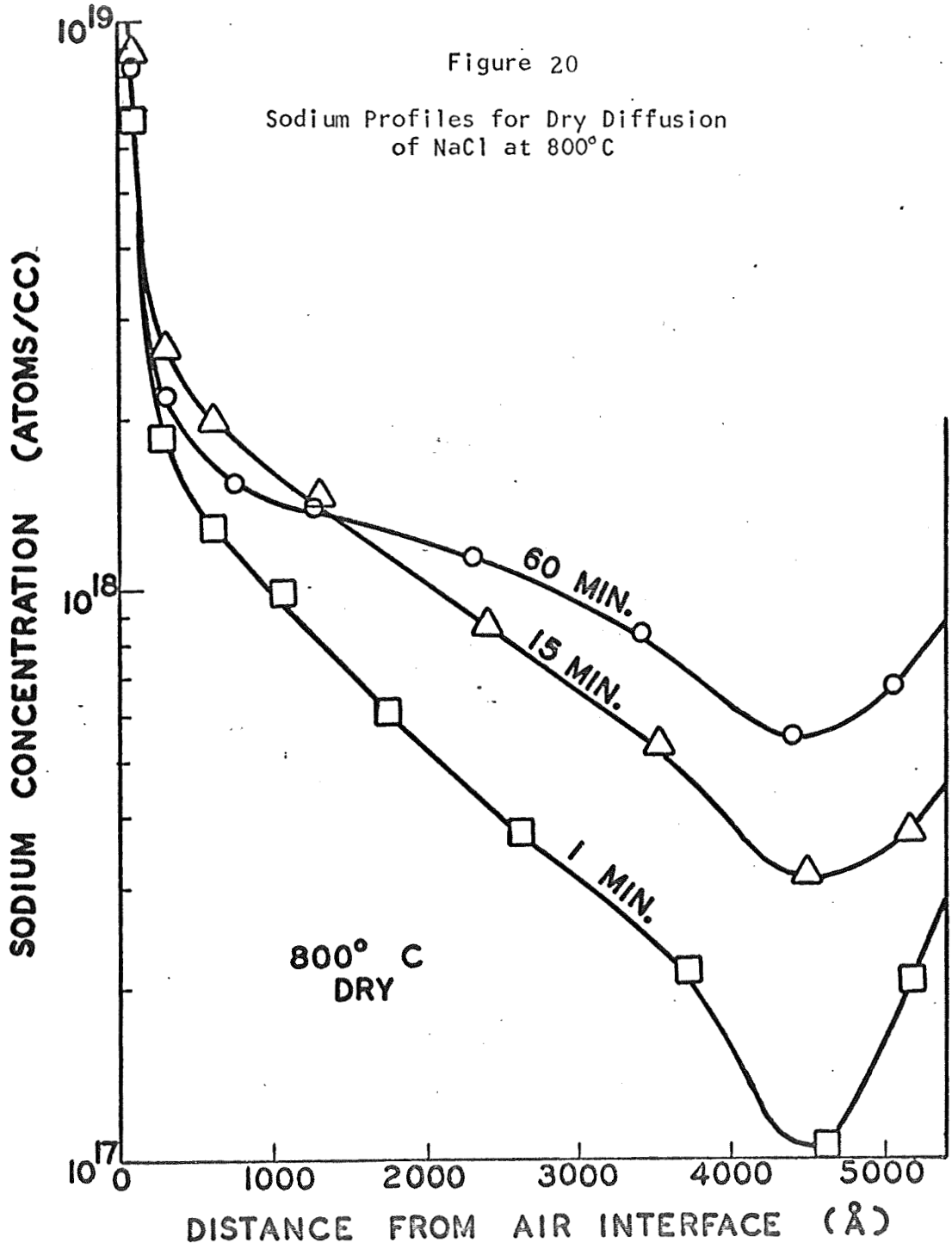

Figure 21

Sodium Profiles for Wet Diffusions
of NaCl at 800°C

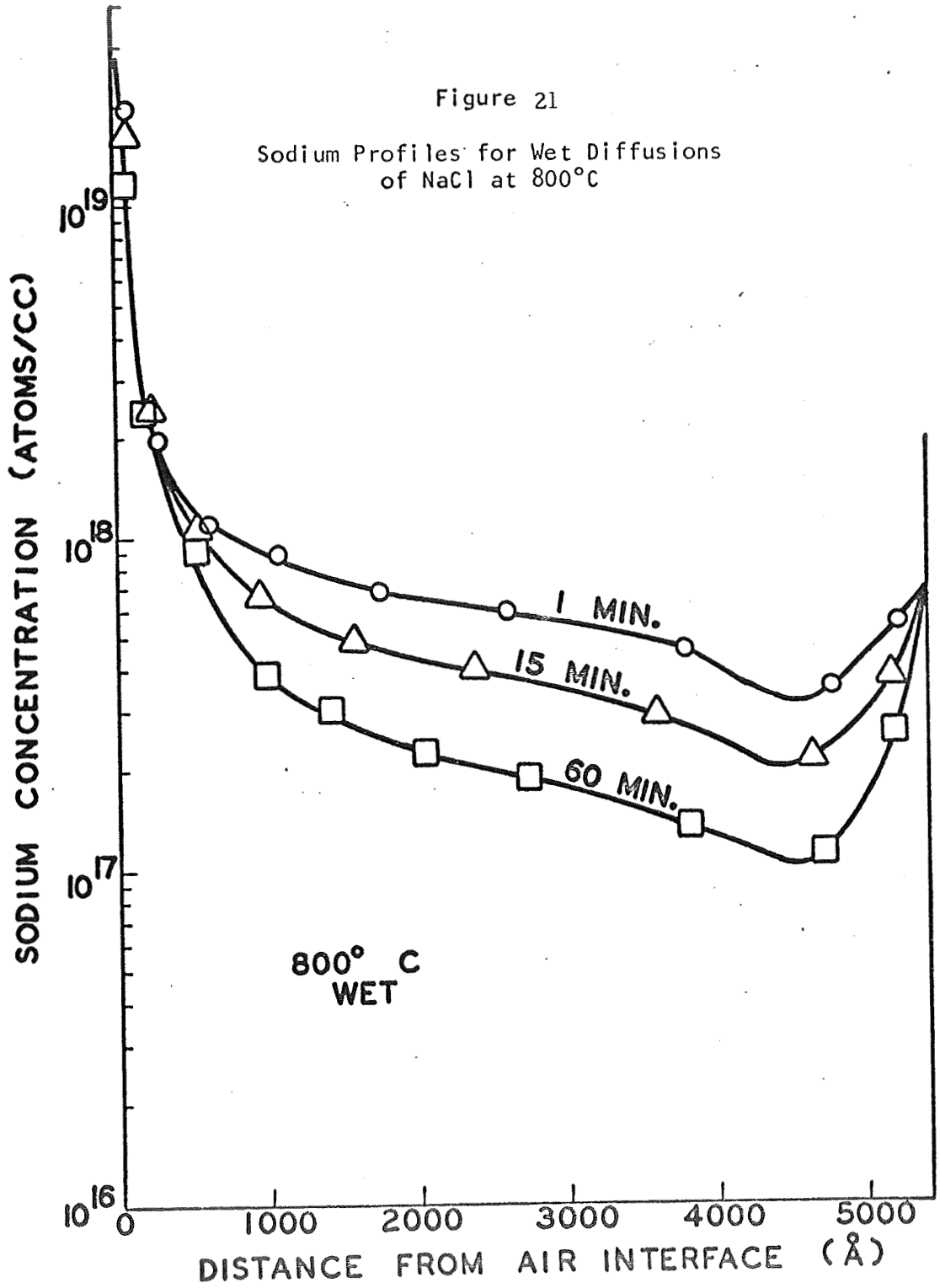

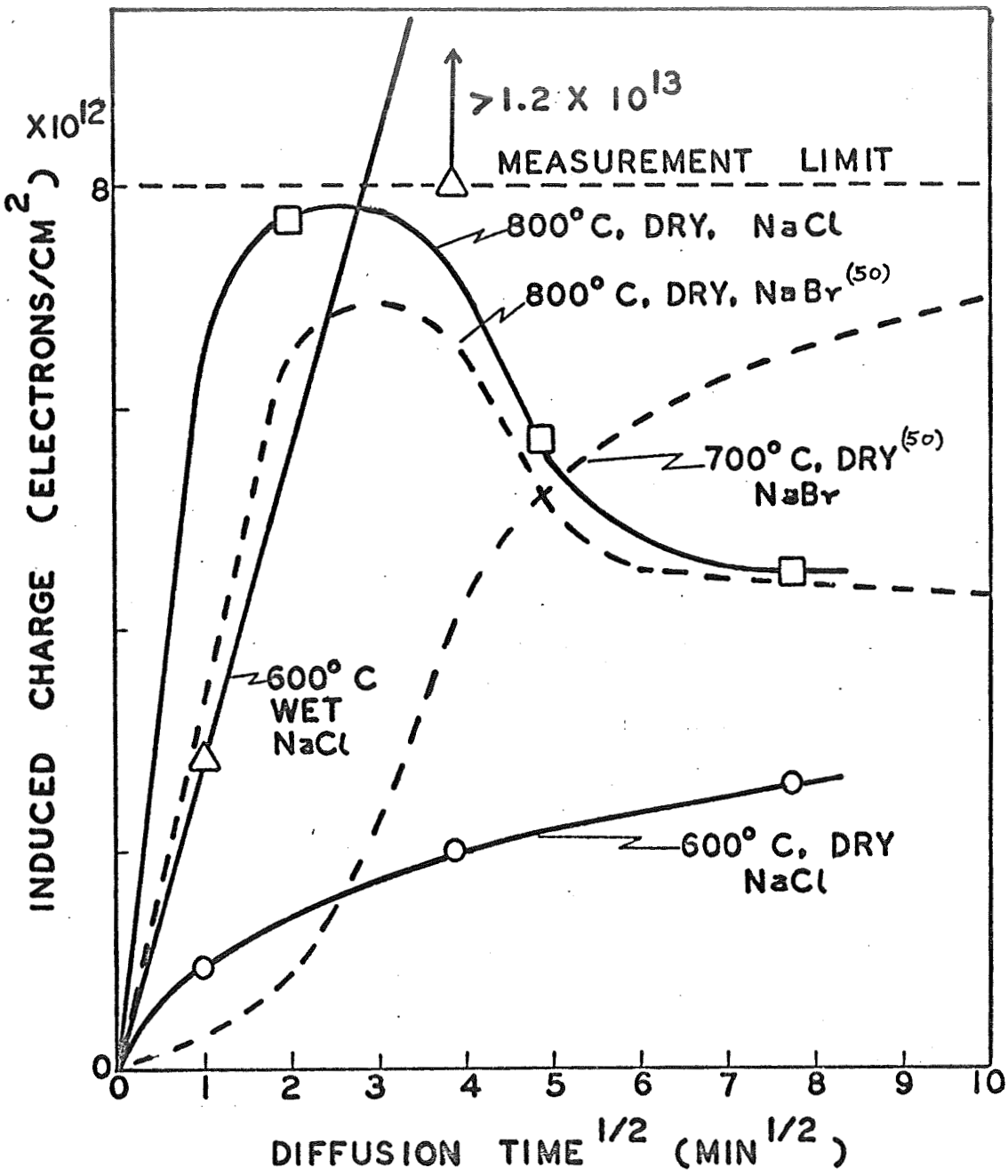

Figure 22

Variation of MOS-Measured Charge with
Diffusion Time for NaCl

Figure 23

Effect of Sodium Contamination on Hydration

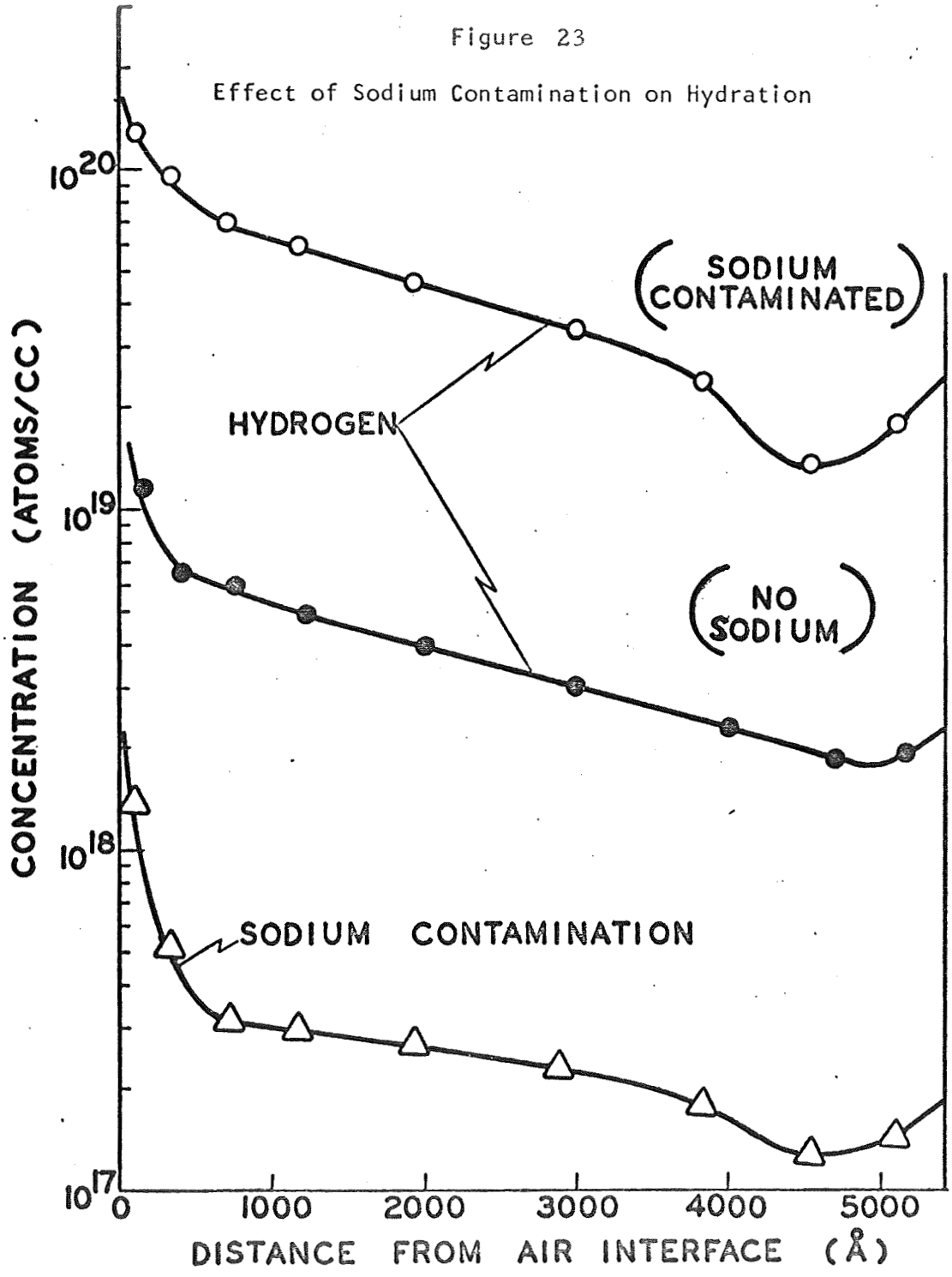

III. INTERFACE STATE MEASUREMENT BY MOS LOW TEMPERATURE TRANSIENT CAPACITANCE

It is the purpose of this investigation to study some characteristics of interface states in the silicon-silicon dioxide system. In particular, features affecting low temperature MOS C(V) characteristics will be stressed.

Theoretical analyses of models proposed for the observed relaxations are presented and compared to experiment.

With the increasing use on solid-state devices of silicon dioxide films for their passivating and masking abilities, the silicon-silicon dioxide interface structure has gained, during the last few years, fundamental importance in solid-state device technology.

One of the major causes of instability and degradation of the electronic properties of these devices is the existence of energy states within the forbidden energy gap at the silicon-silicon dioxide interface. The characterization and understanding of these interface states, therefore, is of major importance.

One of the most successful and powerful techniques used in the investigation of interface states is that developed by Gray and Brown[53]. Their method consists of observing the flat-band voltage shift of the differential capacitance versus bias, C(V), characteristics of metal-oxide-silicon (MOS) structures. Low temperature C(V) characteristics, however, exhibit a complex structure.

Understanding of this structure is fundamental to proper interpretation of information about the density of interface states. Also the possibility arises of extracting additional information from low temperature C(V) characteristics. Considerable effort has been expended in such investigation[54-55].

1. General Observations on the 77°K C(V) Characteristics

An n-type substrate and the existence of interface states will be assumed for illustrative purposes. Characteristics obtained in the dark will be considered first.

Figure 1.1 shows typical C(V) curves at room temperature and at 77°K. For convenience, different regions are identified by the numerals enclosed in circles.

As the temperature is lowered, the flat-band voltage is shifted along the bias axis by an amount, ΔV_{fb}, which depends on the density of interface states, N_{is}, and on the position of the Fermi level.

Thermal generation of carriers is extremely small at 77°K. As a result, when the bias is swept toward the inversion region in the dark, even for very small sweep rates ($\leq$ 10 v./sec.), the minority carriers cannot accumulate at the interface in sufficient numbers to terminate the electric field. Thus, a deep depletion transient is obtained. This is shown in Figure 1.1 as the region

from 1 to 2.

Relaxation in the capacitance takes place throughout the deep depletion transient. If the bias is held constant in this region, the capacitance increases at a rate that decreases rapidly with time. Thus, after a few minutes, the capacitance has risen only about one third of the way toward the theoretical equilibrium value. At this point, it may take hours to detect any further relaxation.

If, after some relaxation has taken place, the bias is increased positively, the capacitance increases in such a way that the slope of the curve thus obtained is the same as the slope of the deep depletion transient curve at the same level of capacitance. The change in electric field, therefore, is being followed by the majority carriers (by an appropriate decrease in the depletion region width). The implication is that the relaxation charge is not only difficult to accumulate at the interface but, once there, is also difficult to remove.

When a certain bias, V_t is reached, the abrupt termination of the deep depletion transient is marked by a sudden increase in the capacitance to a new level, C_t. Relaxation, similar to that corresponding to the deep depletion transient, continues after C_t is reached.

Decreasing the negative bias (moving toward accumulation), will make the capacitance rise to a new level (point 3). When the

bias is about 10 to 30 volts more positive than V_t, another increase in capacitance is observed which levels off within a few volts. This "ledge" or "plateau" (point 4) continues till the curve raises again to meet the accumulation trace, where the curve is retraceable in either direction.

Most of the MOS structures prepared had a thick layer ($\sim 5 \times 10^3$ Å) of Al for the field plate. Even though for this thickness the Al field plate is opaque, light has marked effects on the characteristics. We now discuss these effects.

The relaxation rates throughout the deep depletion transient increase with light intensity, the increase being such that, even for relatively fast bias sweep rates ($\sim$50 v./sec.), the curve is substantially displaced vertically from the corresponding curve in the dark. If the bias is held constant in this region, the capacitance will rise to a level slightly above the "plateau" in a few seconds.

If the light is turned off after some relaxation has taken place, the relaxation rates are immediately reduced to a value which depends on the level of capacitance already reached. The distance to the plateau can be divided roughly in two regions such that relaxation rates immediately after the light is turned off are momentarily negative in the upper region and become practically zero in the lower region.

Since the theoretical thermal equilibrium curve lies between

the deep depletion transient curve and the plateau, it would seem logical to expect this behavior. The argument is that the extra minority carriers generated by the light are responsible for the momentarily negative dC, dt as their concentration is reduced when the light is turned off in the upper region and the system tries to return to equilibrium. No such reduction in the concentration of the minority carriers takes place in the lower region where their number is at all times less than that required by thermal equilibrium.

There exists at present no known method for obtaining experimentally the thermal equilibrium C(V) characteristics at low temperature. The use of the dC/dt behavior under light would seem a plausible way of achieving this. An attempt at obtaining the demarcation line between the two regions mentioned above, however, yielded an erratic curve from which no particular relation with the theoretical thermal equilibrium curve could be observed.

As in the dark, the abrupt termination of the deep depletion transient is marked by a sudden increase in the capacitance, this time when the bias corresponding to the left edge of the plateau is reached. The capacitance then becomes slightly larger (up to 5% of C_{oc}) than the capacitance corresponding to the plateau. The curve can then be retraced in either direction and will follow the contour of the curve obtained in the dark although slightly displaced vertically from it.

It has already been mentioned that the Al metal field plate on most samples is opaque. This implies that either light enters through the edge of the MOS structure, or that the minority carriers generated in the surrounding area communicate with the silicon under the metal field plate. In either case, this is an "edge effect".

In order to investigate to what extent the edge controls the effects of light on the relaxation mechanisms, a special MOS structure was prepared with a thin ($\sim 600\text{Å}$) translucent Al field plate. The shape of the C(V) characteristics for moderate light remained unchanged, indicating that the "edge effect" does not introduce any extraneous effects. Sensitivity to light, however, was greatly increased. Under strong light, the deep depletion transient totally disappeared and the curve was retraceable in either direction. Even under such conditions, however, the plateau remained.

1.1 The Deep Depletion Transient

We now examine more closely the deep depletion transient and the relaxation mechanisms present in it.

The deep depletion transient can be used to obtain the doping profile of an MOS substrate using the relationship

$$N_D(C) = \frac{1}{e\epsilon_s} \quad \frac{C^3}{\frac{dc}{dV}} \qquad (1)$$

Figure 1.2 shows the results of a plot of $(C_{ox}/C)^2$ versus applied bias for two samples of different resistivities. The accompanying table shows the values for the doping density calculated from resistivity measurements (obtained by the four-probe method), $(N_D-N_A)_o$, the ratio of inversion capacitance to oxide capacitance at room temperature, $(N_D-N_A)_1$, and the slope of the $(C_{ox}/C)^2$ versus V plots, $(N_D-N_A)_2$.

It will be seen that for the two samples used, (N_D-N_A) calculated from resistivity measurements is the smallest. This suggests a redistribution of the doping concentration, possibly due to the heat treatments to which the samples were subjected after their resistivity was measured. The discrepancies (average deviation $\simeq$ 13%) can be accounted for by experimental errors such as uncertainties in the oxide thickness, and in the measured values of resistivity.

It should be noted that the plotted points fall very closely in a straight line. This is an indication that the measurements correspond to a deep depletion transient. Measurements taken at bias sweep rates of ~200 v./sec. indicate a much faster relaxation takes place during the first few fractions of a second. This fast component of relaxation has also been observed by Goetzberger[55].

The amount the capacitance relaxes in the deep depletion transient in a given time interval is a function of the bias, decreas-

ing as the bias approaches V_t. This, however, is not in itself evidence that the rate of accumulation of minority carriers at the interface decreases with increasing depletion region width, but rather that the relaxation mechanisms effects on the capacitance are reduced as they compete with an increasing depletion region width.

Some of the theoretical consequences of some models for the relaxation mechanisms have been considered. If we assume that the generation of minority carriers occur throughout the depletion region ω, we obtain

$$\omega = \epsilon_s \left(\frac{1}{C} - \frac{X_{ox}}{\epsilon_{ox}} \right) \qquad (1\text{-}1)$$

where

ϵ_s = relative dielectric constant for silicon.
ϵ_{ox} = relative dielectric constant for SiO_2.
X_{ox} = SiO_2 thickness.

Equation (1-1) is compared to experimental results in Figure 1.3. The plot, for the two samples shown, fails to match that predicted by Equation (1-1).

A relaxation mechanism such that the generation of minority carriers is independent of band bending will yield[53]

$$\frac{1}{[C(o)]^2} - \frac{1}{[C(t_o)]^2} = \frac{2}{\epsilon_s C_{ox}(N_D - N_A)} \int_o^{t_o} dt \qquad (1\text{-}2)$$

where $C(o)$ and $C(t_o)$ are deep depletion capacitances at voltages corresponding to zero and to time and $\dot{P}$ is the rate of change of the number of charges per unit area accumulated at the interface due to the relaxation mechanism.

Figure 1.4 compares this equation to experimental results. Theoretically, the result should be a horizontal line. Agreement between theory and experiment is much improved over Figure 1.3. The low capacitance end of the curves corresponds to a very large ($\sim 10^5$ Å) depletion region width. In this region, the amount of relaxation in capacitance is extremely small and the reliability of the corresponding data is considerably decreased. The high capacitance end of the curves corresponds to the onset of the deep depletion transient, where the assumptions made in the derivation of Equation 1-2 may become questionable. In view of these considerations, it is not surprising to observe that deviations from a horizontal line become more pronounced as either end of the curves is approached.

Consideration of the results of Figures 1.3 and 1.4 suggests the need for a model where the relaxation is independent of the amount of band bending at the interface.

Consider the interface states close to the conduction band of an n-type semiconductor when the system is in the inversion region. Since the height of the potential barrier between any given inter-

face state and the conduction band is a constant, the probability of an electron residing in one of these states being thermally excited over the barrier and into the conduction band does not depend on band bending. As the interface states thus ionized become positive, the depletion region decreases and the capacitance relaxes. This model, then, satisfies our requirements.

The right hand side of Equation 1.2 is proportional to the rate at which the system relaxes, which if our model is to be correct, should be proportional to N_{is}. Averaging the results of the plots in Figure 1.4 yields

$$\frac{N_{is}\ (\text{Sample May 14-B})}{N_{is}\ (\text{Sample May 17-E})} = 2.21$$

whereas the ratio obtained from values of N_{is} measured by the Gray and Brown method is 2.00. The disagreement between the two values can be accounted for by uncertainties in the doping concentration of the silicon and by the fact that the energy range inspected by the low temperature method is somewhat different for the two samples due to their different resistivities.

The theory for the time dependence of such a relaxation model has been evolved for an arbitrary energy distribution of interface states.

Considerable simplification can be made in the equations

if two assumptions are made. Those assumptions are that the energy density of the interface states is a slowly varying function of energy, and that the measurements are taken in a time interval such that the quasi-Fermi level of the interface states traverses a small energy range. The result of these simplifications is

$$\int_{t_1}^{t_2} \dot{P} dt = \bar{N} kT \ln \left[1 + U_2 e^{-U_2 \left(\frac{t_2 - t_1}{\tau}\right)} \right] \qquad (1.3)$$

Figure 1.5 shows the results of a plot of $\int_{o}^{t} \dot{P} dt$ versus $\ln t_o$. The plot is seen to agree well with a straight line. This result is as predicted by Equation 1.3 if it is assumed that, even for the smallest time interval measured (5 sec.),

$$1 << U_2 e^{-U_2 \left(\frac{t_2 - t_1}{\tau}\right)} \qquad (1.4)$$

Equation 1.3 then simplifies to

$$\int_{t_1}^{t_2} \dot{P} dt = \bar{N} kT \ln \frac{U_{2e}^{-U_2}}{\tau} + \bar{N} kT \ln (t_2 - t_1) \qquad (1.5)$$

From the slope and intercept of the plot, then,

$$\bar{N} = \frac{0.96 \times 10^{11}}{kT} = 1.45 \times 10^{13} \text{ cm}^{-2}\text{-eV}^{-1}, \qquad (1.6)$$

and

$$\ln \frac{U_2 e^{-U_2}}{\tau} = 3.61 \qquad (1.7)$$

It should be remembered that the assumption of a slowly varying energy density of interface states implies that the value of $\bar{N}$ given by Equation 1.6 is an average over the energy traversed by the interface states quasi-Fermi level in the time interval under consideration. The value is in agreement with those found by Gray and Brown for interface states energy density close to the conduction band. They report interface states energy densities in the range 1 to 5×10^{13} cm^{-2}-eV^{-1} for a sample with a total density, N_{is}, of about 1.5 times our sample's N_{is}.

A rough estimate of the position of the interface states quasi-Fermi level, E_Q, can be obtained by comparison of our value for the energy density of interface states with those obtained by Gray and Brown for the same total density of interface states. In terms of U, this method yields $U \simeq 23$. Since $U(t=0) \simeq 7$, this would seem to invalidate our assumption that ΔU is small. It should be remembered, however, that a "fast" component of relaxation exists during the first few fractions of a second. This component will, therefore, be responsible for most of the change in U. Time intervals taken after that, therefore, allow relatively small changes in U to occur. This is borne out by the agreement between the

plot of Figure 1.5 and a straight line.

2. Summary of Results

The following list summarizes our investigation of relaxation during the deep depletion transient.

1. Best fit to the data corresponds to a model where relaxation rate is independent of the amount of band bending.

2. The above leads us to consider a model where relaxation is due to thermal discharging of interface states.

3. Theory for the time dependence of such a model is developed. Simplifications of the theory, verified experimentally, allow the experimental determination of average values of interface state energy density in rough agreement with those found by Gray and Brown. τ is also estimated from the same simplified theory.

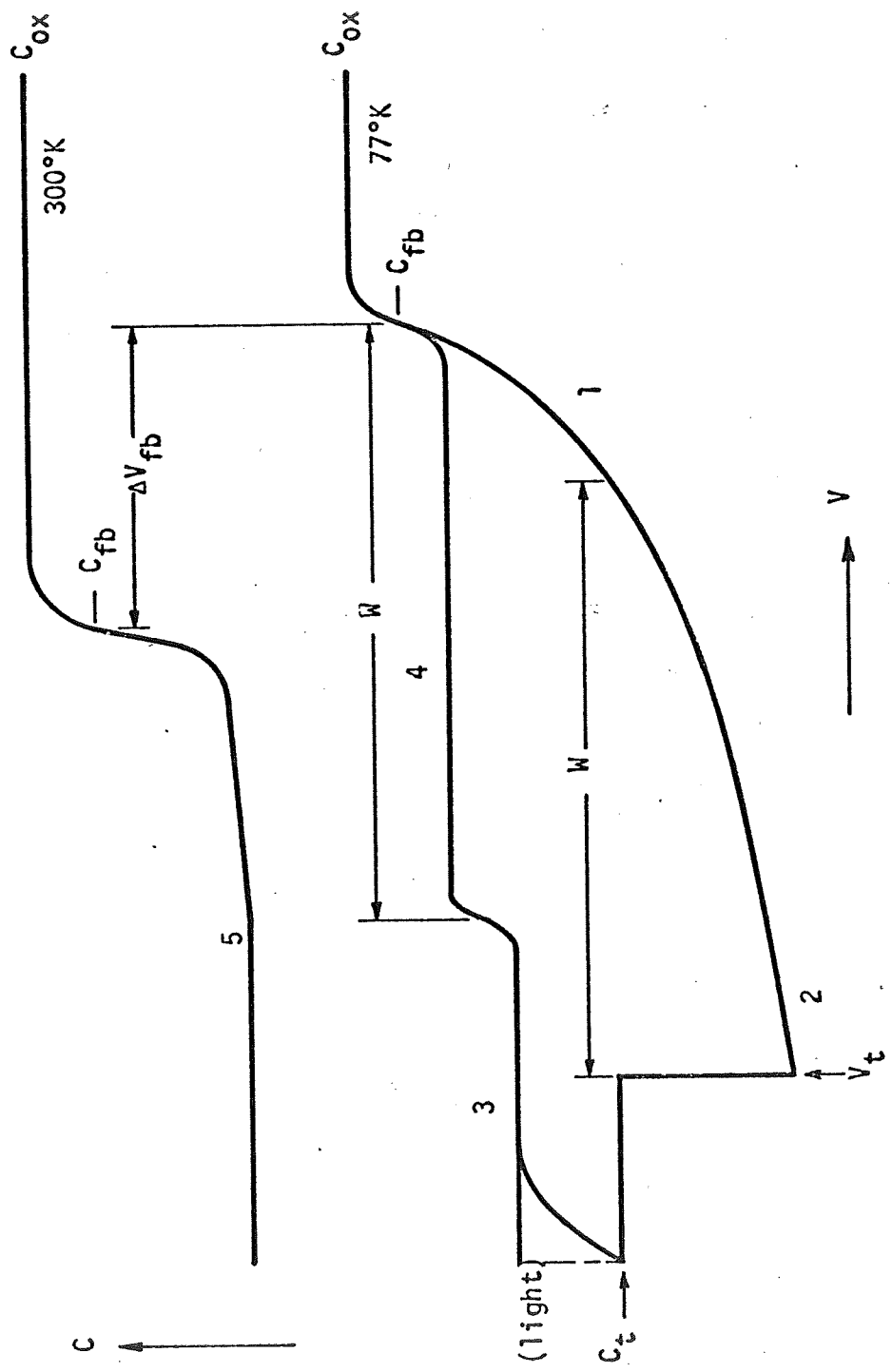

Figure 1.1. Typical C(V) Characteristics of an N-Type MOS Structure at 300 and 77°K.

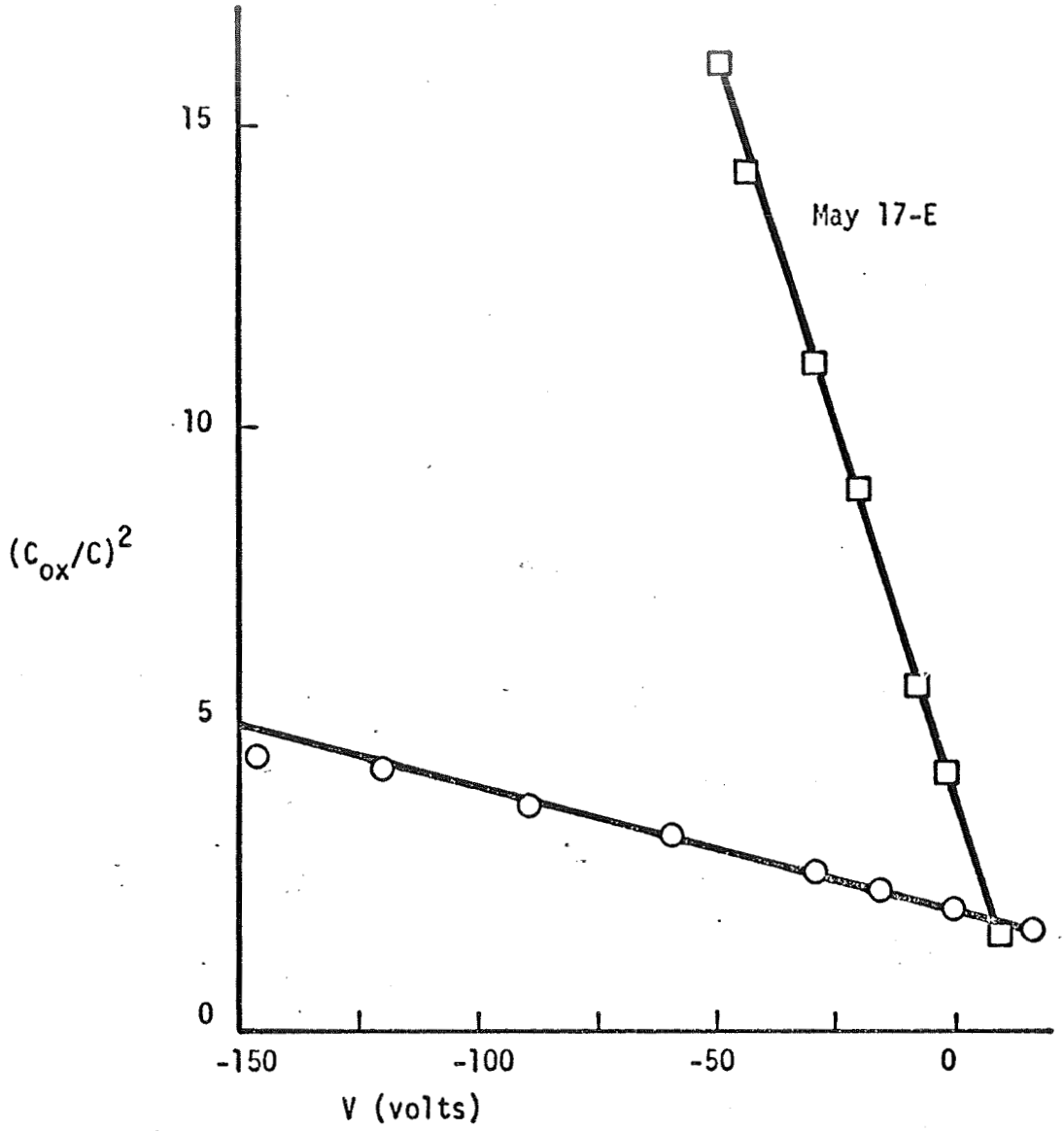

Figure 1.2 $(C_{ox}/C)^2$ versus V within the deep depletion transient region. The table below is discussed in the text.

Sample	$(N_D - N_A)_0$ x 10^{15} cm^{-3}	$(N_D - N_A)_1$ x 10^{15} cm^{-3}	$(N_D - N_A)_2$ x 10^{15} cm^{-3}
May 14-B	15	19.4	23.7
May 17-E	1.7	2.3	1.95

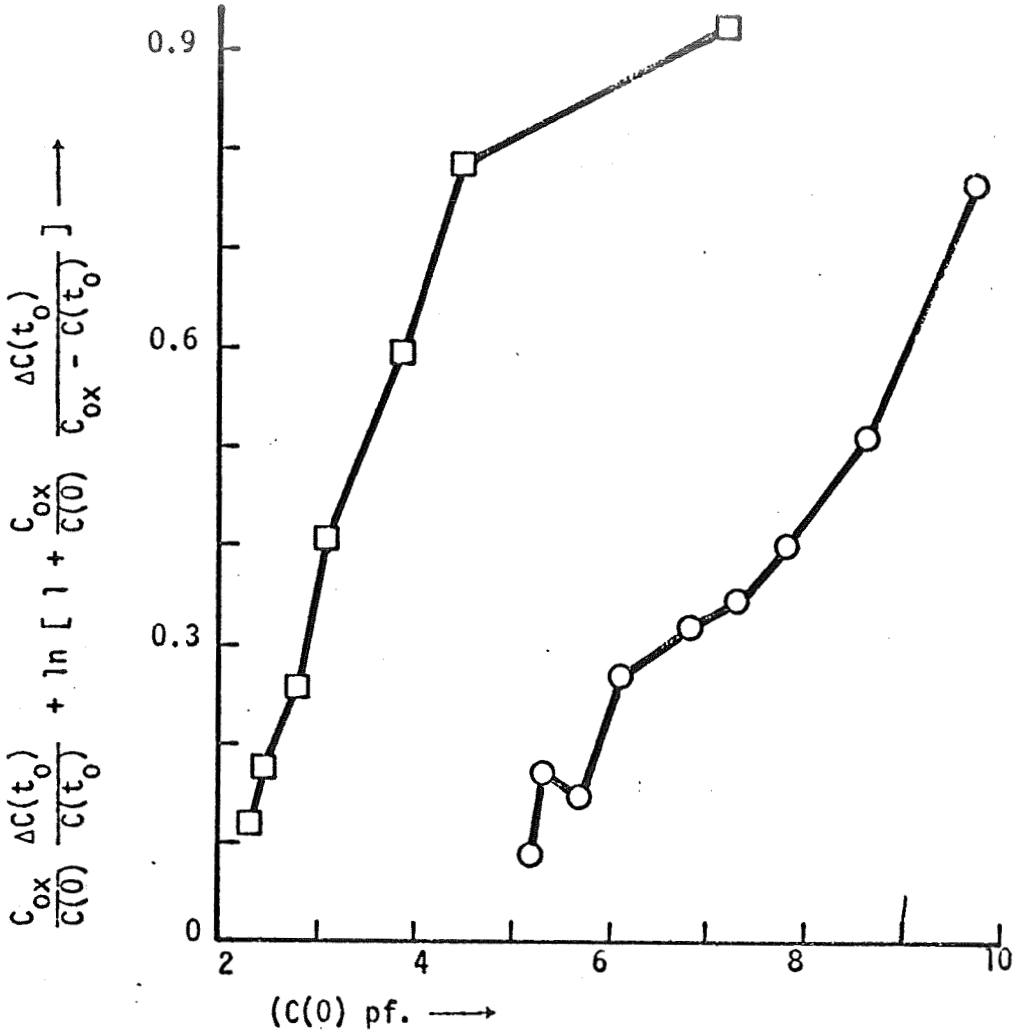

Figure 1.3 Experimental results compared with Equation for t_o = 10 sec. Theory predicts a horizontal line. For both samples: 111 orientation, n-type Si, 5400 A of thermally grown SiO_2. Resistivities are 2.73 and 0.41 Ω-cm. for samples May 17-E and May 14-B respectively.

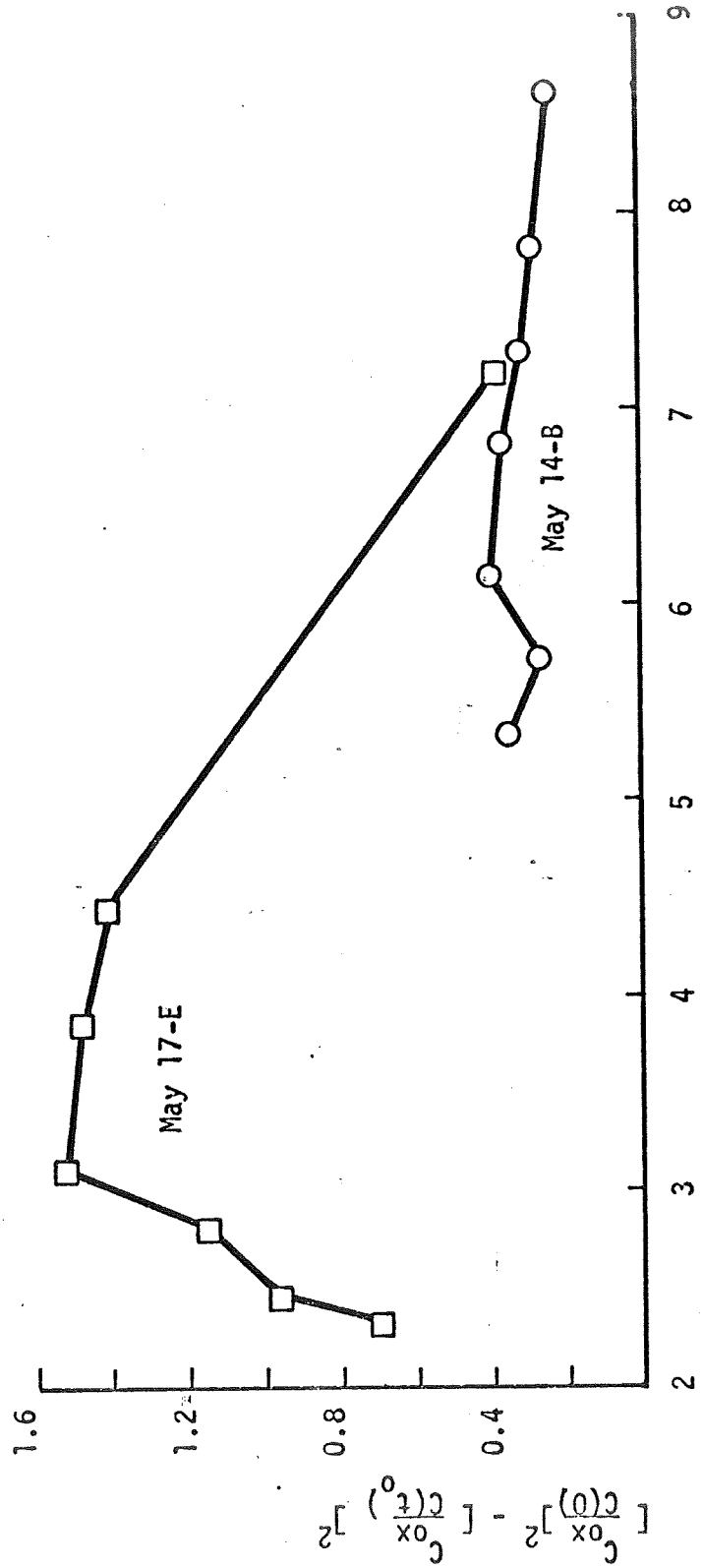

Figure 1.4 $[\frac{C_{ox}}{C(0)}]^2 - [\frac{C_{ox}}{C(t_o)}]^2$ versus C(0) for t_o = 10 sec. Theory predicts a horizontal line. Same samples as in Figure 4.3.

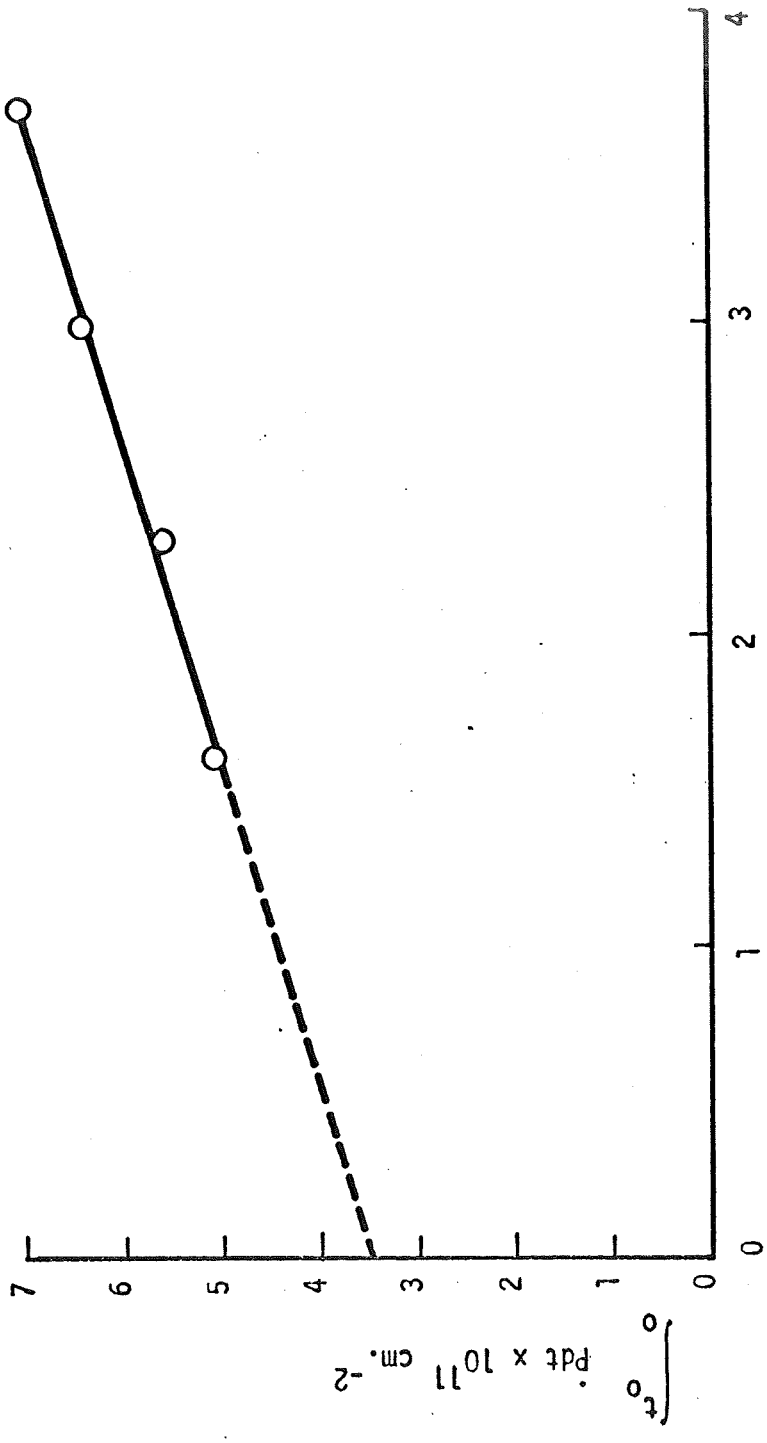

Figure 1.5 $\int_0^{t_o} P dt$ versus ln t_o (t_o in sec.) for Sample May 14-B at V = -15 v. Slope is 0.962×10^{15} m^{-2}.

IV. DEVICE SCREENING TESTS

Mobile ions present on the outer surface of planar silicon devices have an important influence on the device long term stability and performance characteristics. Many investigators have studied the effects of surface ion migration on device characteristics[57,58,59]. Qualitative correlation of device failure mechanisms related to the presence of surface ions on the device oxide and techniques for minimizing the effects of these mechanisms have been presented[60-64]. Actual measurement of ionic transit times have been performed by Schlegel et. al.[65]. The effort of this research is to develop a quantitative screening technique which would indicate the presence and effective quantity of mobile surface ions in a completed device package. This technique should be applicable to standard devices and require no special test structures being incorporated with the device. The technique should also be capable of separating the contribution of surface ions from those produced by other process related failure mechanisms.

Several techniques have been investigated for their applicability of measurement of surface ion effects. These are:

1. Water-film Conductance Measurements.
2. Transient Differential Quench.
3. Low Temperature Reverse Current Characterization.

These techniques and the results obtained using them will be explained in the following sections.

1. Water-film Conductance Measurements

Initial experiments were first directed toward the measurement of current over the surface of oxide passivated devices. The test setup is shown schematically in Figure 1. In the setup shown, the leakage current over the surface of the glass header feedthrough is being measured. The ambient humidity is being established in the Dewar by the use of saturated salt solutions. The particular solutions used are shown in Table I. Leakage tests were made over the surfaces of various glasses at 25°C. The results of one of these tests are shown in Figure 2. The original proposal of this type technique embodied the possibility of observing an easily identifiable conductance anomaly at the ice point of water and the use of this anomaly in the measurement of the quantity of surface ions present on the structure. The anomalous effect can be observed as seen in Figure 3 at high relative humidity. At lower humidity levels, the detection of this anomaly became increasingly difficult. However, as a result of low temperature measurements, an idea for a new approach to the measurement of surface ions developed. The method centered around the use of a transient temperature test to distinguish surface conductance over the oxide from the bulk conduc-

Table I

CONTROL OF R.H. BY SATURATED AQUEOUS SALT SOLUTIONS

% R.H. at 25°C	Salt	gms/100 ml. H_2O for saturation
0%	Drierite	
12	$LiCl$	64g.
33	$MgCl_2 \cdot 6H_2O$	167
66	$NaNO_3$	100
80	NH_4SO_4	76
100	distilled H_2O	

tance. For example, referring to Figure 1, if the copper can were cooled faster than the sample, surface ion contribution from a water film would be reduced as the film was distilled from the sample. This approach, which was called the Transient Differential Quench (TDQ) technique was tested by quenching the test unit from room temperature to approximately $0^{\circ}C$. In Figure 1 a copper tube is shown connected to the test header. In this case, the test samples cooled at approximately the same rate as did the outer can. By removing the copper tube, the sample was isolated and cooled more slowly than the can after quenching. Results of this test are shown in Figure 4. As seen, a delay of approximately 6 minutes was seen before the buildup of channeling current occurred. By the measurement of a sensitive parameter, this simple technique might detect incipient surface failure devices.

2. Transient Differential Quench (TDQ)

Having demonstrated that a TDQ effect could be seen on glass surface conductance in humid encapsulation, a test setup was designed so that commercial devices could be evaluated using this technique. This test offers the possibility of screening poorly encapsulated or surface - dependent devices which have passed static testing. The method used for evaluation consists of quenching the sample and can at different rates and measuring a specific param-

eter as a function of time. The temperature excursion used in the test can be small. The major question to be answered is whether reverse current is a sufficiently sensitive parameter at the low humidity environments normally encountered in device packages.

The test setup for the TDQ techniques using TO-5 devices is shown in Figure 5. The quench temperature used in these tests is $0^{o}C$. The TO-5 can may be heated using the plug heater to accentuate desorption from the can. The leakage current is measured in this setup using a Keithley 610.

Three transistor types were used in these tests. The devices used, and their electrical characteristics, are listed in Table II. Moderately high breakdown collector junctions were used. P-type collectors are expected to be more sensitive to this type measurement because of the known tendency for oxidized silicon surfaces to invert from p type to n type. Two of the transistors that were selected therefore, were pnp. A range of junction areas was selected as evidenced by the C_{OB} values to accentuate junction perimeter effects.

Before transient testing, static I_{CBO}-V_{CB} data were taken on all transistors. This data is shown in Figure 6-9. These Figures will be referred to later.

The I_{CBO} characteristics exhibited a wide range of variation for all device types used. In every case one unit failed to meet

Table II

SILICON TEST TRANSISTOR PARAMETERS

	2N3053	2N2904	2N3741
Mfgr.	RCA	MOT.	MOT.
Config.	NPN	PNP	PNP
Type	Planar	Epi, Annular	-----
Power	medium	low	high
f_T (MHz)	20	200	-----
Header	TO-5	TO-5	power
V_{CBO} (max.V)	60	60	80
I_{CBO} (max)	0.25 ua (30v)	0.02 ua (50v)	0.1 ma (60v)
C_{OB} (pf. max, 10v)	15.	8.	100.
Thermal res. jcn-base	35°C/w.	----	----

I_{CBO} limits set by the manufacturer.

The results of the TDQ evaluation were negative. Typical results are shown in Figure 10. The quench temperature used was $0^{o}C$. The system was well behaved, with quenching of the header resulting in faster cooling than quenching of the can. The current relaxed in one minute and the effects were similar at current levels ranging from nanoampere to microampere range. One limiting problem here is that the limiting thermal transient is set by the semiconductor package. If heat flow is sufficiently fast from the package can to the header, little transient response will be seen.

The experiments did reveal, however, that there was a detectable time - dependence of I_{CBO} at constant V_{CB} . The quench results showed a dependence not only to the timing of the start of the quench but also to the timing of the application of voltage to the junction. This result is indicated in Figure 11 where relaxation of the I_{CBO} of sample No. 6 continues for approximately one minute after reverse bias is applied at room temperature. The standard state for these tests was the diode being short-circuited before time t=0 . The significant fact to note is that the static I_{CBO} characteristics shown in Figure 6 shows virtually no difference between sample No. 6 and No. 7 . The results shown in Figure 11 indicate that sample number 7 responds with the overshoot and relaxation characteristics of the undercompensated long-

time constant of the system. With the same test at the same current loads, sample 6 indicates a clearly observable additional time constant. This implies a time dependent relaxation mechanism which may be surface dependent. Please note in Figure 11-16 that the zero level of current has been suppressed in all plots.

The results of the application of this test procedure to the rest of the similar sample types are shown in Figure 12. It should be noted that sample number 5, which indicated excess I_{CBO} values in room temperature static tests, shows a large, noisy slow relaxation indicating possible surface or hermiticity problems.

It should be noted that a "soft" diode characteristic need not be due to a time dependent surface mechanism. In Figure 13, the transient relaxation characteristics of the collector - base 2N2904 transistor are shown. Sample 4, which had a high static I_{CBO} current, again indicates a large I_{CBO} value, but the transient response shows only system relaxation. The conclusion that is implied is the leakage mechanism for the device is bulk related and not surface dependent.

It was found that the high input impedance of the Keithley 610 picoammeter could lead to serious changes in relaxation times if the full scale range of the instrument was change. This is shown in Figure 14 where overshoot characteristics change as the current range changes. To be useful, therefore, the test procedure

should compare devices against reference devices at the same system settings.

Figure 15 shows that very little change is seen in an "ideal" device by performing the transient test at $0^{o}C$ compared to room temperature. Also shown is the system response to a fixed resistance value. It can be seen that the diode - system interaction introduces a transient of approximately 2 seconds duration which is short compared to the relaxation times that are attributed to surface instability.

In Figure 16, the effect of variation of V_{CB} on the relaxation characteristics of an "ideal" device are shown. The choice of V_{CB} used in the test appears not to be critical.

This technique appears to reveal anomalies which are not seen in static tests and may be capable of distinguishing between surface and bulk incipient failure. Upon consideration, it is seen that what is being measured by this technique can also be determined by examination of the time swept V-I junction characteristic particularly in the time hysteresis exhibited by the characteristic. An evaluation of this was made in the low temperature reverse current characterization.

3. Low Temperature Reverse Current Characterization

Walsh[66] has presented a low temperature technique which

appears to be useful in determining the life capability of semiconductor devices. His technique resolves itself into the following general approach[66].

A. Examination of the electrical charge activity of the "ideal" part using specified design information. If design information is not attainable, then empirically observed data from a measurable V-I characteristic over an extended temperature range is used.

B. Selection of levels of voltage temperature and current that are likely to indicate the presence of extraneous conduction mechanisms in the device.

C. Performance of evaluation tests to determine the level and rates of charge of the conduction mechanisms.

D. Establishment of screening test parameters.

The data presented extends over a temperature range of $+75^{o}C$ to $-125^{o}C$. Walsh was successful in isolating device failures as produced by elevated temperature - stress experiments. His results did not indicate the following:

A. The actual mechanism producing the diode failure i.e. whether the diode exhibited some flaw, produced during the device processing and evidenced under high power optical examinations.

B. The presence of time dependent current leakage mechanisms.

Since his data was taken from measurements at discrete points (10 volt increments) it is doubtful if data was taken to indi-

cate time dependent mechanisms. Cocca[67] investigated the low temperature voltage current characteristic using techniques which can indicate time varying mechanisms. His results indicate that some of the devices investigated indicated breakdown voltage increasing with decreasing temperature and the presence of low temperature increase in reverse current at constant voltage. These devices failed during temperature stress evaluation. It was the results of this work which initiated the low temperature device performance research effort in our laboratory. It should also be pointed out that, chronologically, Cocca's results preceeded both the TDQ and Low Temperature Device test results.

Following Cocca's initial work, low temperature measurements of the reverse bias voltage current characteristics as a possible screening test were initiated.

A test cell was constructed, shown in Figure 17, to investigate these effects. Temperature is controlled by varying the power to the jacket heater, working against a cold reservoir of liquid nitrogen. The test circuit has the capability of plotting a point-by-point voltage characteristic as well as automatically sweeping the diode voltage at a rate of 0.001 Hz to above 10Hz. In order to remove effects of current conduction through moisture condensation across the outside of the diode package, a steady flow of dry nitrogen was maintained across the test diode throughout the tempera-

ture cycle.

The instrumentation setup was evaluated for "built in" hysteresis effects by obtaining the V-I characteristics of a 22 meg-ohm carbon resistor. The upper sweep frequency that could be reliably used without introducing readout errors was determined by obtaining the system response to a step input. Figure 18 indicates the step response of the system. To improve overall response, the system is somewhat undercompensated. The maximum sweep speed will be kept below 0.5Hz to minimize lag in recorder response which can be mistakenly identified as hysteresis.

The devices used in this test were glass-encapsulated 1N3605 diodes. 100 units were used in the evaluation lot. Of the 100 diodes, 5 diodes failed to meet room temperature reverse current leakage tests. The units were separated into two groups. Group A were diodes meeting room temperature specifications and Group B were diodes not meeting specifications. Diodes were then cooled from room temperature to -196^{o}C. V-I characteristics were measured at 25^{o}C increments. The results of these tests are as follows:

(1) Over 20% of the units tested indicated the negative-going hysteresis characteristics of what Cocca has referred to as a non-ideal diode. Figure 19b is an example of this hysteresis.

(2) Diodes of Group B did not indicate the hysteresis of non-ideal diodes.

(3) No change in breakdown voltage was seen for diodes exhibiting non-ideal hysteresis.

(4) In some cases hysteresis characteristics changed as the temperature was lowered. Specifically shown in Figure 19a and b, the hysteresis characteristics of an "ideal" diode were seen at -50°C (Fig. 19a). These characteristics changed at a temperature of -100°C to the non-ideal case.

These diodes were then electrically loaded to 80 milliwatts dissipated power in the forward mode and placed in an ambient of 75°C. The diodes were connected in banks of 6 parallel units and the total current to each bank was continuously monitored. If any device failed, raising the total supply current, the failure would be automatically recorded. At the end of this contract period approximately 1000 hours of test have elapsed with no diode failures observed. At 3,000 hours, the test will be interrupted and all diodes subjected to a complete low temperature evaluation. It is planned that any defective device will be opened and examined in an attempt to determine the cause of failure. These results will be reported as they become available.

The point which still remains unproven is the overall sensitivity of this test procedure to the presence of surface ions. In an attempt to quantitatively determine this, a special diode test structure was designed and fabricated. This structure consists of several diodes having varying perimeter to area ratios and two metal

pads on the surface of the oxide. The complete structure is contained in a .040"x.040" cross-sectional area. The main objective is to construct diode structures which should have varying degrees of sensitivity to the presence of surface ions. These structures will be encapsulated in hermetically sealed flat packs of 5 microliters volume in controlled ambients from 0% RH to greater than 50% RH. The effects of premature breakdown at the junction wall will be controlled by varying the effective radius of curvature at the wall edge. The passivating oxide thickness will also be varied. The thinner the oxide is made, the more susceptible the diode structure should be to the presence of surface ions since the field modifying the Fermi level at the silicon surface will vary inversely as the oxide thickness for a given amount of surface charge on the oxide. The diode structures constructed for evaluation are listed in Table III.

Wafers having the diode structure diffused to a depth of one or three microns were processed in such a way as to have either 1,000, 2,000 or 5,000Å of passivating oxide present at the completion of processing. After the wafers were probed and scribed, one sample from each specific group (i.e. 1μ and 1,000Å, 1μ and 2,000Å, etc.) were placed in the flat pack and wired. The package was then sealed in a specified ambient.

No low temperature measurements have been taken at the

Table III

SPECIAL DIODE TEST STRUCTURE

Substrate:	N type <111> 1Ω-cm
Diode Periphery to Area Ratio:	1.2/mil, 0.6/mil, 0.25/mil.
Dopant Surface Concentration :	10^{21}/cc. Boron
Oxide Passivation:	1,000, 2,000 and 5,000Å
Junction Depth:	1 micron and 3 microns

conclusion of this reporting period. Room temperature measurements indicate, as expected, that the diodes having high periphery to area ratio and thin passivating oxides were extremely sensitive to the presence of humidity in the surrounding ambient. As these tests proceed, complete results will be reported.

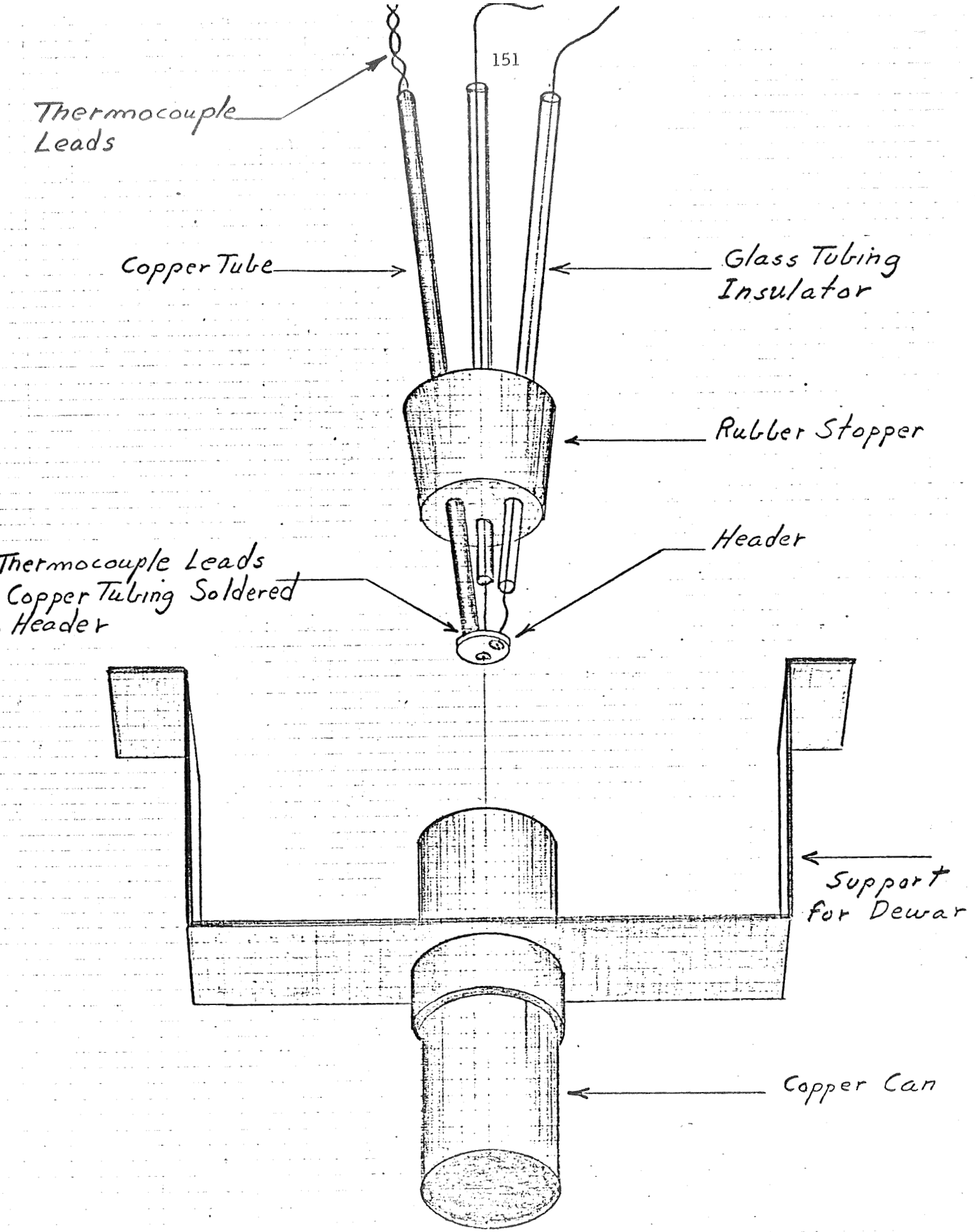

Figure 1. Water-film Conductance Measurement.

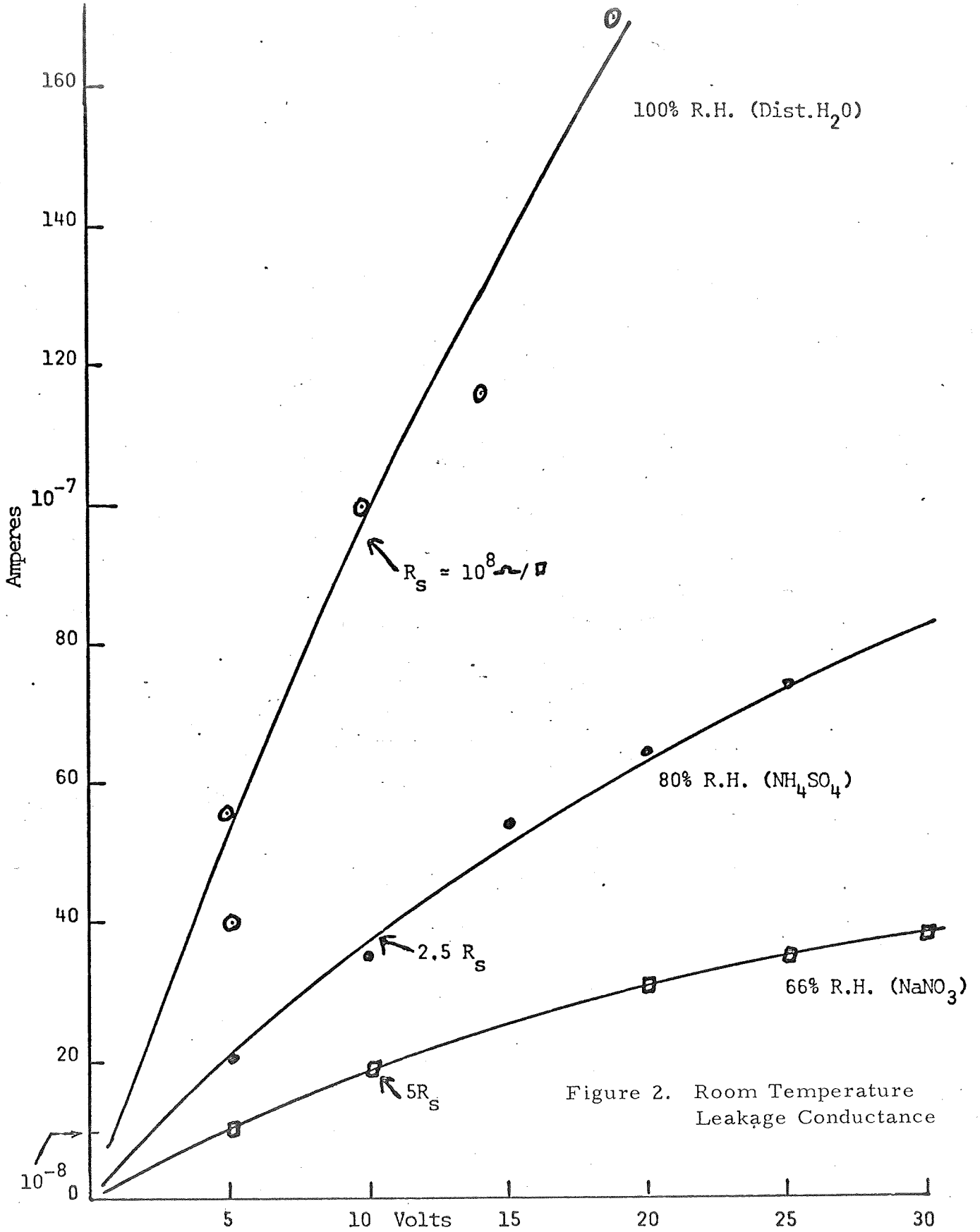

Figure 2. Room Temperature Leakage Conductance

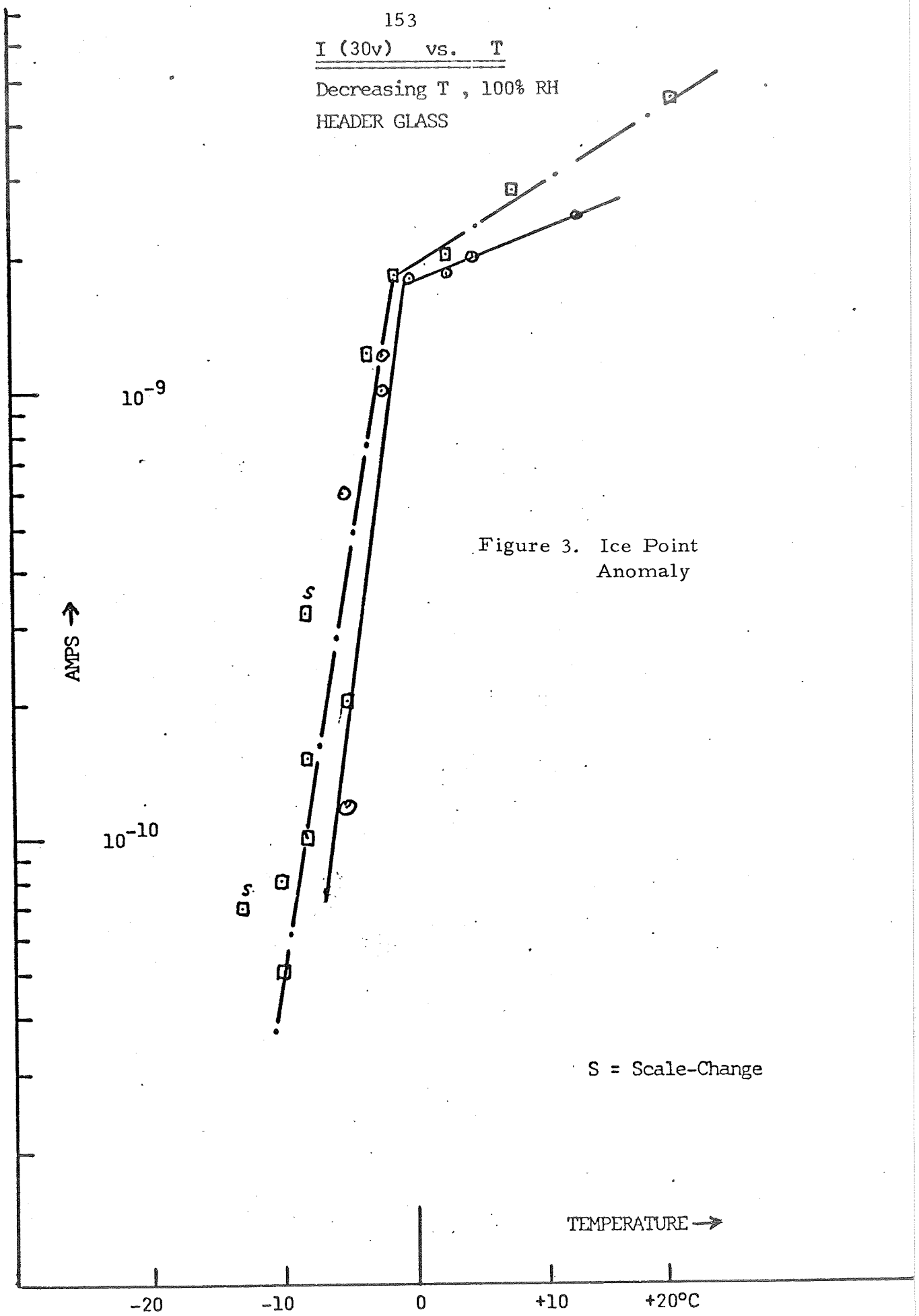

Figure 3. Ice Point Anomaly

S = Scale-Change

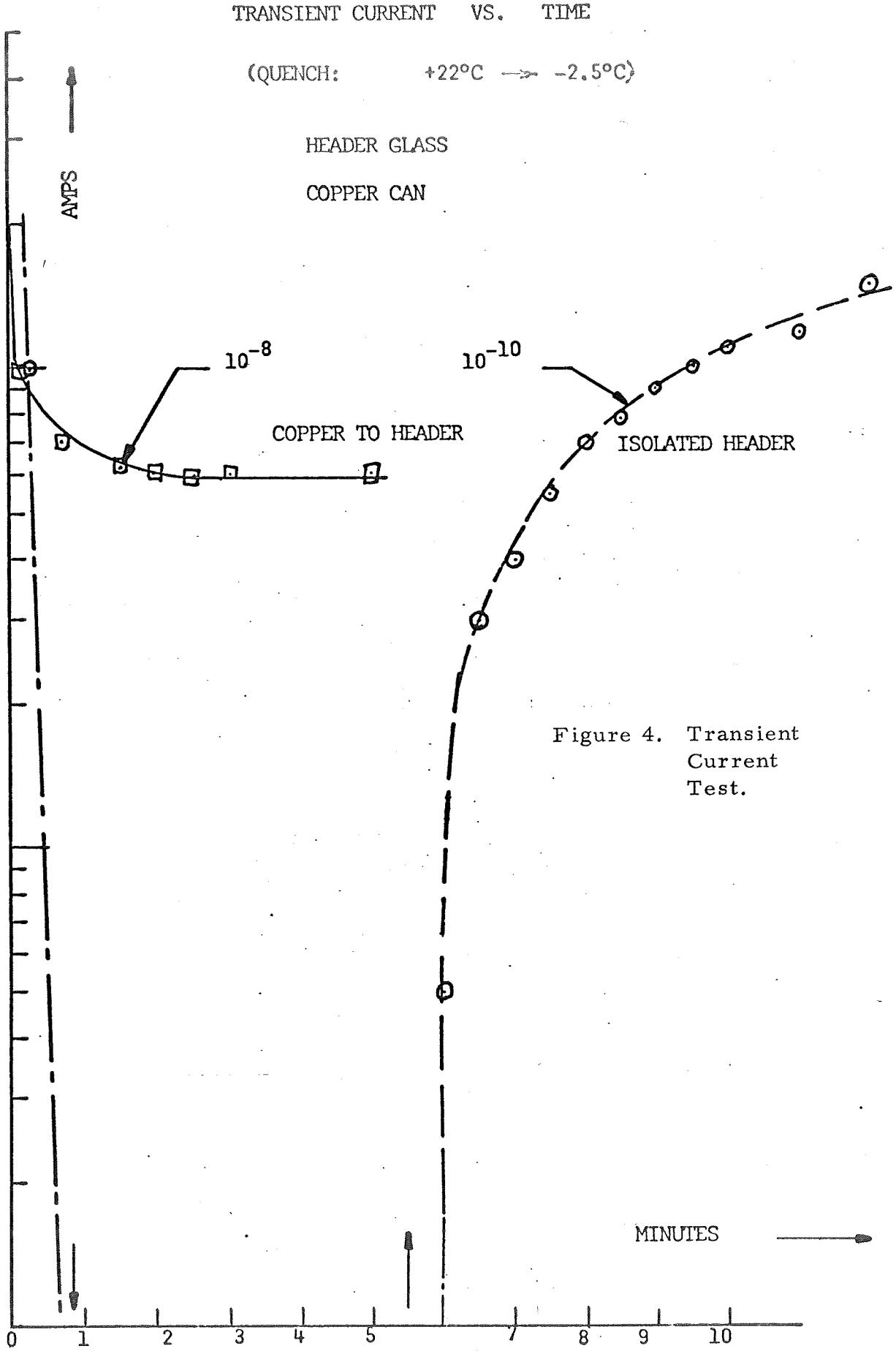

Figure 4. Transient Current Test.

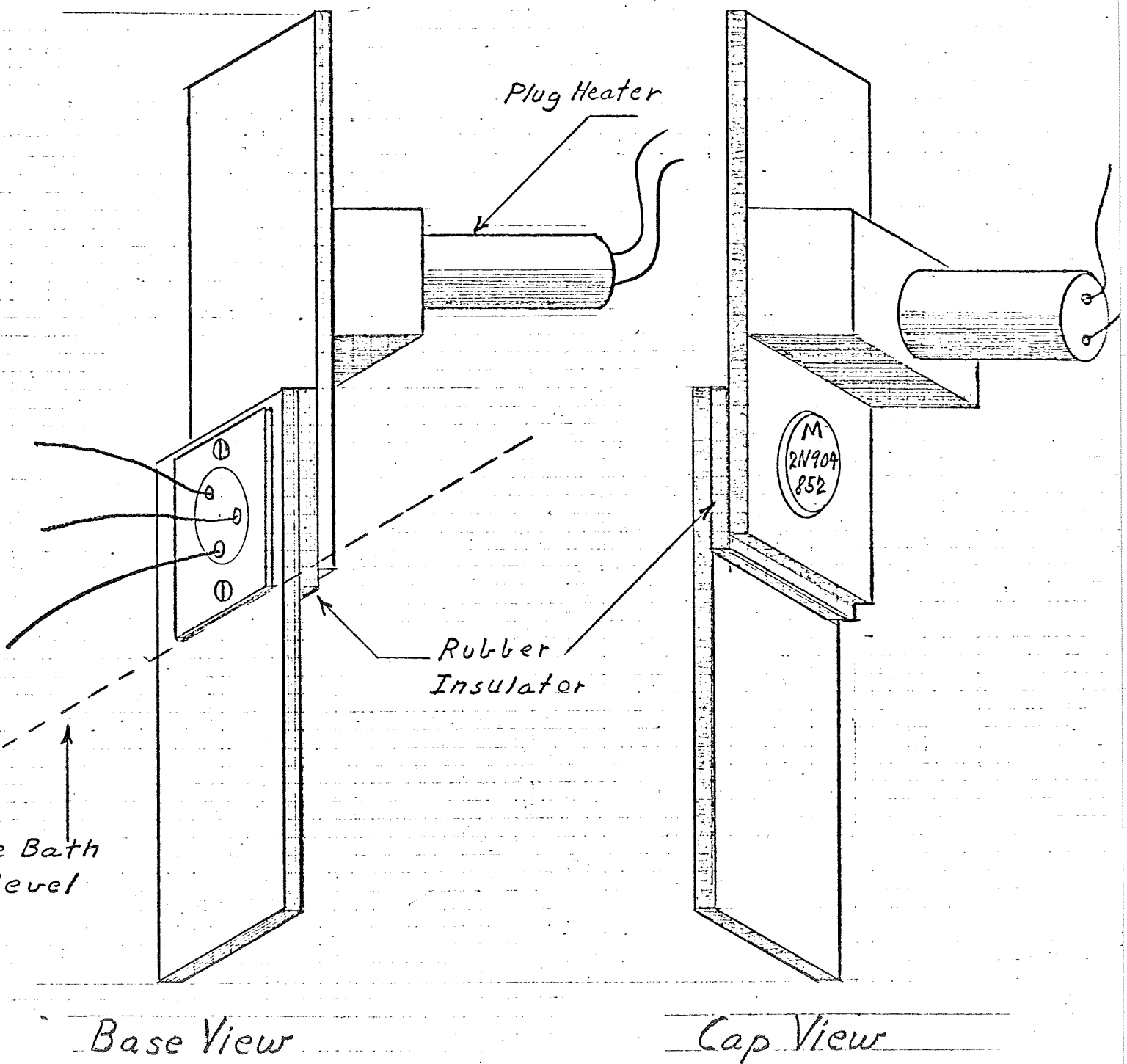

Figure 5. TDQ Test Setup

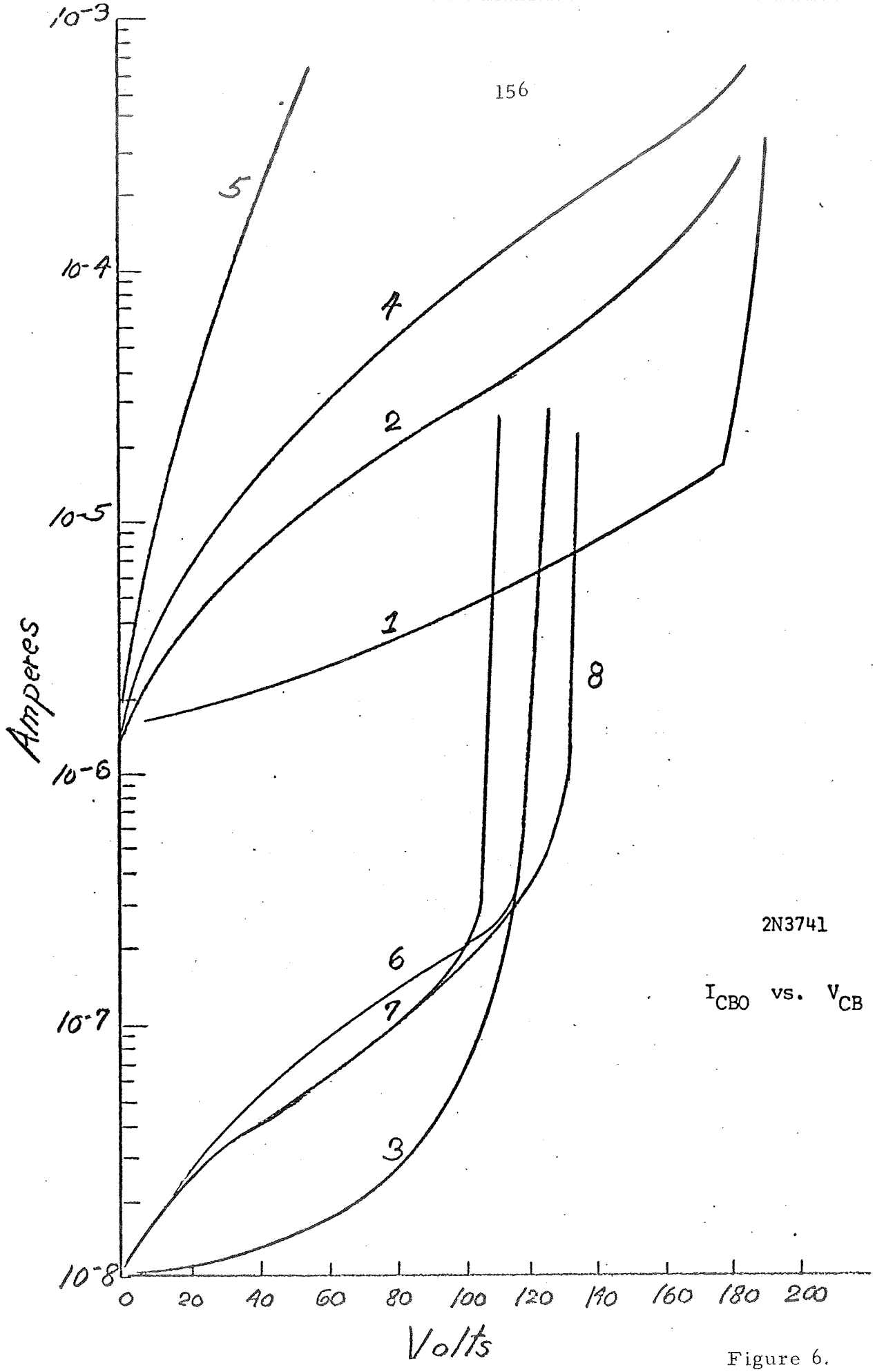
10-3
10-4
10-5
10-6
10-7
10-8
Amperes
0
20
40
60
80
100
120
140
160
180
200
Volts
1
2
3
4
5
6
7
8
2N3741
I_{CBO} vs. V_{CB}

Figure 6.

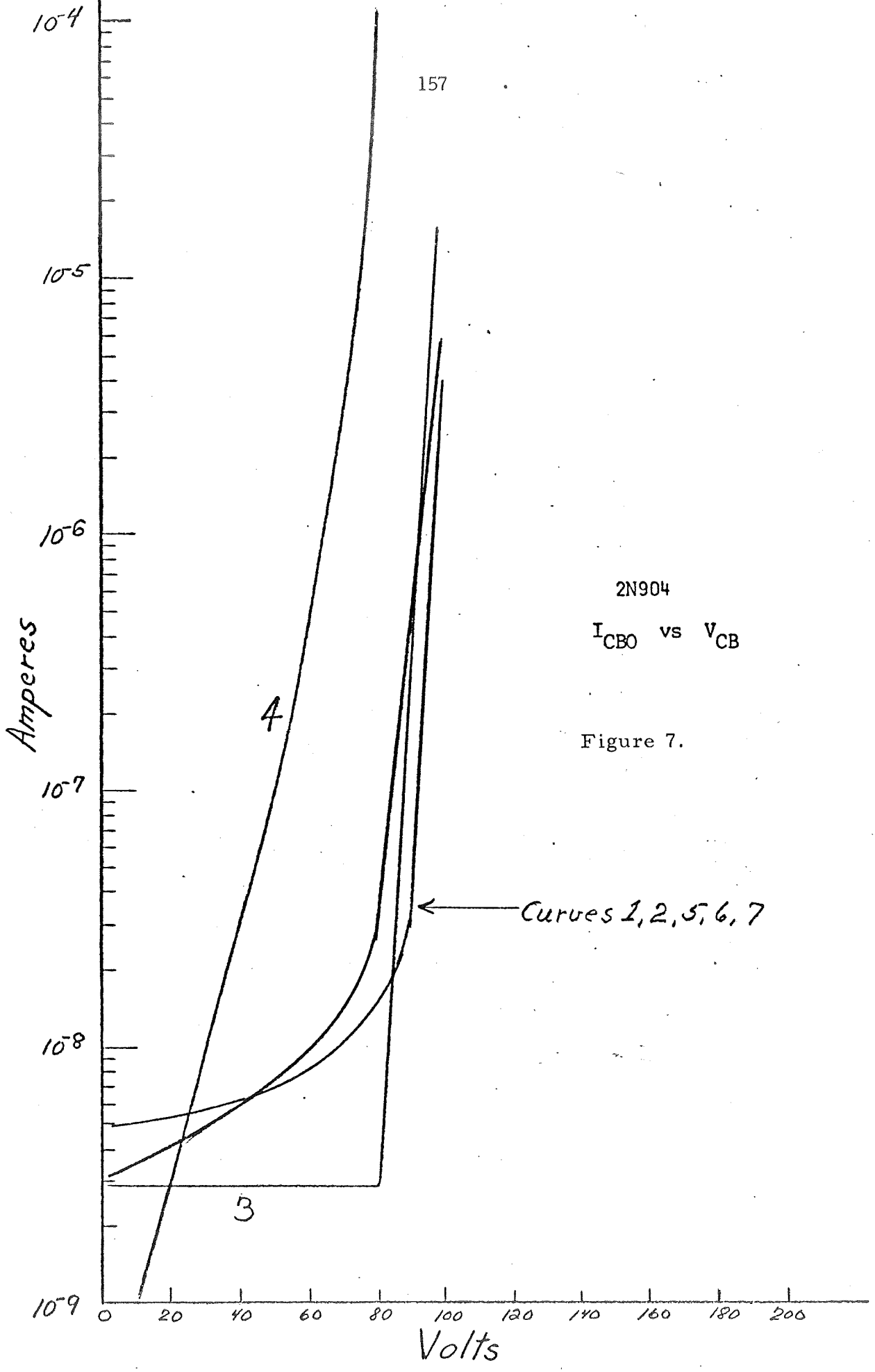

2N904

I_{CBO} vs V_{CB}

Figure 7.

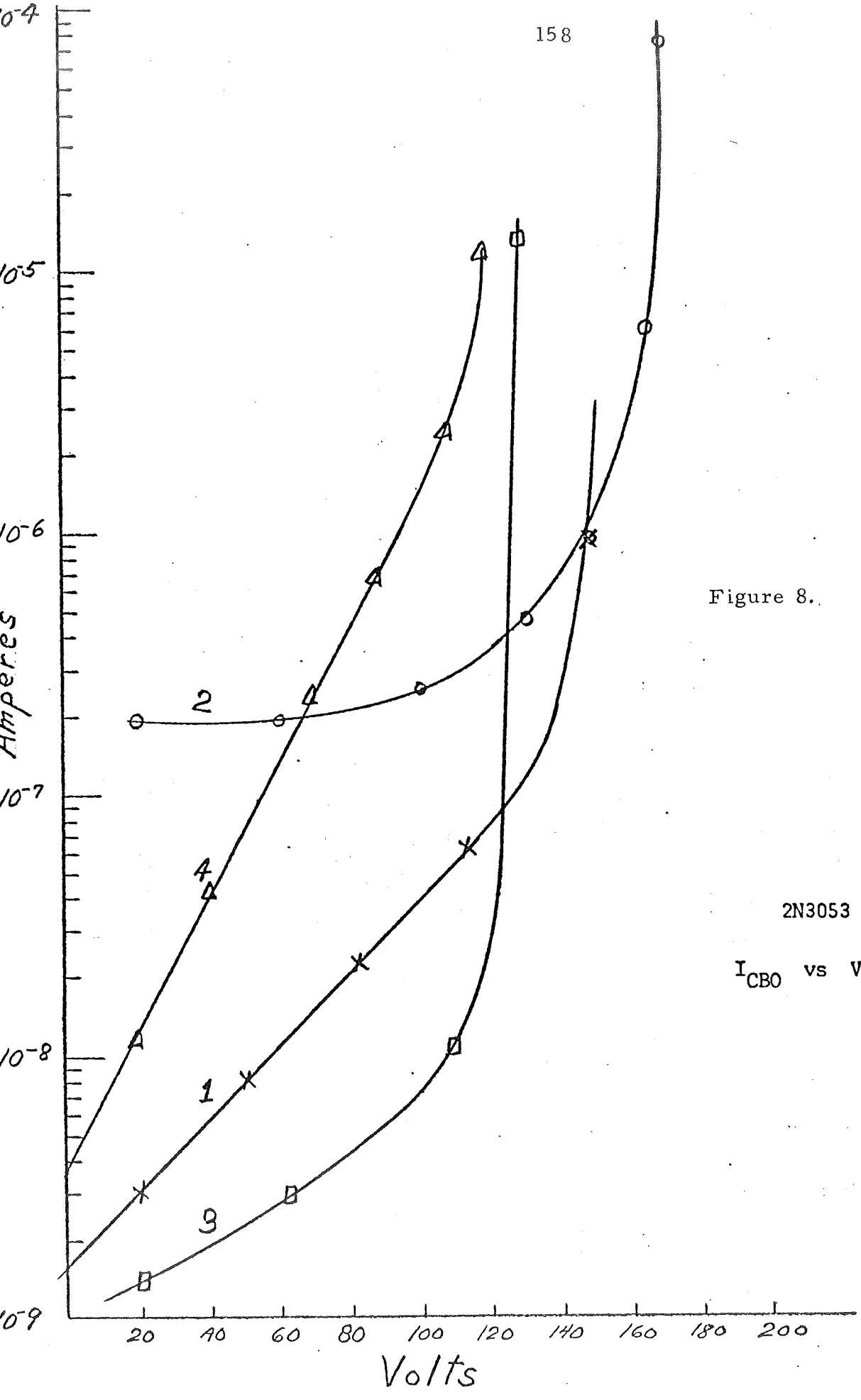

Figure 8.

2N3053

I_{CBO} vs V_{CB}

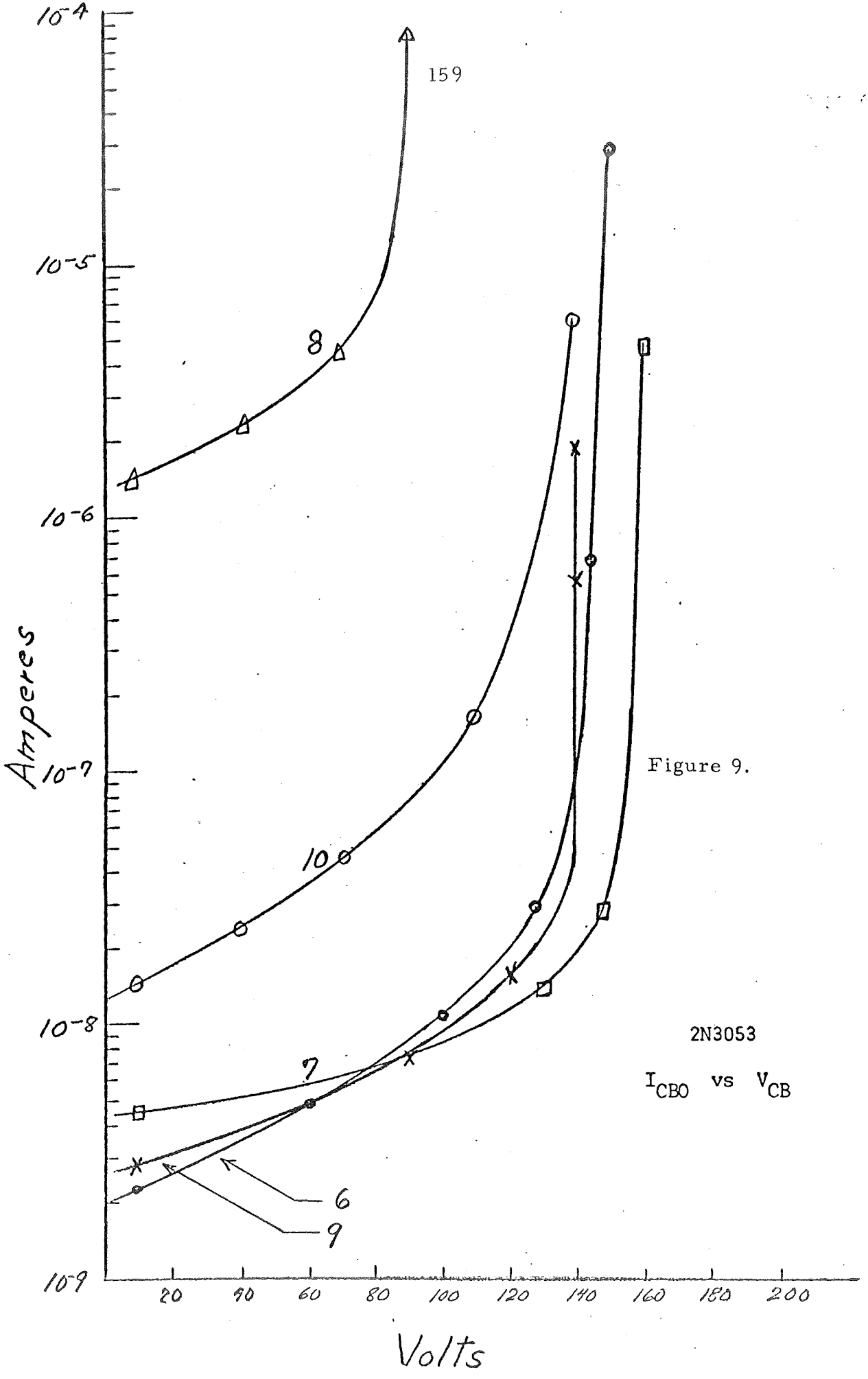

Figure 9.

2N3053

I_{CBO} vs V_{CB}

TDQ --- I_{CBO} vs TIME

QUENCH BATH = 0°C

V_{CB} = 10V

C = CAN QUENCHED
H = HEADER

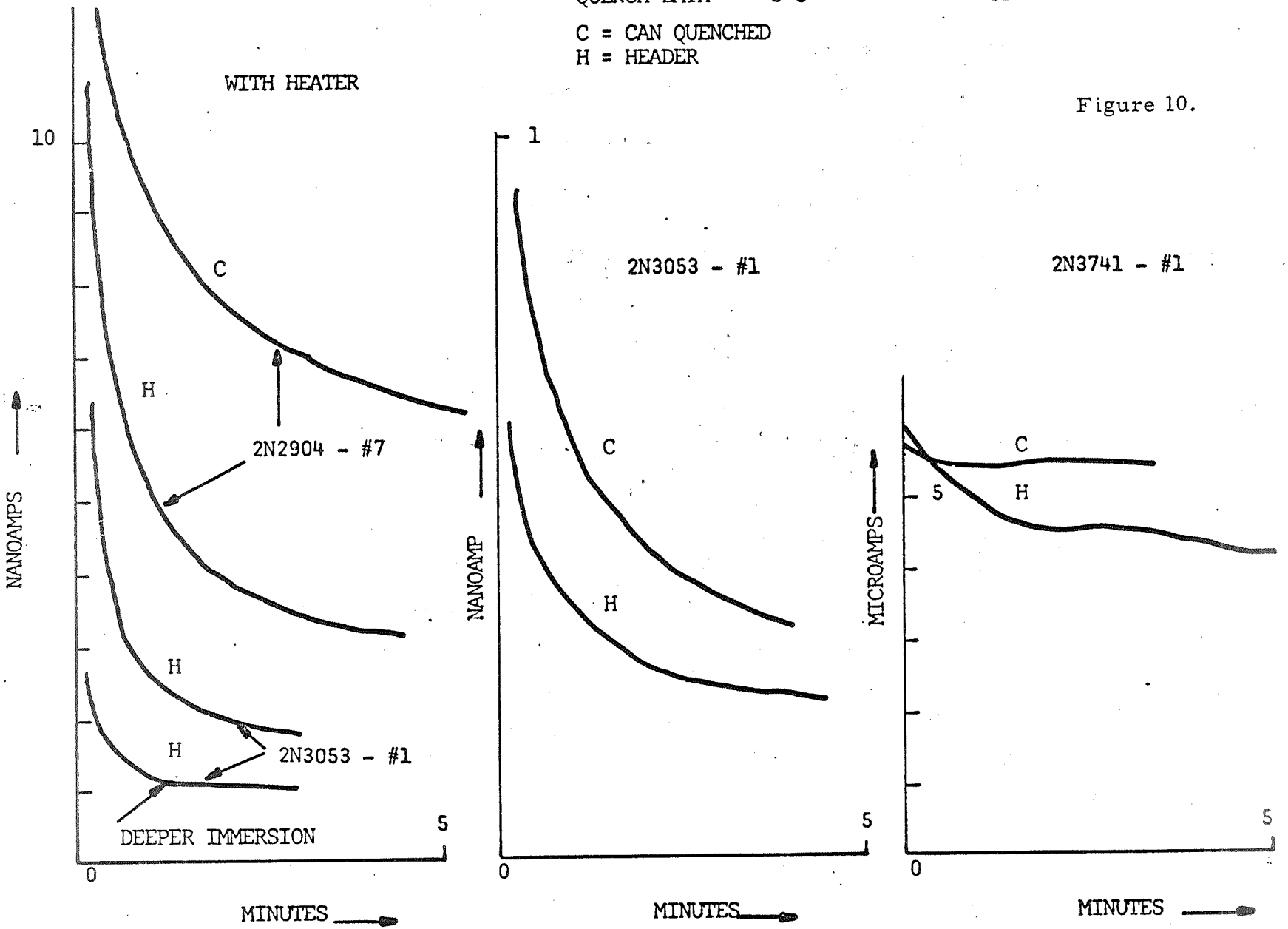

Figure 10.

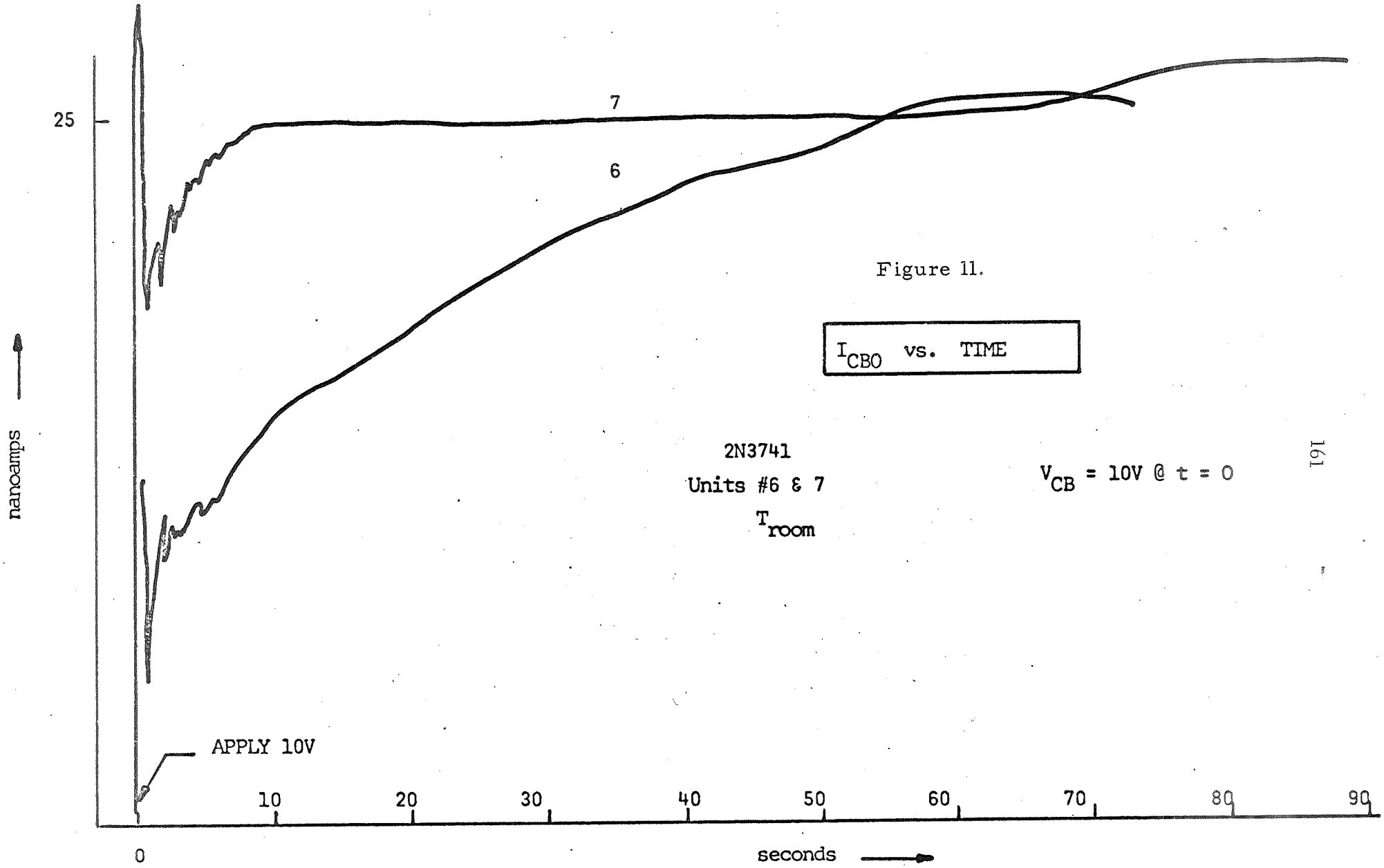

Figure 11.

I_{CBO} vs. TIME

2N3741
Units #6 & 7
T_{room}

V_{CB} = 10V @ t = 0

Figure 12.

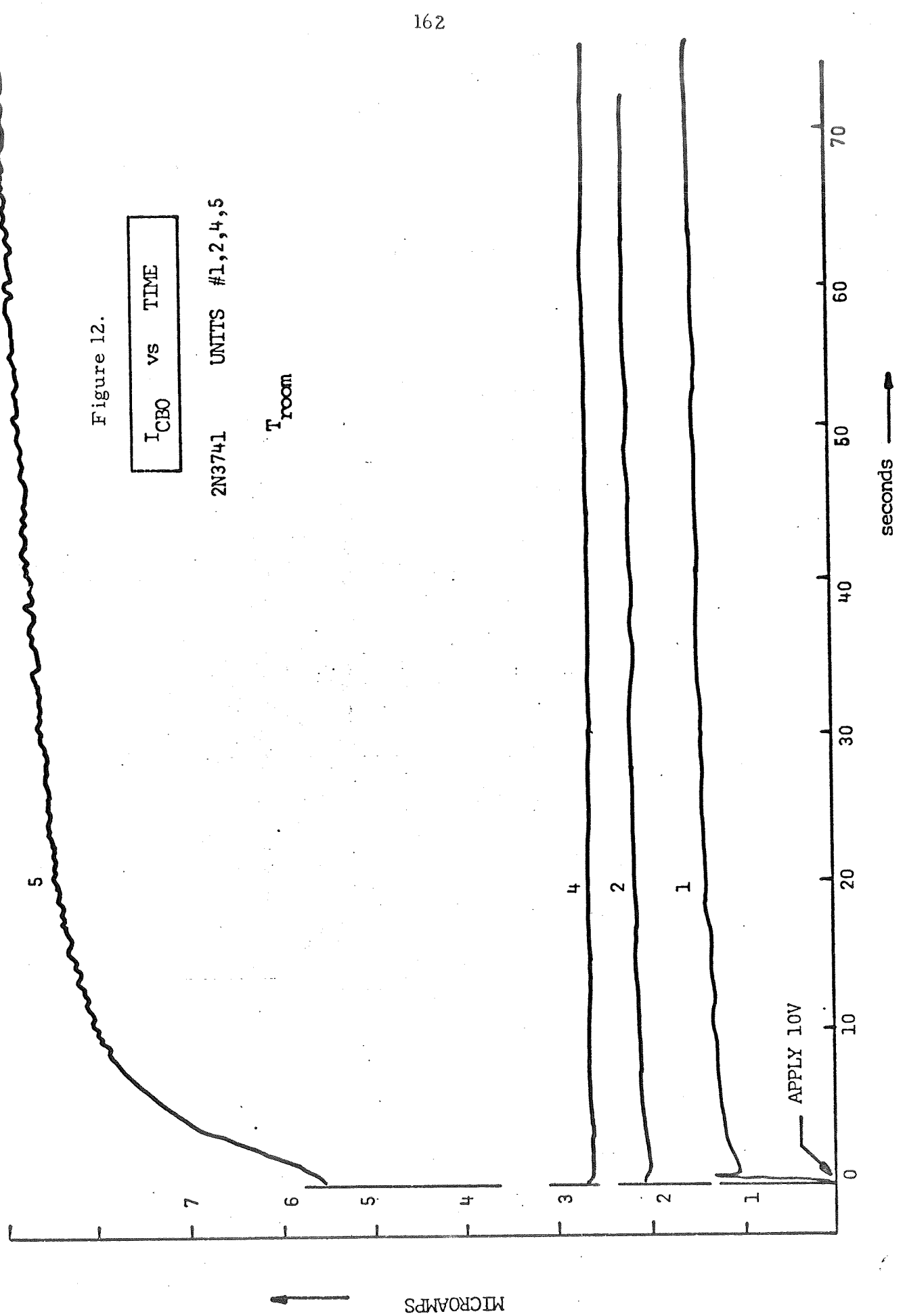
I_{CBO} vs TIME
2N3741 UNITS #1,2,4,5
T_{room}
MICROAMPS
seconds
APPLY 10V
5
4
2
1
0
10
20
30
40
50
60
70
1
2
3
4
5
6
7

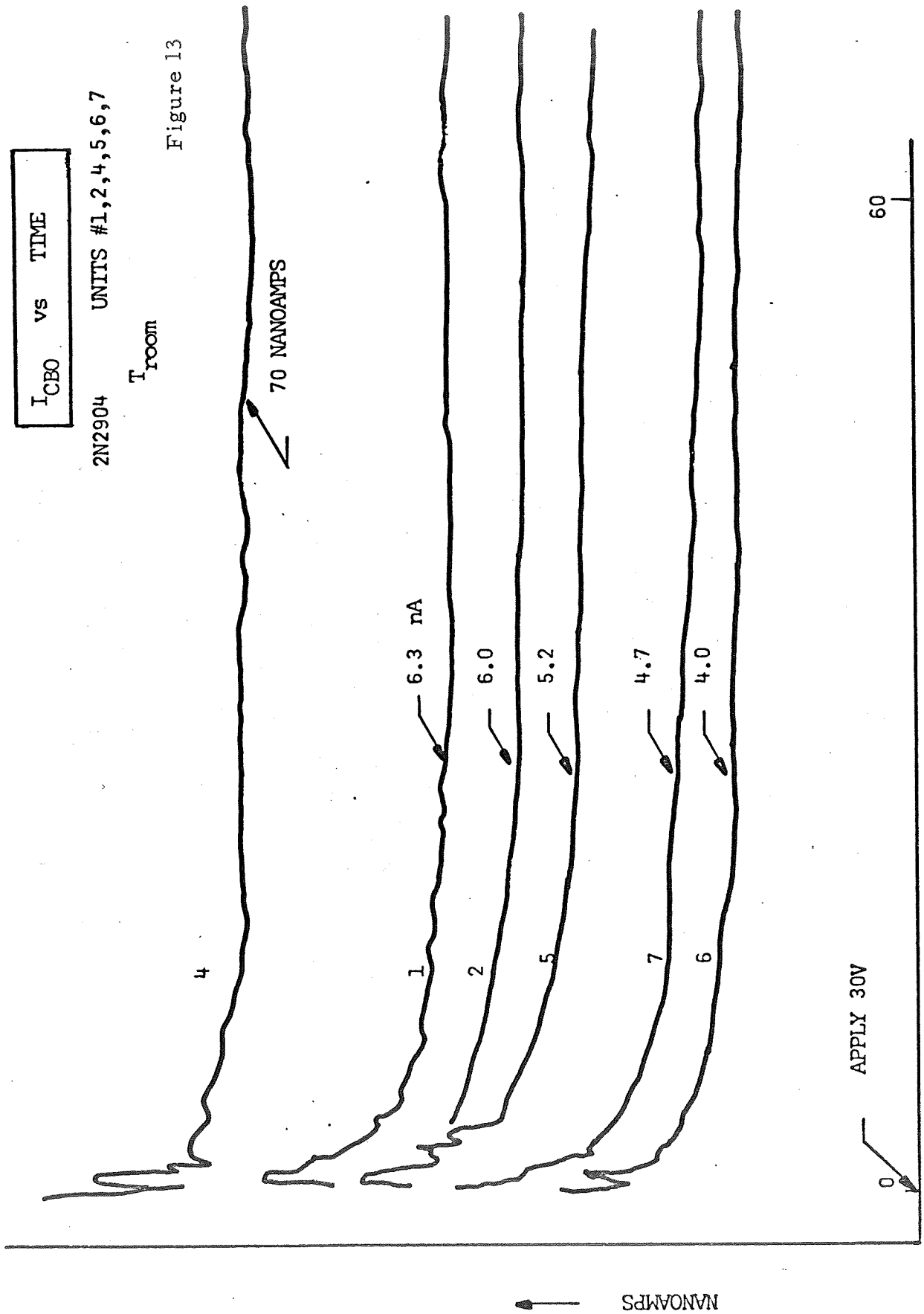
I_{CBO} vs TIME
2N2904 UNITS #1,2,4,5,6,7
T_{room}
70 NANOAMPS
6.3 nA
6.0
5.2
4.7
4.0
4
1
2
5
7
6
APPLY 30V
0
60
seconds
NANOAMPS

Figure 13

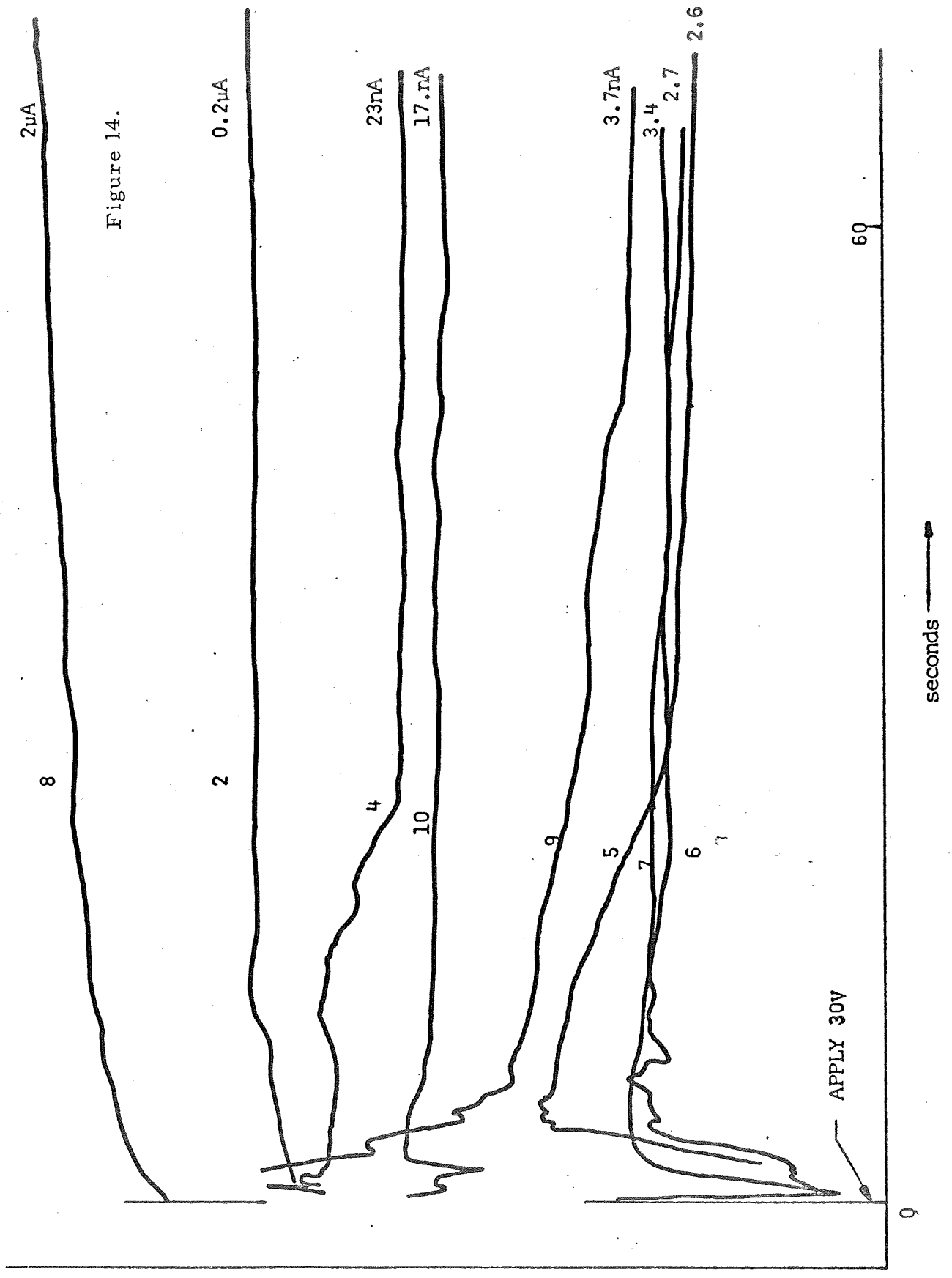
I_{CBO} vs TIME
2N3053 UNITS #2,4,6-10
2μA
0.2μA
23nA
17.nA
3.7nA
3.4
2.7
2.6
8
2
4
10
9
5
7
6
APPLY 30V
0
60
seconds
CURRENT

Figure 14.

Figure 15.

EFFECT OF TEMPERATURE

I_{CBO} vs TIME

2N3741 UNIT #1 at 0°C and T_{room}

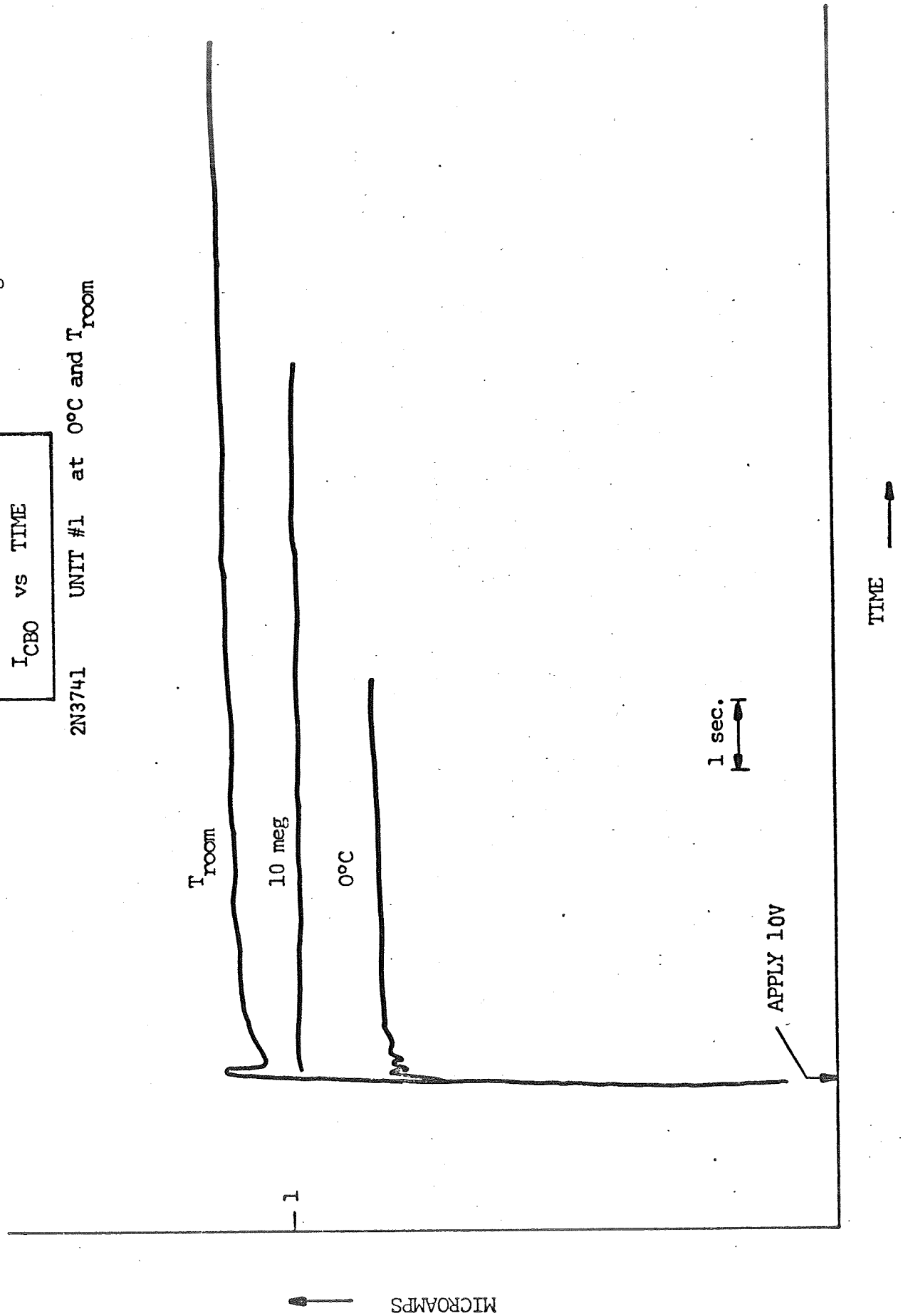

Figure 16

EFFECT OF REVERSE BIAS

I_{CBO} vs TIME

2N3741 - #1 T_{room}

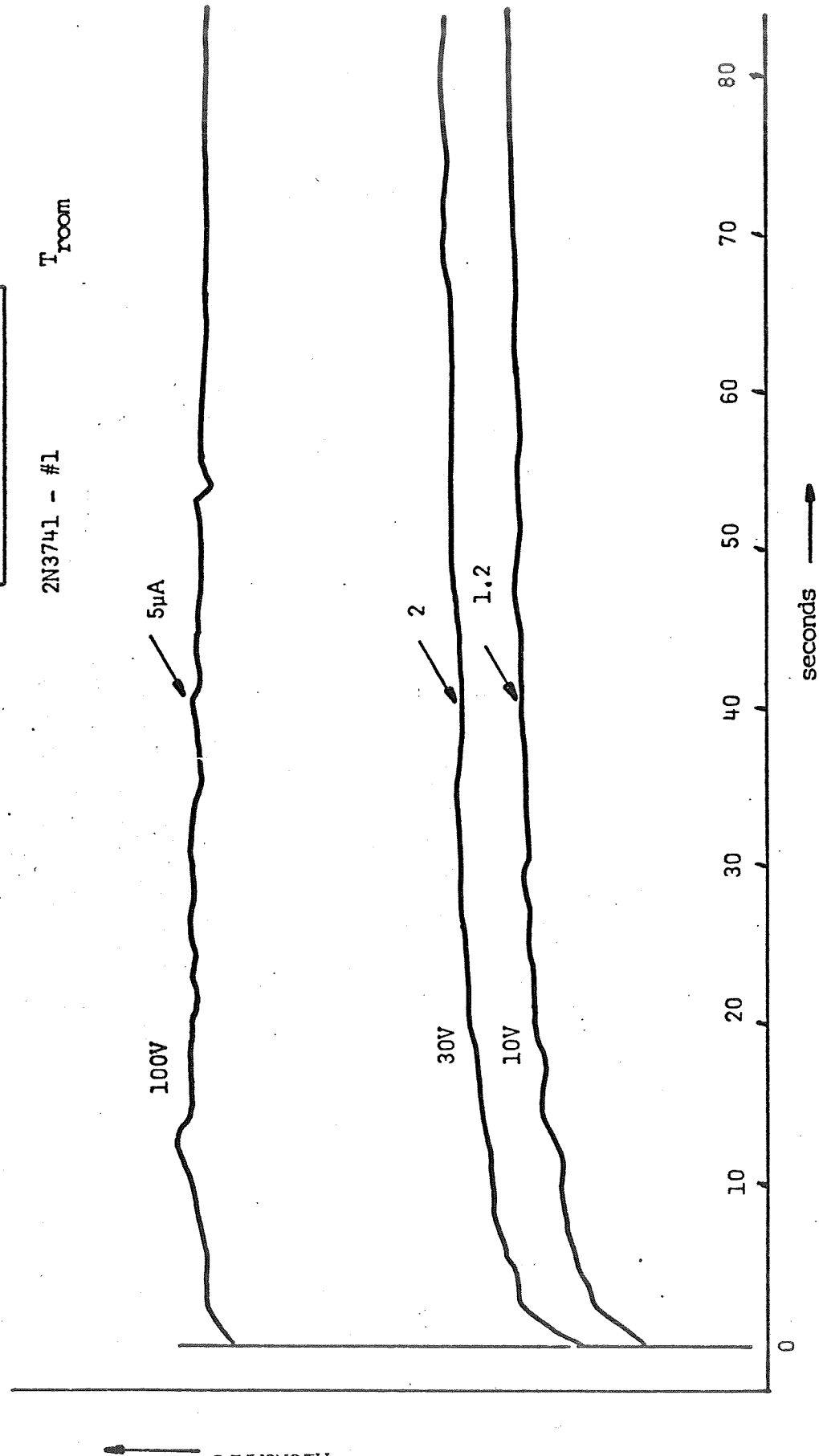

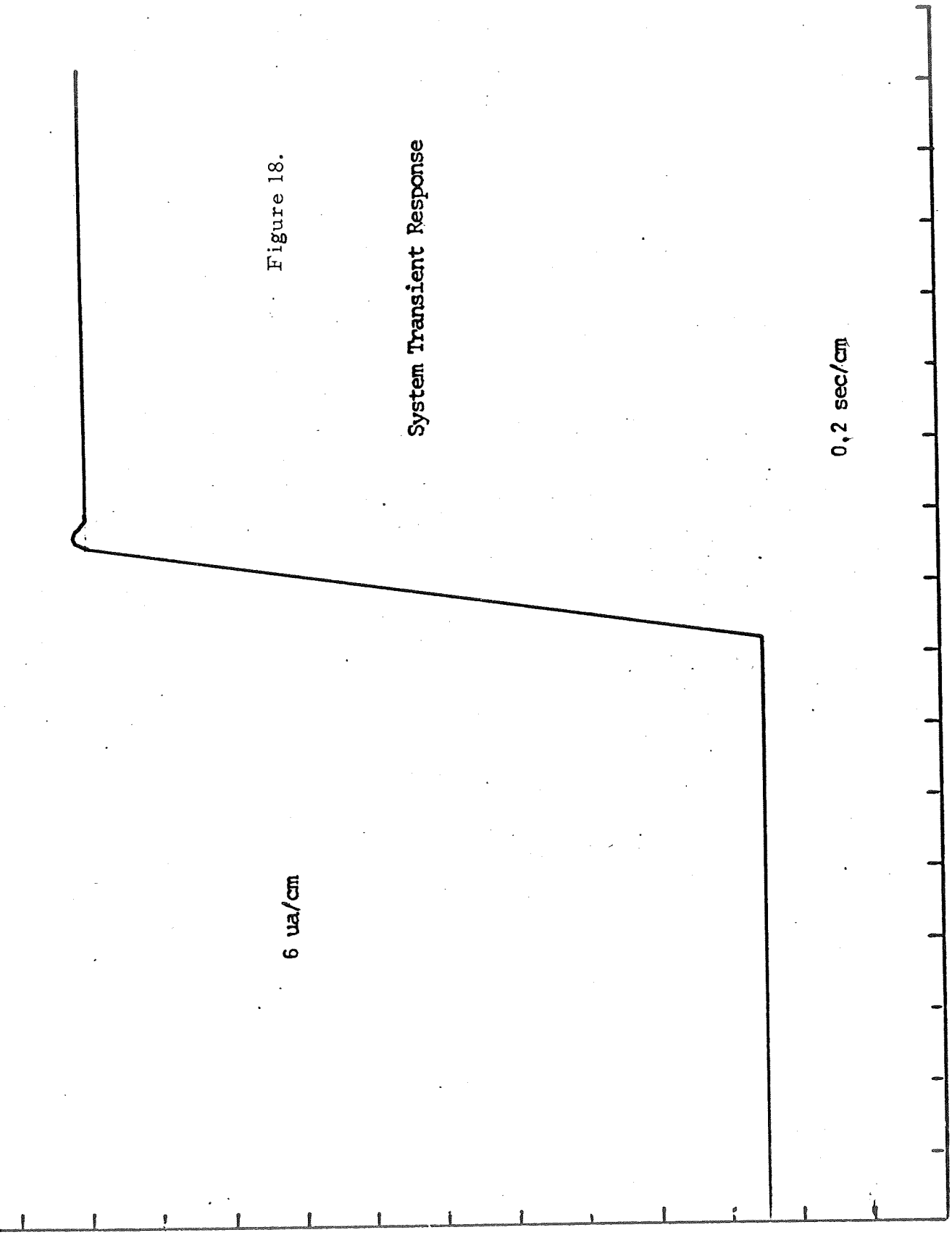

Figure 18.

REFERENCES

1. W. M. Bullis, Solid State Electronics, Vol. 9, p. 143, 1966.

2. S.F. Cagnina and E.H. Snow, J. Electrochem. Soc., Vol. 114, p. 1165, 1967.

3. D.R. Collins, J. Appl., Physics, Vol. 39, p. 4133, August 1968.

4. E. Yon, W.H. Ko and A. B. Kuper, IEEE Trans. on Electron Devices, Bol. ED-13, p. 276, February 1966.

5. E.H. Nicollian and A. Goetzberger, Bell System Technical Journal, Vol. 46, p. 1055, July 1967.

6. A.J. Moulson and J. P. Roberts, Trans. Far Soc. 57, 1208, 1961.

7. T. Drury and J. P. Roberts, Phys. Chem. Glasses 4, 79, 1963.

8. G. J. Roberts and J. P. Roberts, Phys. Chem. Glasses 5, 26, 1964.

9. G. Hetherington and K.H. Jack, Phys. Chem. Glasses 3, 129, 1962.

10. T. Bell, G. Hetherington and K.H. Jack, Phys. Chem. Glasses 3, 141, 1962.

11. R. W. Lee, Phys. Chem. Glasses 5, 35, 1964.

12. G. Hetherington, K.H. Jack, M. W. Ramsey, Phys. Chem. Glasses 6, 6, 1965.

13. G.J. Roberts and J. P. Roberts, Phys. Chem. Glasses 7, 82, 1966.

14. A.E. Owen and R.W. Douglas, J. Soc. Glass Tech. 43, 159, 1959.

15. A.G. Revesz, Phys. Stat. Sol. 24, 115, 1967.

16. B.E. Deal and A.S. Grove, J. Appl. Phys. 36, 3370, 1965.

17. R.J. Jaccodine and W.A. Schlegel, J. Appl. Phys. 37, 2429, 1966.

18. A.B. Kuper and E.H. Nicollian, J. Electrochem. Soc. 112, 528, 1965.

19. E.H. Nicollian and A. Goetzberger, Appl. Phys. Letters 7, 216, 1965.

20. E. Kooi, Philips Res. Repts. 21, 477, 1966.

21. P.V. Gray and D.M. Brown, Appl. Phys. Letters 8, 31, 1966.

22. D.M. Brown and P.V. Gray, J. Electrochem. Soc. 115, 760, 1968.

23. S.R. Hofstein, IEEE Trans. Electron Devices ED-13, 222, 1966.

24. J.R. Ligenza and W.G. Spitzer, Phys. Chem. Solids 14, 131, 1960.

25. W.G. Spitzer and J.R. Ligenza, Phys. Chem. Solids 17, 196, 1961.

26. P.J. Burkhardt, J. Electrochem. Soc. 114, 196, 1967.

27. T.E. Burgess and F.M. Fowkes, J. Electrochem. Soc. 113, 63C, 1965.

28. S.R. Hofstein, IEEE Trans. Electron Devices ED-14, 749, 1967.

29. S.W. Ing, Jr., R.E. Morrison and J.E. Sandor, J. Electrochem. Soc. 109, 221, 1962.

30. L.A. D'Asaro, Solid State Electronics 1, 3, 1960.

31. E. Yon, W.H. Ko and A.B. Kuper, IEEE Trans. Electron Devices ED-13, 267, 1966.

32. A.D. Lopez, J. Electrochem. Soc. 113, 89, 1966.

33. E.T. Yon, Ph.D. Thesis, Case Institute of Technology, Nov., 1966.

34. A.G. Revesz and K.H. Zaininger, RCA Review 29, 22, Mar. 1968.

35. T.E. Burgess, et. al., J. Electrochem. Soc. 115, 69C, 1968.

36. V. Garino-Canina and M. Priqueler, Phys. Chem. Glasses 3, 43, 1962.

37. R.J. Charles, J. Appl. Phys. 29, 1549, 1958.

38. R.D. Evans, The Atomic Nucleus, New York, McGraw-Hill, 195, 1955.

39. R.H. Conditt and J.B. Holt, J. Electrochem. Soc. 111, 1192, 1964.

40. L.W. Hunt and W.H. Miller, Anal. Chem. 37, 1269, 1965.

41. A. Choudhury, et. al., Solid State Comm. 3, 119, 1965.

42. G. Amsel and D. Samuel, J. Phys. Chem. Solids 23, 1707, 1962.

43. D.W. Palmer, Nucl. Instr. Methods 38, 187, 1965.

44. R.W. Ollerhead, E. Almqvist, and J.A. Kuehner, J. Appl. Phys. 37, 2440, 1966.

45. F.N. Hayes, B.S. Rogers and P.C. Sanders, Nucleonics 13, 46, Jan., 1955.

46. F.N. Hayes, et. al., Nucleonics 13, 38, Dec., 1955.

47. F.N. Hayes, D.G. Ott and V.N. Kerr, Nucleonics 14, 42, Jan., 1956.

48. M.S. Patterson and R.C. Greene, Anal. Chem. 37, 854, 1965.

49. J.C. Fisher, J. Appl. Phys. 22, 74, 1951.

50. C.J. Slabinski, M.S. Thesis, Case Institute of Technology, 1966.

51. E.H. Snow, A.S. Grove, B.E. Deal and C.T. Sah, J. Appl. Phys. 36, 1644, 1965.

52. A.G. Revesz and K.H. Zaininger, IEEE Trans. Electron Devices ED-13, 246, 1966.

53. P.V. Gray and D.M. Brown, Appl. Phys. Letters 8, 31-33, 1966.

54. D.M. Brown and P.V. Gray, J. Electrochem. Soc. 115, 760, 1968.

55. A. Goetzberger and J.C. Irvin, IEEE Trans. Electron Devices, ED-15 No. 12, 1009-1014, 1968.

56. A. Goetzberger, IEEE Trans. Electron Devices, ED-14, No. 11, 787-789, 1967.

57. M.M. Atalla, A.R. Bray and R. Lindner, "Stability of Thermally Oxidized Silicon Junctions in Wet Atmospheres," Proc. IRE, London, 106, 1130-1137, 1959.

58. W. Shockley, H.J. Queisser and W.W. Hooper, "Charges on Oxidized Silicon Surfaces", Phys. Rev Letters, 11, 489-490, 1963.

59. W. Shockley, W.W. Hooper, H.J. Queisser and W. Schroen, "Mobile Electric Charges on Insulating Oxides with Application to Oxide Covered Silicon P-N Junction", Surface Science, 2, 277-287, 1964.

60. E.D. Metz, "Silicon Transistor Failure Mechanisms Caused by Surface Charge Separation", Second Annual Symposium on the Physics of Failure in Electronics, Chicago, September 25-26, 1963; RADC Series in Reliability, PHYSICS OF FAILURE IN ELECTRONICS, 2, 163-172, 1964.

61. G.L. Schnable, E.S. Schlegel and R.S. Keen, "Failure Mechanisms in Reverse-Biased Oxide-Passivated Silicon Diodes", Third Annual Symposium on the Physics of Failure in Electronics, Chicago, September 29 - October 1, 1964; RADC Series in Reliability, PHYSICS OF FAILURE IN ELEC-

TRONICS, 3, 108-121, 1965.

62. W. Schroen, "Reliability Physics Studies on Transistors", RADC-TR-65-141, First Quarterly Report, 1965.

63. W. Schroen, "Accumulation and Decay of Mobile Surface Charges on Insulating Layers and Relationship to Reliability of Silicon Devices", Fourth Annual Symposium on the Physics of Failure in Electronics, Chicago, November 16 - 18, 1965; RADC Series in Reliability, PHYSICS OF FAILURE IN ELECTRONICS, 4, 291-314, 1966.

64. K.D. Kang, "Detailed Study of Deleterious Effects on Silicon Transistor", RADC-TR-65-35, Final Report, 1965.

65. "Study of Failure Modes of Multilevel Large Scale Integrated Circuits", NASA Contract NAS - 12-544, Performed by Philco-Ford Corporation, Microelectronics Div., Blue Bell, Penna.

66. T.M. Walsh, "A Technique for Determining the Life Capability of Individual Semiconductors", Proc. 1969 Annual Symposium of Reliability, pp. 86-90, 1969.

67. F. Cocca, "Effects of Low Temperature on Reverse I-V Characteristics of Silicon Diodes", NASA, ERC Internal Publication, May 1969.